Binding site contribution in high resolution records of nicotinic receptor channel currents

vorgelegt von

Patrick Maria Stock

aus Schweinfurt

Würzburg, 2011

Eingereicht am: …………………………………

Mitglieder der
Promotionskomission

Vorsitzender: …………………………………

Gutachter: …………………………………

Gutachter: …………………………………

Tag des Promotionskolloquiums: …………………………………

Doktorurkunde ausgehändigt am: …………………………………

Table of Contents

1. Summary

The nicotinic acetylcholine receptor of the skeletal muscle is one of the best-investigated synaptic proteins and often serves as model for the entire family of pentameric ligand gated ion channels (pLGICs). Receptors of this superfamily share a common architecture. After binding the agonist the characteristic C-loop structure closes in around the ligand-binding site and triggers a wave of conformational changes spreading through the protein finally resulting in the opening of the channels gate.

As shown before, high-resolution single channel data can hardly be described by simple kinetic mechanisms (Parzefall et al., 1998, Hallermann et al., 2005). Recent advances in the field of kinetic modelling on receptor currents demonstrate that the introduction of additional short lived shut states in kinetic schemes enhances the quality of rate estimates. The additional shut states that immediately follow ligand bound states in the mechanism are suggested to resemble the closing movement of the C-loop (Lape et al., 2008; Mukhtasimova et al., 2009). Albeit it has not been described yet whether and how the structural differences of the 2 binding sites of the receptor influence the opening behaviour. To address this question, high-resolution single channel recordings, in combination with agonists that are known to exhibit different binding site selectivity, were performed. Thereby, a detailed description of the binding site dependent generation of channel currents is possible.

At the embryonic mouse muscle receptor used in this study the ligand binding sites are located at the α-γ and α-δ subunit interfaces. By allocation of opening characteristics to the α-δ and α-γ sites it is possible to show the binding site dependent activation of distinct kinetic states. Furthermore, direct evidence is found that the recently introduced short-lived shut states sufficiently describe high-resolution single channel data. Finally an enhanced kinetic mechanism based on the 'primed states' model, published in 2009 by Mukhtasimova et al., will be presented. The model is able to support the structurally diverse α-δ and α-γ binding sites eliciting kinetically distinguishable characteristics. Thus the

complex kinetic characteristics of the embryonic receptor while using high-resolution techniques can be described coherently.

2. Zusammenfassung

Der nicotinische Acetylcholin-Rezeptorkanal des Skelettmuskels zählt zu den bestuntersuchten synaptischen Proteinen und gilt als Modell für die Familie der Liganden gesteuerten pentameren Ionenkanäle. Rezeptoren dieser Großfamilie besitzen als charakteristisches strukturelles Merkmal ein Cystein-Schleifen-Motiv (C-loop), welches sich nach Bindung eines Agonisten um die Bindungstasche herum schließt und eine Kette weiterer Konformationsänderungen nach sich zieht.

Wie in früheren Publikationen festgestellt wurde, ist es nur schwer möglich hochauflösende Messdaten mit konservativen kinetischen Modellen ausreichend zu beschreiben (Parzefall et al., 1998; Hallermann et al., 2005). Aktuelle Fortschritte auf dem Gebiet der kinetischen Modellierung von mechanistischen Rezeptormodellen auf Rezeptorströme, zeigen, dass die Einführung zusätzlicher kurzlebiger Geschlossenzustände in den kinetischen Mechanismen die Qualität der Voraussagen der Modelle verbessert. Diese zusätzlichen Geschlossenzustände, welche Zuständen mit gebundenen Agonisten des Rezeptormodells folgen, spiegeln höchstwahrscheinlich die Schließung des Cystein-Schleifen-Motivs wider (Lape et al., 2008; Mukhtasimova et al., 2009). Trotz der jüngsten Fortschritte wurde bisher nicht beschrieben wie und ob die strukturellen Unterschiede der 2 vorhandenen Bindungsstellen sich auf die Charakteristika des Öffnungsverhaltens auswirken. Die Bindungsstellen für Agonisten befinden sich am embryonalen nicotinischen Acetylcholinrezeptor des Muskels der Maus an den Schnittstellen der α-δ und der α-γ Untereinheiten.

Um der Frage des Einflusses der Bindungsstellendiversität auf den Grund zu gehen, wurden hochauflösende Einzelkanalmessungen unter der Verwendung von unterschiedlichen Agonisten, für die bekannt ist, dass sie unterschiedliche Selektivitäten zu den Bindungsstellen besitzen, durchgeführt. Hierdurch ist es möglich ein detailliertes Bild der bindungsstellenbedingten Auslösung definierter Öffnungscharakteristika zu beschreiben.

Durch die Zuweisung der Öffnungscharakteristika zu den α-δ und α-γ Bindungsstellen gelingt es die bindungsstellenabhängige Aktivierung von

einzelnen kinetischen Zuständen zu zeigen. Darüber hinaus werden direkte Anhaltspunkte dafür gezeigt, dass es möglich ist mit den angeführten kurzlebigen Geschlossenzuständen hochauflösende Einzelkanaldaten kinetisch hinreichend zu beschreiben. Schließlich wird ein erweiterter kinetischer Mechanismus vorgestellt, welcher auf dem ‚primed-states' Modell, das 2009 von Mukhtasimova veröffentlicht wurde, basiert. Zusätzlich ist dieser in der Lage die komplexen kinetischen Charakteristika des embryonalen nicotinischen Rezeptorkanals, unter hoher zeitlicher Auflösung der Messdaten, zu beschreiben.

3. Introduction

Nicotinic acetylcholine receptors (nAChR) are cation permeable ion channels that mediate the transmission of neuronal signals at chemical synapses when binding the presynaptically released neurotransmitter acetylcholine. The muscle type nAChR in particular mediates all fast synaptic excitation in voluntary muscle in vertebrates. When an action potential reaches the presynaptic ending of its motoneuron, synaptic vesicles are released that cause high local concentrations of acetylcholine ($\sim$300 µM) in the synaptic cleft (Katz & Miledi, 1973b; Kuffler & Yoshikami, 1975). ACh diffuses rapidly through the synaptic cleft, transiently binds to postsynaptically located nAChR and causes short openings of the cation selective channel. The inflow of cations leads to depolarization of the surrounding membrane. The locally altered electric field causes voltage-gated Na^+- channels to open and thus elicits muscle action potentials that are conducted along the muscle membrane. Subsequent steps involve the activation of calcium permeable voltage dependent dihydropyridine receptors and ryanodine receptors of the sarcoplasmic reticulum. The massively elevated calcium level finally triggers the movement of motor-proteins causing the muscle contraction.

3.1. The nicotinic acetylcholine receptor and the pLGIC superfamily

nAChRs are part of the pentameric ligand gated ion channel family (pLGIC) that share a common architecture (Figure 1) while differing in agonist specificity and ion selectivity, as well as conductance characteristics. The superfamily consists of cation selective nicotinic ACh receptors and $5HT_3$ receptors as well as anion selective $GABA_A$, $GABA_C$ and glycine receptors in vertebrates and are widely expressed in the central and peripheral nervous system regulating excitability and neurotransmitter release (Corringer et al., 2000; Lester et al., 2004; Sine & Engel,

2006; Kalamida et al., 2007; Taly et al., 2009). Also in Invertebrates members of this family are found: glutamate, 5HT, histidine and acetylcholine gated anion selective channels (Raymond & Sattelle, 2002).

Cys-loop receptor dysfunctions are thought to be involved in a variety of diseases and disorders including Alzheimer's disease, Parkinson's disease, epilepsy, schizophrenia, myasthenic syndromes, depression and substance abuse (Jackson, 1999). As a result, the pLGICs serve as molecular targets for a variety of clinically important drugs, such as muscle relaxants, tranquillizers, anti-convulsants and anti-emetics. Hence, these receptors are critical targets for the development of therapeutics to treat a variety of neurological diseases and disorders.
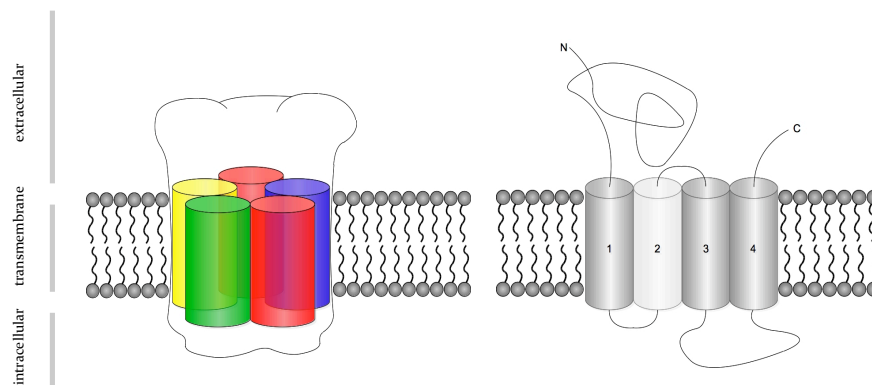
Figure 1: General features of the pentameric ligand gated ion channel superfamily (pLGICs). pLGICs share a common architecture. They are built of 5 subunits arranged around a central ion-conducting pore (left side). The subunit composition for each receptor type varies depending on species and place of action. The colour-code of the subunits matches the muscular nicotinic acetylcholine receptors, having 2 similar α-subunits (red). Right side: pLGIC-subunits exhibit similar molecular features: a large N-terminal extracellular domain, four α-helical transmembrane domains (1 to 4), a more or less extensive intracellular loop between the third and fourth transmembrane domain, and a extracellular C-terminal portion.

The nAChR in particular is involved in pathologies such as congenital myasthenia, autosomal dominant nocturnal frontal lobe epilepsies, sudden infant death syndrome, attention deficit hyperactivity disorder and nicotine addiction. Understanding nAChR structure and the conformational transitions, linking binding of the agonist to the opening mechanism of the channel pore, is essential for understanding these disorders and will help to design novel therapies.

The nicotinic acetylcholine receptor has been subject to scientific investigations for over one century now, since John Newport Langley was the first to show that nicotine and curare directly act on the muscle tissue and not on the neural side of the motor endplate. He concluded that "it is convenient to have a term for the especially excitable constituent, and I have called it the *receptive substance*. It receives the stimulus and by transmitting it causes contraction" (Langley, 1906). In addition, nAChRs were the first membrane receptors of a neurotransmitter to be isolated and chemically identified and are now among the best-known membrane proteins involved in synaptic signal transduction (Colquhoun D, 2003) and often serve as model for other receptors (Colquhoun & Sivilotti, 2004).

3.2. Structure of nicotinic acetylcholine receptors

The muscle-type ACh receptor macromolecule is composed of five subunits, point symmetrically arranged around a central membrane-spanning pore (compare Figure 1 and 2) with a total molecular weight of about 290 kDa. The subunits are similar in amino acid sequence and show the same topology. Each subunit has a large extracellular amino-terminal domain, four predicted α-helical membrane-spanning segments, M1 to M4, with a large cytoplasmic loop between M3 and M4 (Figure 1) of strongly varying sequence and length and a small extracellular C-terminal domain (Miyazawa et al., 2003). The same characteristics are found in all members of the pLGIC superfamily of receptor channels, therefore also called the nicotinic family.

The muscle type receptor channel has the subunit composition $(\alpha 1)_2$, β, γ, δ in embryonic or denervated muscle. Some of the embryonic type receptors aggregate in dense small clusters (hot spots) that are randomly distributed over the myotube surface. During development, the distributed embryonic muscle type receptors will be reinternalized on activation by the outgrowing motoneuron reaching its target cell; adult receptors will be expressed and

exposed instead. In the adult muscle-type receptor, the γ-subunit is exchanged for an ε-subunit. These adult muscle receptors are clustered at the postsynaptic membrane, exhibiting higher single channel conductivity and altered kinetic characteristics in comparison to embryonic type receptors.

Compared to the neuronal nicotinic receptors, far more is known about the muscular AChR. The main reason is that a very similar receptor to the muscle-type is present in great abundance in the electric organ of the Torpedo ray. The name derives from the Latin word *torpere*, which means to be stiffened or paralyzed. When the electric organ is discharged to paralyse a potential prey the electric shock can reach, species dependent, up to 220 Volts. To accomplish this very special task, modified muscle cells of the electric organ are densely packed with embryonic like nAChRs, partially forming crystalline arrays (Kistler & Stroud, 1981). This has allowed purification of the receptor subunits and cloning of the corresponding genes. Since then, it was possible to study the properties of defined nAChR subunits and their interactions necessary for binding and gating using a broad spectra of techniques, like biochemics, molecular genetics and electrophysiology (Karlin, 2002; Corringer et al., 2000).

For structural analysis by electron microscopy it was of great importance that tubular crystals of *Torpedo ray* receptors, still embedded in their native lipids, can be easily grown from isolated postsynaptic membranes. These are the basis of almost all of the quantitative structural studies of the whole nAChR and for the entire nicotinic superfamily (Kistler & Stroud, 1981; Miyazawa et al., 1999). However, two major discoveries have lately increased the understanding of structure and fuction in nAChRs and related proteins. The first was the cloning and characterization of the molluscan ACh-binding protein (AChBP, Brejc et al., 2001; Smit et al., 2001). Since the protein was found to be analogous to the extracellular domain of pLGICs and is soluble, it allows deeper structure analysis compared to membrane bound receptors. The second was the refined structure of *Torpedo* nAChRs by 4 Å resolution (Unwin, 2005), which provided a complete picture of the receptor in near-physiological conditions, including ligand binding

domain, the aqueous pore and the intracellular domain. Most recently the discovery of bacterial homologues to pLGICs, the so-called ELIC and GLIC channels, brought the possibility to provide even further refined structural insights (Corringer et al., 2010).

The electric organs of *Torpedo* contain only the embryonic γ-form of the receptor. However, all subunits share a high degree of homology of about 31 to 41% pair wise identity to the α subunits, depending on species. The most likely arrangement around the pore, viewed from the extracellular space is α, γ, α, β, δ in clockwise order. The acetylcholine molecules bind to both α subunits at or close to the neighbouring γ or δ subunit, respectively (Karlin, 1993; Sine et al., 1995; Xie & Cohen, 2001).

3.2.1. Overall structure

The cylindrical appearing receptor has a diameter of ~70Å and measures ~160Å from its bottom at the intracellular space to its extracellular top (Figure 2). The 5 rod-shaped subunits that constitute the receptor are arranged in a nearly 5-fold point-symmetric manner, thereby forming the conducting pore in the core of the macromolecule. The subunits all have a similar size and the same 3-dimensional fold. Essentially, each subunit is a 3-domain transmembrane protein and partitions naturally in its extracellular domain (ECD) containing the ligand binding sites, membrane spanning domain and intracellular part (compare also Figure 1 and 2).

3.2.2. Special conformations of α-subunits

The subunits of the closed channel have two alternative conformations: that of the two α subunits and the other for the three non-α subunits (Unwin et al., 2002), that mainly involve the inner sheets of the β-sandwich that composes the ECD and are twisted about 10° relative to non-α subunits (Unwin, 2005). Several interactions have been identified, stabilising the special conformation of the α subunits. These intra and inter-subunit interactions are similar or same for both

α subunits and their three-dimensional structures are therefore deemed to be the same, except for differences at the binding site, where the C-loop of α_δ is disordered (Unwin, 2005) and of variations in side-chain conformations, that could not be resolved so far.
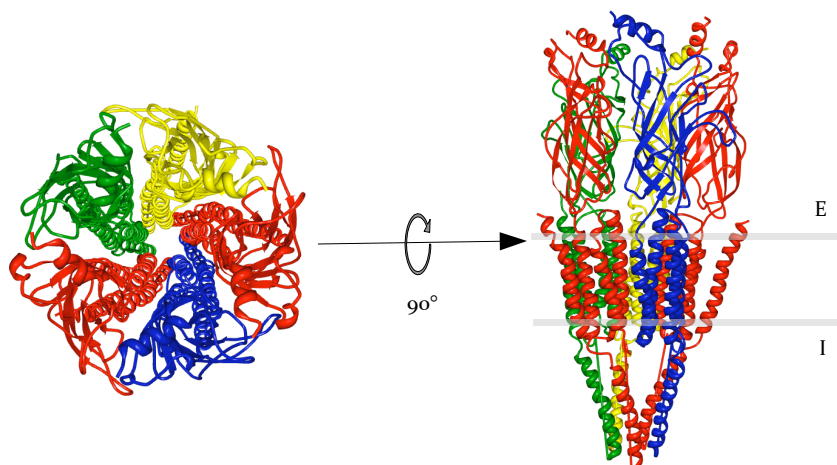
Figure 2: Structure of the nAChR. Structural data based on data from N. Unwin, 2005. The left side shows the top view of the nAChR macromolecule as seen from the synaptic cleft. The subunits are coloured in red for the two equivalent α-subunits, in blue for the γ-subunit, green for β-subunit and yellow for the δ-subunit. The ligand binding sites are situated at the αδ- and αγ-interfaces. Right side: The nAChR is rotated 90° to give a side view. The inner sheet (I) and the external sheet (E) of the lipid bilayer are shown as grey bars. The subunits show a natural spatial division into extracellular domain expanding the macromolecule into the extracellular space (top part), transmembrane domain mainly located between the inner and outer sheets of the lipid bilayer (gray bars) and intracellular domain expanding into the cell lumen (lower part). The ligand binding sites are located in the upper half of the extracellular domain.

3.2.3. Agonist binding and the conformational wave

The special conformation of the two α subunits can also be called "distorted", since the α subunits convert to a conformation more similar to the non-α form upon agonist binding. This conformation resembles very much the form of the protomers of the AChBP, when agonist is bound to all subunits (Unwin et al., 2002). Accordingly the binding is thought to overcome this distorted (or tense) state, by triggering a conformational wave spreading through the receptor. Loops B and C of the ECD close in around the agonist molecule on binding, which results in a local reorganization, mainly involving rigid body movements of the

inner and outer parts of the β-sandwich. The rearrangement reduces the stability of the tense form of the α subunit in favour for the relaxed form. A more extended conformational change of the α subunits takes place, when the β1-β2 loop rotates and therefore is displaced next to the pore lining M2 α-helix. The unlocking of M2 helices, allows their rotation, thereby destabilizes the weak hydrophobic interactions that keep the channel gate closed and finally opens the pore.

The gating itself appears to occur by fast cooperative movements of the pore lining helices, while the ligand–binding domain may act as a controlling device that blocks or facilitates these structure changes. In this respect a clear distinction can be made between ligand binding at the α subunits and the movements in the membrane-spanning domain, where a more symmetrical conformational change occurs and the subunits contribute equally to the opening sensitivity of the gate (Labarca et al., 1995).

3.2.4. The ion conducting pathway

The transmembrane domain (TM) is formed by α-helical segments (M1 to M4) and the functional important M1-M2 and M2-M3 loops. The TM is covalently connected to the ECD at the end of M1 and additionally interacts through the M2-M3 loop with the β1-β2 and Cys-loops. The central ion-conducting pore is lined by the M2 segments of each subunit. The constriction zone is the narrowest part of the open channel and located near the cytoplasmic membrane surface (Miyazawa et al., 2003). The constriction zone is critical for selectivity and permeation of the channel (Galzi et al., 1992; Corringer et al., 1999; Gunthorpe & Lummis, 2001).

Furthermore, the central tube is constituted of a ~20Å wide outer vestibule, reaching about 65Å deep, narrowing down to the smaller transmembrane pore. The end of the tube is formed by the cytoplasmic parts of the subunits, forming an inverted pentagonal cone, shaping a spherical inner vestibule of ~20Å

diameter. The cavity connects the tube to the intracellular space via ~8-9Å wide windows between subunits, located directly under the inner membrane surface (Unwin, 2005).

The most likely physiological role of the vestibules is to serve as pre-selectivity filters for ions, exposing charged groups at the vestibule entrances and the inner walls of the vestibules. By concentrating cations close to the narrow membrane spanning pore the efficiency of transport may be amplified (Kelley et al., 2003; Hansen et al., 2008). In analogy to the molecular design of the ACh-esterase enzyme, the protein surface may play a crucial role in producing an electrostatic field, guiding the positively charged ACh molecules towards the enzymatic active site (Ripoll et al., 1993).

In comparison to the extracellular one, the cytoplasmic vestibule is differently designed. Negatively charged groups that are arranged at the window borders exert strong local ion selectivity. The windows are not significantly wider than the diameter of an ion with its first hydration shell. Thus, the lateral windows are equally, or more constricting than the narrowest part of the transmembrane domain and therefore may even restrict the ion flux through the channel, like it was shown for 5-HT$_3$ receptors (Kelley et al., 2003).

3.3. Electrophysiology

3.3.1. Historical development

As mentioned above, the general idea of postsynaptically located "receptive substance" was first described by Langley in 1906. In 1936 Dale and his colleagues then accomplished the subsequent identification of acetylcholine as the transmitter acting on the muscular receptors in detail. Many important discoveries followed with short delay, e.g.: in 1938 Göpfert & Schäfer accomplished the first recordings of neuromuscular postsynaptic potentials, using extracellular electrodes, and Feldberg and colleagues were able to show electrochemical transduction at the electrical organ of *Torpedo marmorata* by

applying ACh and measuring the response (Feldberg et *al.*, 1940). Further important steps were the recording of postsynaptic currents by means of intracellular electrodes (Eccles et *al.*, 1941; Fatt & Katz, 1950, 1951, 1952) and the controlled iontophoretic stimulation of the receptors (Nastuk W, 1953; del Castillo & Katz, 1955a, 1955b, 1957a, 1957b; Kuffler & Yoshikami, 1975).

The first single channel recording of nicotinic receptor currents using the patch clamp technique was accomplished in 1976 by Neher & Sakmann and revolutionized electrophysiology. The patch clamp technique brought electrophysiology to the molecular level and provided the possibility to expand electrophysiological studies to most cells. The combination of electrophysiology and molecular biology brought the possibility of structure-function analysis. The currents of the nicotinic receptor appeared as several ms events, invariable in amplitude and of the same average duration over a wide concentration range.

The development of the gigaseal (Sigworth & Neher, 1980) by applying slight suction to the recording pipette allowed recordings with less noise. This method improved current resolution and finer details in the kinetics of channel gating were revealed. The establishment of the various recording configurations: cell-attached/inside-out/outside-out/whole-cell (Hamill et *al.*, 1981) further broadened the spectra of applications and allows for experiments to be undertaken with a controlled environment on both sides of the membrane patch.

With the higher resolution of gigaseal patch clamp, it became clear that channel opening events are truly bursts of openings, separated by very short closings (Colquhoun & Sakmann, 1981). While performing a broadly organized characterization of nAChR kinetics, using agonists with different binding properties, David Colquhoun and Bert Sakmann delivered a very detailed description of the electrophysiological features that were interpreted in the background of structural knowledge in 1985. Compared to today, only little was known about the detailed structure of the nicotinic receptors and their binding sites. Using a cut-off frequency (f_c) of 4-9kHz a consistent resolution of 40µs for

shut times and 60µs for openings could be achieved (Colquhoun & Sakmann, 1985). At this resolution they found individual channel activations (bursts) to be interrupted by gaps of short and intermediate duration and showed that the shorter gaps appear to be of agonist dependent duration, varying from 71µs to 13µs, but do not depend on agonist concentration. Furthermore they were able to discern the distribution of bursts that revealed to have two components: a shorter component that mainly consists of single openings, whereas the longer burst component contains sequences of longer openings. The gap frequency and the mean number of gaps in bursts were shown to be dependent on the nature of the agonist, but only little dependence on agonist concentration was found. They further concluded that brief openings do not originate from singly liganded receptors only, since the persistence of a small portion at high concentrations provided a contraindication to this presumption.

The models shown in Figure 3 were fitted to the experimental data using a maximum likelihood approach, so that the rate constants of the kinetic scheme were varied to maximise the probability of observing the data previously recorded. The two mechanisms gave comparable good result, when the association and dissociation rates of the Model 1 mechanism were not constrained to each other. At this time there were mainly biochemical evidences that the 2 binding sites might differ (Sine & Taylor, 1981). Assuming for simplicity that the rate constants for binding are independent from each other (no co-operativity) the improvement over the simpler Model 1 was restricted to a better match for the occurrence of the intermediate gap component. In addition their rate constants turned out to give a zero opening rate for one of the binding sites, referring to the inability to resolve a third intermediate opening component, that could be observed for the first time, when in 1998 Parzefall and colleagues presented the first electrophysiological data derived by high-resolution patch clamp records (Parzefall et al., 1998). Using this improved method Parzefall and colleagues were able to push the physical resolution barrier so that events down to 6µs length could be reliably detected for mouse muscle nAChRs.

Model 1 according to Karlin (1967)
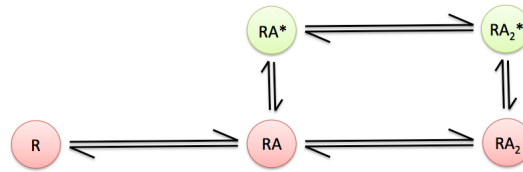
Model 2 according to Colquhoun & Sakmann (1985)
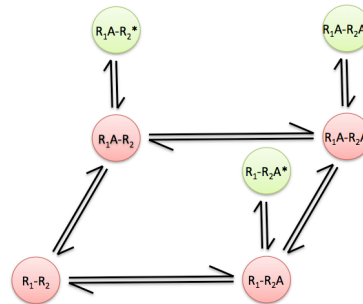
Figure 3: Kinetic models distinguishing binding and gating for the nAChR. R denotes the shut receptor molecule (R_n depicts the discrimination of the 2 binding sites), A denotes the agonist molecules bound to the receptor and asterisks (*) label the open states (additionally depicted in greenish). Model 1 presumes that the 2 binding sites are indistinguishable or show co-operativity (depending on rate-constraints in the mechanism) and that only one distinct open state can be detected from singly liganded receptors, whereas the second model presumes that the 2 subunits are non-equivalent in binding and dissociation behaviour and may allow for different kinds of openings from the two singly liganded receptor states.

The improved method of high-resolution patch clamp recording was mainly based on the use of a low noise amplifier that was additionally optimised by incorporation of an alternative pipette holder made of Teflon and the application of thick-walled quartz glass pipettes (Parzefall et al., 1998; Dudel et al. 2000). The sophisticated setup allowed the exposure of at least 3 different open states, when ACh was used to activate the channel: single openings with mean durations of 1.2 and 25μs and bursts of 10ms mean duration, composed of on average 800μs openings intervened by 16μs gaps (Parzefall et al., 1998).

Subsequent work of Hallermann and colleagues (2005) employing the high-resolution technique and fitting the mechanistic receptor Model 2 (Figure 3) using the maximum likelihood approach accurately predicted the main physiological properties of the nAChR for one concentration of the agonist. Trying the same approach simultaneously for a range of Suberyldicholine

concentrations revealed the frequency of short and intermediate openings to be poorly predicted by this mechanism and therefore unlikely to arise from monoliganded states solely.

3.3.2. Recent findings

One recent example for the interconnection of these two research fields is the work of Auerbach & colleagues on muscle receptors that provided an overall picture of the sequential nature of receptor gating upon binding of the agonist. By measuring the rate-equilibrium free energy relationships referring to point mutations in ligand-binding and pore domains, that were deemed to be crucial for binding to gating conformational changes or the gate opening (Zhou et al. 2005), they have been able to describe blocks of coordinated motion. The cascaded movement starts with the $\beta4$-$\beta5$ linker and the C-loop (increasing agonist affinity), followed by the transition zone (the $\beta1$-$\beta2$ linker) and subsequent movement of the pore region (M2-domains) finally resulting in gating of the channel (Grosman et al., 2000, Chakrapani et al., 2004). The propagational wave, excluding the activation-barrier of agonist binding, moves through the receptor protein via Brownian motion and is thought to take not more than ~1µs and thus reflects the minimal unit time needed for receptor opening isomerisation (Chakrapani & Auerbach, 2005).

The movement of the pore-lining M2 domains was refined (Purohit et al., 2007) to be further divided into a 3-step mechanism of gate activation. The early movement of most of the M2 residues is followed by delayed repositioning of residues restricted to the mid section of M2. Purohit and colleagues suggested that the pore conductance does not increase dramatically until the late rearrangements of mid section residues of the M2 transmembrane domain.

More recently Lape et al. (2008) proposed the existence of a new functional state in kinetic models of nAChRs and glycine receptors, the so-called "flip" state, to help explain partial agonism of these receptors. The flip state (see Figure 4, denoted as F in Model 3) is one of a number of brief intermediate closed states, immediately preceding the channel opening state, with a higher affinity for

agonist than the closed states. According to their model, partial agonism is the result of the reduced ability to reach the flipped state (Lape et al., 2008) in contrast to activation by full agonists, without having any agonist or concentration dependent effect on the rate of channel opening (β) and closing (α). Using partial agonists the group was able to improve the agonist-induced discrepancy on entering the flipped state compared to full agonists. Based on phi-value analysis, they suggested the additional brief shut state to reflect an early conformational state after binding of the agonist molecule, most probably the closing in of the C-loop around the bound agonist.

Another recent study of Mukhtasimova and colleagues provided an even further extended gating scheme by introduction of so-called primed states. Using mutational studies they detected 2 transient closed states, called singly primed and doubly primed state, that immediately precede brief and long-lived channel openings respectively, which they suggest to reflect the closings of the C-loops (Mukhtasimova et al., 2009). They found the singly primed state to have intermediate duration while triggering short openings, and the doubly primed state to have brief duration whilst allowing long-lived openings.

Model 3 according to Lape and colleagues (2008)
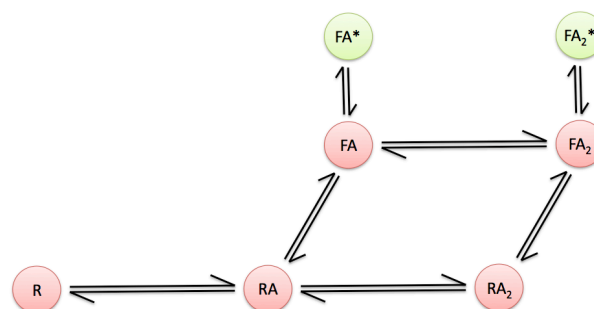
Model 4 according to Mukhtasimova and colleagues (2009)
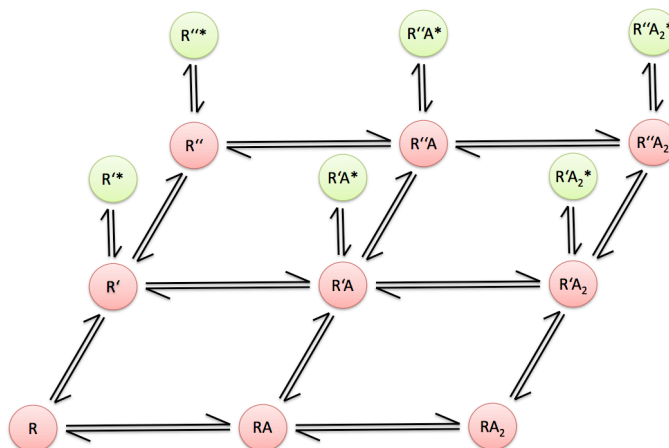
Figure 4: Recently published models of channel kinetics distinguishing different conformational states of the channel. Both models exhibit additional shut states directly preceding the open states of the channel. Both models do not discern the structurally differing binding sites. In Model 3 proposed by R. Lape and colleagues, a so-called "flip state" was introduced that directly precedes channel opening. Channel opening and closing rates from the flipped states were shown to be independent of the nature of the agonist. Mukhtasimova and colleagues proposed a model with 2 transient closed states directly preceding the open states on basis of mutational receptor studies. The singly primed state is of intermediate duration, triggering short openings, while the doubly primed state is of brief duration and allows for long openings.

3.4. Agonists for analysis of binding site diversity

The nAChR has two main functional modules: the extracellular portion, which recognizes and binds the neurotransmitters at specific subunit interfaces, and the transmembrane module, forming a gated ion selective channel. The question, how the binding of the transmitter to the extracellular compartment controls the opening and closing of the channels gate has been a long-standing question in the field. A variety of diverse advanced allosteric mechanisms has been proposed in the last ten years (Grosman et al., 2000; Chakrapani et al., 2004; Gao et al., 2005; Taly et al., 2005; Sine & Engel, 2006; Lape et al., 2008; Mukhtasimova et al., 2009).

Although the nAChR subunits have been explored in the most sophisticated ways the relationship between binding site diversity and gating kinetics has not been

resolvable to a satisfying level (most likely) due to hardly resolvable short opening events. Despite the availability of the high-resolution patch-clamp technique for some years, this advanced method has been ignored for the generation of data as basis for development of advanced kinetic mechanisms. It is still not clear whether agonists with different preferences for the two binding sites show altered gating properties in respect to short and intermediate openings that can only be observed using high resolution single channel recording techniques. Even the observation of residual short openings at high agonist concentrations remains a long standing question in the field of electrophysiology and demands to be solved.

To address this topic I combined the technique for high-resolution single channel recording and the application of agonists differing in affinities for both binding sites to dissect the contribution of unequal binding on channel opening behaviour. The use of high-resolution single channel data allows a detailed evaluation of gating events below the physical resolution barrier of 6μs by interpretation of dwell time distributions and accordingly fitted probability density functions as described before (Parzefall et al., 1998; Hallermann et al., 2005). The observed gating characteristics will be interpreted in the framework of several kinetic gating schemes.

To address the influence of binding site diversity, agonists with unequal affinities for the αγ and αδ binding pockets of nAChRs will be applied. Differing binding properties lead to diverse efficacies in channel gating of the heterogeneous macromolecule and the influence on openings from the singly liganded states may only be detected by the application of ultra high resolution patch clamp recording techniques as described by Parzefall and colleagues in 1998.

Site selectivity depends on the species of the animal and the subtype of the non-α subunits. Adult receptors from human or mouse show either little or undetectable site selectivity (Ohno et al., 1996; Akk et al., 1996; Wang et al.,

1997). However, the embryonic type nAChRs of mouse muscle present some site specifity in activation and will be used in this study.

Three agonists were employed to activate such nACHR channels: acetylcholine (ACh) the natural occurring transmitter; carbamylcholine (CCh) that happens to be a weaker agonist then ACh, and epibatidine (Ebd) that differs greatly in binding site preference and exhibits enhanced efficacy as compared to ACh.
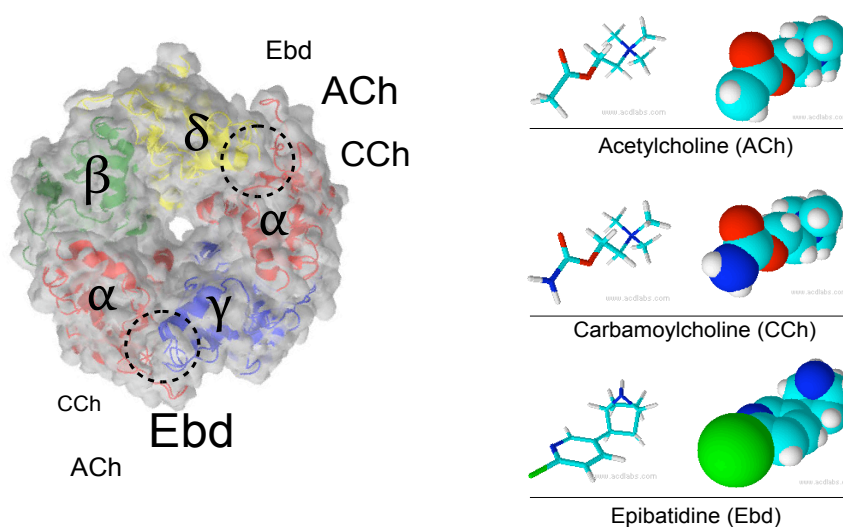
Figure 5: Agonists with diverse binding affinities at the mouse musle embryonic type nAChR. Left side: The nAChR is shown as surface view as seen from the synaptic cleft and the arrangement of subunits is depicted. The location of the binding sites at the αδ- and αγ-interfaces are roughly labelled by dotted lines. The abbreviations for the agonists used in this study visualize the relative binding properties of the molecules in that way, that larger letters mean depict a higher affinity for the binding site they are located next to. Right side: 3-D atomic structure of the selected agonists as stick model and spacefill-representation. Atoms and bonds are coloured according to their nature: turquoise: carbon, white: hydrogen, red: dioxygen, blue: nitrogen, green: chlorine. For better comparison the front most part of the agonists is always directed to the central axis of the receptor molecule, when the agonist is bound.

ACH activates the mouse muscle nAChRs of the embryonic type with 30 fold site selectivity for the αδ-binding site compared to the αγ-binding site (Zhang et al., 1995). CCh activates the embryonic type receptor with similar site selectivity but less efficient compared to the naturally occurring transmitter ACh. Ebd activates the embryonic muscle receptors quite differently from ACh (Zhang et al., 1995). The αδ-binding site forms the low affinity binding-site, whereas the αγ-interface

is the high affinity site. The αγ-site is selected 75 fold over the αδ-site in the embryonic type of the receptor (Prince & Sine, 1998a, 1998b).

4. Methods

4.1. Cell culture and treatment

4.1.1. Preparation

To gain cells that are suitable for cultivation of myotubes, we prepared interossal toe muscles of the hind feeds of neonatal wild type mice. According to national guidelines, it was ensured that the animals did not suffer needlessly. After derotomy of mice not older than postnatal day 7 (P 7), the muscles were excised and incubated in enzyme solution for 1h at 37°C to dissociate the cells and remove presynaptic nerve terminals (Költgen et al., 1991; see Figure 6 for overview). The solution was constituted of standard Ham's F12 culture medium (Invitrogen Co., Carlsbad, CA, USA), 460 Units/ml Collagenase V, 2 Units/ml Protease IX and 100 Kunitz-Units/ml Deoxyribonuclease I (all from Sigma-Aldrich Co., St. Louis, MO, USA). After enzyme treatment, cells were mechanically triturated and centrifuged for 10 min at 1800 r.p.m. After resuspension of the pellet in standard Ham's F12 containing 20% fetal calf serum and 100 Units/ml Penicillin/Streptomycin (both Invitrogen) the cells were plated out on collagen coated cover slips. When the cultivated cells reached confluence after 3-4 days Arabinofuranosyl Cytidine (Ara-C, Invitrogen, c=3.1 µmol/l) as antimetabolic agent was supplemented to retain cells from further mitoses and overgrowth. 12h later culture media was changed to remove Ara-C: D-MEM (Dulbecco's modified eagle's medium) containing 5% fetal calf serum, 5 % horse serum (Invitrogen) and 100 Units/ml Penicillin/Streptomycin.

4.1.2. Culture

During development of the embryo, muscle cells express different types of receptors. At the very beginning nicotinic Acetylcholine Receptors (nAChRs) are of the embryonic type. They are constituted of 5 subunits: 2 α, β, γ, δ, have a conductance of about 40 pS and are evenly distributed over the entire muscle cell

surface but will form much denser small clusters a little later. These so called hot spots are still randomly distributed over the myotube surface (Vogel et al., 1972). When outgrowing motoneurons reach the myotubes and neuromuscular junctions are built, embryonic type receptors are exchanged for adult type receptors. The latter posses a different subunit composition with the δ subunit replaced by an ε subunit. The adult receptors therefore show a higher conductivity of about 60 pS and kinetics are changed to show a reduced duration in postsynaptic currents (Brenner & Sakmann, 1983). As the presynaptic apparatus is artificially removed by the enzyme treatment, resorption of the adult receptors takes place and embryonic type receptors are expressed and translocated to the surface again. To ensure that the embryonic type receptor is the only to be exposed on the myotubes cell surface cells were kept in culture for at least 7 days, like described in Franke et al. (1992). The cells were used for 1 to 2 h for the cell attached mode patch clamp recordings.
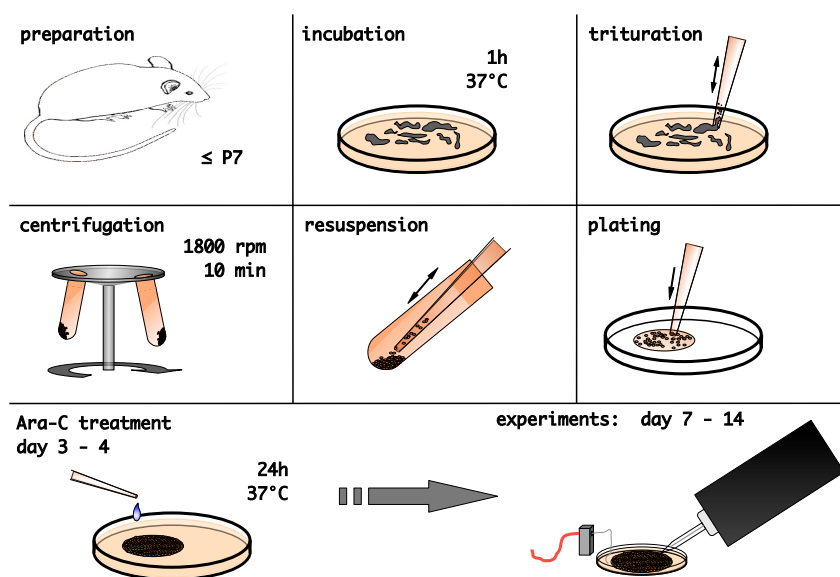
Figure 6: Preparation of myotubes uniformly expressing the embryonic type nAChR. The figure gives a short overview of the tissue preparation and cell culture from top left to bottom right. The treatment ensures that all exposed nAChR channels are of the embryonic or denervated muscle type of the $\alpha_2\beta\gamma\delta$-subunit composition.

4.2. Electrophysiology

4.2.1. Patch clamp recordings in the on cell mode

For recordings the cover slips were transferred into Petri dishes with physiological solution: 162.0mM NaCl, 5.3 mM KCl, 2.0 mM $CaCl_2$, 0.67 mM NaH_2PO_4 and 15 mM HEPES adjusted to pH 7.4 using NaOH. The same solution was used for the pipette tip, but additionally contained one of the used agonists (ACh, CCh, Ebd) in defined concentration (0.003 to 300 µM). All recordings were performed at room temperature (20±2°C).

The patch clamp technique in voltage clamping mode was used to carry out the measurements. The on cell patch clamp configuration (Hamill et al., 1981) is achieved by tightly sealing a low resistance glass pipette of about 5 to 20 MΩ to the cell surface by slight suction. By this procedure a "gigaseal" in the order of 10^9 Ω is formed allowing the separation of background noise and channel currents. To improve the signal to noise ratio furthermore the patches were constantly hyperpolarized to -200 mV, so that the potential across the membrane patch should be about -250 mV respectively.

4.2.2. Low noise modifications for high-resolution records

The resolution of detectable single channel events is limited by noise. The changes to the setup are guided by optimizations that were first proposed by Parzefall et al. in 1998. Till now the best instrument for low noise recordings available on the market is the Axopatch 200B amplifier (former Axon Instruments, now Molecular Devices, Inc., Sunnyvale, CA, USA) with cooled input field-effect transistor and capacitive feedback input. Since the customary very long silver wire, connecting the pipette to the input resistor acts as a very effective antenna for electromagnetic fields and the polycarbonate material of the enclosed pipette holder generates unacceptable dielectric losses, a Teflon holder as described previously (Parzefall et al., 1998) was used. The custom-built holder is largely contained in the metal housing of the headstage and makes it possible to shorten the silver wire to ≈ 3 cm length. The latter was directly soldered onto

the input resistor. To fix the pipettes on the headstage an improved 3-point holder was used (Hallermann et al., 2005). The pipette length was ≈ 12mm and was filled with extracellular solution at the very tip for less than 1 mm. Special care had to be taken to not cause any extra noise-increasing fluid films on the inside of the pipette. The inverted microscope was optimized with a grounded table and objective. Additionally a Petri dish with hydrophobic glass inlay was used, where the cover slip of 20 mm diameter perfectly fitted. To ensure a very low immersion depth of about 300 μm, the extracellular solution level in the recording chamber was optimized by adding only 80μl extracellular solution after the transfer of the wet cover slip from the culture dishes.

Borosilicate glass pipettes produce substantial noise because of salt solutions creeping up the inner and outer wall of the pipette. The better alternative is using quartz glass tubes to pull pipettes. Quartz glass has a hydrophobic surface and does not support creeping of fluid films. Additionally quartz glass has superior electrical characteristics compared to borosilicate glass, thus reducing the input capacitance of the pipette and decreasing RC noise produced in combination with the input resistor. The negative aspect is the very high melting point of 1580°C, which cannot be reached by use of usual micropipette pullers with electric heating filament. The DMZ Quartz puller (Zeitz Instruments, Martinsried, Germany) is operated by an oxy-hydrogen burner, which makes it possible to produce thick walled quartz glass pipettes with short tapper (Dudel et al., 2000). Using tubes with 2 mm outside and 1 mm inside diameter generation of pipettes with resistances of about 20 MΩ is possible, reducing the membrane capacity of the patch.

4.3. Data acquisition and analysis

4.3.1. Acquisition and processing

The conventional Axopatch 200B Amplifier offers several filtered outputs with integrated 4 pole Bessel filtering from 1 to 100 kHz. On removal of the 4 pole internal 100 kHz filter the bandwidth of the amplifier is the limiting factor. By directly feeding in square root pulses of defined amplitude and frequency, the bandwidth of the amplifier could be determined to 130kHz at -3dB cutoff. The data stream was converted using either a micro1401 A-D device (Cambridge Electronic Design Limited, Cambridge, England) at 400kHz sampling rate or a power1401 at 1MHz sampling rate, respectively. The data was stored directly on a regular personal computer running Windows XP professional (Microsoft Corporation, Redmond, WA, USA), using CED's *Signal3* Software.

For further analysis, using the "DC analysis programs" Software package from David Colquhoun's lab at University College of London (available from www.ucl.ac.uk/pharmacology/dc.html, further denoted as "DC-Progs"), the data had to be exported as 16bit integer formatted data. The recordings were analyzed as described earlier by Hatton et al. (2003) and Colquhoun et al. (2003).

Using *filtsamp* (DC-Progs) the 16 bit integer data was transformed into continuous sample (*consam*) file format. Likewise *filtsamp* is a utility to omit points and/or filter a *consam* record with a digital Gaussian filter. In the case of data that was acquired at 1 MHz sampling rate, only every third point was used, resulting in an effective sampling rate of 333 kHz for the following filtering and idealization process. Since the internal bandwidth of the Axopatch 200B was tested to 130 kHz (-3dB) we used, according to the equation below, a digital Gaussian filter of 30832.2 Hz (-3dB) to get a final filter cutoff frequency (f_c) of 30 kHz at -3 dB attenuation of the maximum amplitude.

$$\frac{1}{f_c^2} = \frac{1}{f_1^2} + \frac{1}{f_2^2}$$

With a final filter cut-off frequency f_c of 30 kHz (-3 dB) the typical filter rise time T_r is 11.07 µs:

$$T_r = \frac{0{,}3321}{f_c}$$

4.3.2. Idealization by time course fitting

For reliable detection of events a signal to noise ratio (s.n.r.) of at least 10 is necessary. With the optimized low-noise setup used here the mean r.m.s. (root mean square) noise of our recordings was 0.85±0.013 pA and the mean amplitude is 11.37±0.42 pA, resulting in a mean s.n.r of 13.38 . For idealization of recordings the program SCAN (DC-Progs) was used (Colquhoun & Sigworth, 1995).

In SCAN the data trace is scrolled across the screen until an event is detected by a threshold-crossing method. The threshold was set to 5µs to ensure that no event of 6µs and longer was missed. After the detection of an event the trace on the screen expands and SCAN makes initial guesses for all positions of transitions and amplitudes (Figure 7). Transition times and amplitudes for events longer than 2 T_r, are fitted simultaneously by an implemented least squares fitting routine. Shut times shorter than 2 rise times have their amplitudes fixed to zero. Openings of less than 2 T_r duration can be detected reliably down to 6µs, as their amplitude is fixed to be the same as that of the closest open event that is longer than 3 rise times. The fitted curve is presented to the operator for acceptance, rejection or modification. Once accepted by the operator, the time point of transition and the respective amplitude are stored as idealized dataset. The advantage of this method is that the resolution of measurements can be somewhat greater than can be obtained by using a threshold-crossing method. As there will be ambiguous events in the recordings the method forces the operator from time to time to make subjective decisions about the most likely interpretation of the data. In this point it is crucial that the operator is aware of what the program is doing. In recordings with reasonable good s.n.r. these events are sufficiently rare and misinterpretation of artifacts, e.g. like the spikes

produced by reset of the capacitive feedback element, can be avoided by this method. The produced idealized record has the form of an event list, which contains the duration of each event in the record and the corresponding single channel current amplitude.
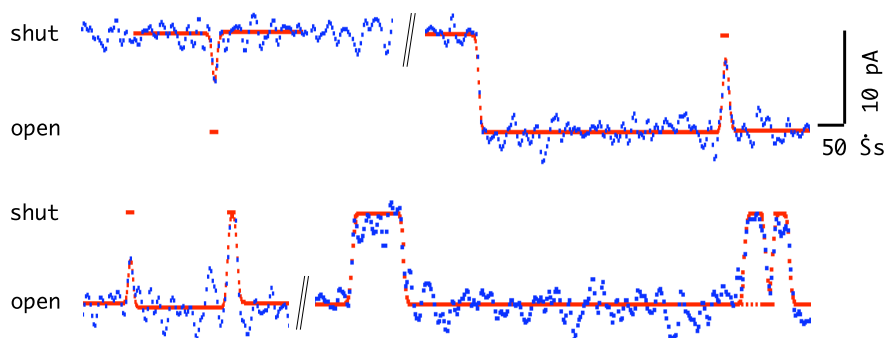
Figure 7: Idealization method using the program SCAN. The data trace at a sampling rate of 333kHz is shown in blue and the least squares fit performed by the program is shown in red. Noise at 30kHz filter cut-off was 1.0 pA at maximum, allowing the detection of very short events down to 6 μs. Top row, left: short openings down to 6 μs can be reliably detected. For events shorter than 2 t_{rise} the amplitude is constrained to the next neighboring event, which is longer than 3 t_{rise}. The constrained is marked by the short dash right over the fitted event. Right: Transition from shut to open (467μs) followed by a short shutting of 10 μs. Bottom row: long opening with intermittent shuttings of different length. The first two shuttings are shorter, the following ones longer than 2 t_{rise}. The sequence, beginning with the open state is: open, 6 μs, 185 μs, 19 μs, open, 97 μs, 642 μs, 41 μs, 13 μs, 32 μs, open.

4.3.3. Stability plots

The idealized records were analyzed using the EKDIST (DC-Progs) utility. Before doing any histograms the operator has to decide, which resolution has to be imposed on open times and shut times, ensuring that all events of at least this length have been detected in idealization, and which amplitude difference is reliable to be distinguished. Since all recordings have been made in the on cell patch clamp configuration, all measurements have been made at equilibrium conditions, which means that the average behavior of the channel in the records should not be changing over time. After imposing a resolution of 6 μs to open and shut times the idealized records were checked for stability of the fitted amplitudes and open probability.
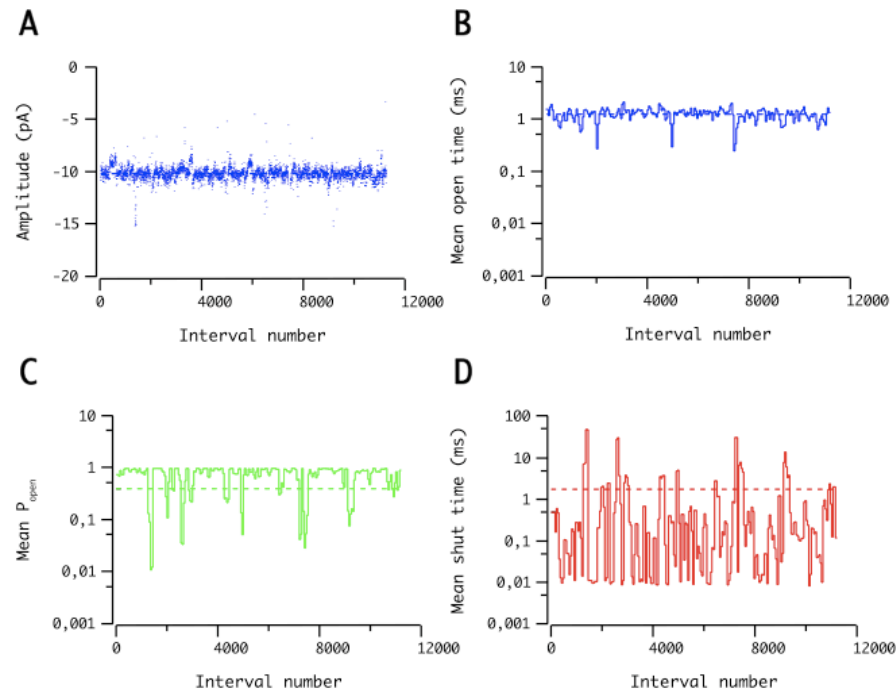
Figure 8: Examples for different stability plots. (A) amplitude stability as plot of open event amplitudes longer than 2 t_{rise} . No decrease in amplitude could be detected. (B) to (D): stability plots using a sliding window, averaging 50 events and shifting 25 events in each step. The dashed line illustrates the overall mean for the respective method (B) mean open time (C): mean open probability (P_{open}) (D) mean shut time. The high variability resembles the broad range of shut times occurring during the recording.

From amplitude stability plots the constancy of the current amplitudes throughout the recording was evaluated (see Figure 8 for example plots). The stability of mean amplitude was tested with plots of sliding averages of 50 successive openings and a step width of 25 openings. In the next step the stability of mean open times, shut times and the stability of the open probability were inspected using the same sliding window method. In the case of any observed instability the whole recording was refused to ensure that only faultless records were used for analysis.

4.3.4. Open period, shut time and burst time distributions

Plot of dwell time distributions:

Open time, shut time and burst length distributions were calculated with EKDIST for further analysis. All dwell time histograms are shown at logarithmic scale with logarithmic binning for the abscissa and root scale for the ordinate as

proposed by (Sigworth & Sine 1987) and (McManus et al. 1987). Thus, the number of exponential components, which can be fitted to the histogram, can easily be seen as local maximums (e.g. see Figure 9). Probability density functions can directly be fitted to the distributions in EKDIST to determine the main components.

To justify the number of components fitted to open time distributions the logarithmic likelihood ratio (LLR) of fits using n and n-1 components was calculated. The probability of erroneously accepting n components, although n-1 components were correct is smaller than 1 % if the LLR exceeds the value of 4.6 (Rao, 1973; Horn, 1987). Because the likelihood in our case is calculated as though dwell times were independent, the approach used to fit exponentials is only an approximation to true 'maximum likelihood'. Since dwell times are actually dependent on neighboring events it might have an effect on the LLR distribution, thus questioning the trustworthiness of this test. For the estimation of initial parameters for the fitting process of mechanisms the consequence is negligible.

Open time distributions:

In case of open time distributions, there are in principle two differing possibilities of displaying opening events: As "open time distribution", at which the transitions from one level to a higher level and back are considered as individual openings, just like the record was idealized. An alternative way is to plot "open period distributions". In this case all dwell times between two full closings are considered as one fused opening regardless of amplitude. The danger of the first method is that baseline fluctuations of sufficient amplitude would be interpreted as determinable openings. Consistent with our findings from observation of amplitude histograms, nAChRs open to one conductance level only, we therefore preferred the open period distribution.
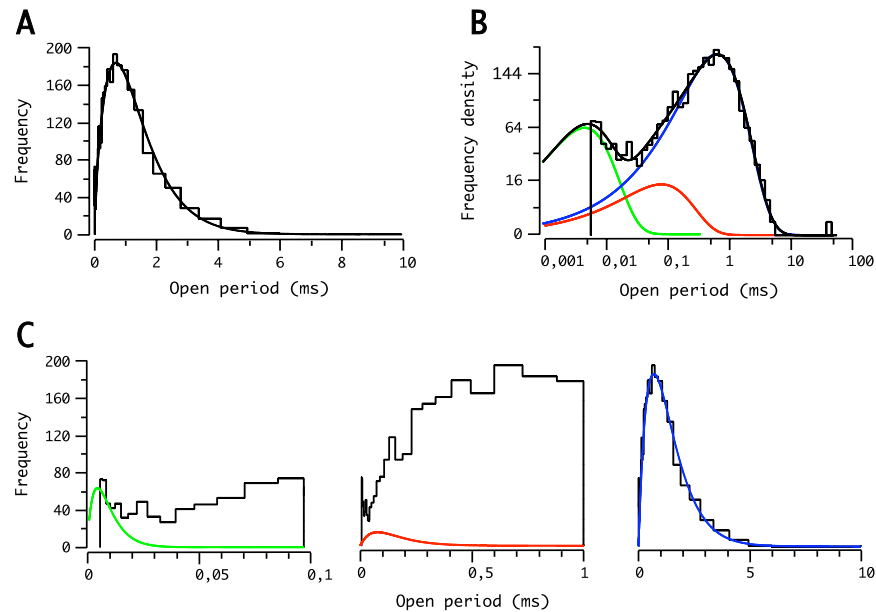
Figure 9: Optimized display of dwell time distributions. Example plots for event distributions and fitted probability density functions (pdfs) using arithmetic or logarithmic/root scaled axes are shown. (A) open period distribution using standard arithmetic scaled display. Only the main component of approximately 1 ms is obvious. (B) logarithmic scaled abscissa and root scaled ordinate facilitate the identification of components in distributions. Event histogram and calculated pdf using the EKDIST least squares fitting routine are depicted in black. Green, red & blue lines: short intermediate and long components of the pdf. 2 main components (green & blue) become directly obvious, when observing the histogram, only a third intermediate component shown in red is hard to identify from the stepped polygon. (C) separate arithmetic display of the three components at higher resolution. Colors of the components equal to (B).

Shut time distributions:

Shut time distributions were plotted to allow visual inspection of gap durations. All distributions have been fitted using pdfs with 5 components. Only in some cases of low agonist concentration a sixth component was necessary to comply with the broader dispersion of values due to the longer shut times in the record.

Burst time distributions:

Openings occur in bursts (successive openings with short intermittent closings), separated by long silent periods (Colquhoun, Sakmann 1985), rather than at random (exponentially distributed). In common a burst of openings can be defined empirically as any series of openings divided by shuttings that are all shorter than a defined duration (t_{crit}). In terms of mechanisms one would like to

have a more precise definition for bursts. Once a critical shut time is defined, a gap within a burst can be defined as a sojourn in a particular short-lived state (or set of states). Gaps between bursts, exceeding t_{crit} are then similarly defined as sojourns in a different long–lived state or set of states, that can't be distinguished. In this way it depends on an interpretation of the observations made from open and shut time distributions and structural knowledge that is consolidated when a putative mechanism is constructed. Conversely, the distribution allows inferences about mechanism from the observations that can be made. Since the choice of mechanism and the choice of a critical shut time for creation of a burst length distribution interfere with each other - theory connected with observation. Because of that it is not to be automatically and empirically applied to a set of data regardless of the following interpretation. The exact choice of t_{crit} for definition of bursts and interpretation in terms of mechanism will be given in the results part.

4.3.5. Statistical analysis

While plotting the determinants for fitted pdfs against the used agonist concentrations it became obvious that most parameters do not obey simple linear concentration relationships, but change in a logarithmic concentration dependent manner. To test for the according model that describes the observed data in the most convenient way, we performed regression analysis using a simple linear function (1) and a semi-logarithmic function (2).

$$y = y_{intercept} + slope * x \qquad (1)$$

$$y = y_{intercept} + slope * \log(x) \qquad (2)$$

The fitted functions of the two types were compared by standard statistical methods for significantly better fitting results of the semi-log function. If this was not the case the simpler linear function was used to describe the observed dependencies. The slope of both function types is of the μM^{-1}–type, independent

of whether component length, component areas or other parameters were plotted versus concentration. When the function type was determined, subsequent tests for significant concentration dependent changes versus the steady zero-slope model of the same function were performed. The according level of significance will be given in the results part as probability (P) of erroneously accepting a concentration dependent (non-zero) slope, even though concentration independency would have been correct. To test whether parameter groups e.g. of different agonists show diversity analysis of variance (ANOVA) or students t-tests, if there were only two groups to compare, were performed.

The number of records carried out for each concentration differs between agonists and concentrations and the exact number will be given in the results part when needed. A complete overview of records used for histograms and obtained parameter values will be summarized in tabular form in the appendix of this publication. Most parameters in the text will be given in the form mean±s.e.m. (standard error of the mean) unless otherwise stated and will be found in the tabular overview in the appendix as well.

5. Results

5.1. General features of agonist induced single channel currents

All measurements show a remarkable low noise level of less than 1.27 pA r.m.s. at 30 kHz filter cut-off frequency (-3 dB). The overall mean r.m.s. noise level is 0.850±0.013 pA. The mean amplitudes for all acetylcholine (ACh), Carbamoylcholine (CCh) and Epibatidine (Ebd) channel openings are 11.44±0.419 pA, 10.95±0.375 pA and 12.02±0.333 pA (mean±s.e.m.) respectively. No significant correlation of amplitude to ligand concentration can be observed.
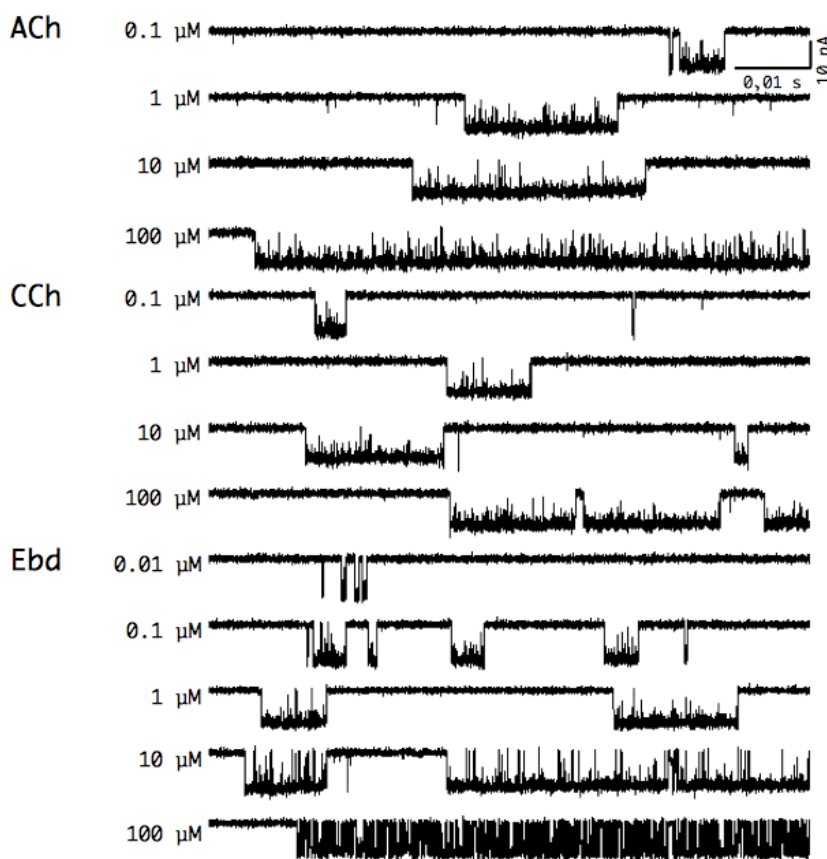
Figure 10: Elementary currents of the nAChR elicited using different agonists and concentrations. Independent of the nature of the agonists single activations, consistent of many short openings and intermittent short channel closures, become more prominent, whereas long shut periods become less eminent. In case of

Epibatidine (Ebd) it is obvious, that at least at 100 μM a heavy blocking of the channel takes place, with intermediate non-conducting events comprised in activation periods.

A coarse examination of the recorded single channel currents as depicted in Figure 10 reveals a substantial blocking effect tacking place in high concentrations of Epibatidine. The blocking seems to introduce a great number of short additional gaps in periods of activation in the 100 μM trace. The same phenomenon can sparsely be observed in the 10 μM measurement as well. Regarding the high concentration records for acetylcholine (ACh) and carbamoylcholine (CCh) no blocking effect could be observed for high agonist concentrations, even though a slight amplitude reduction for 2 of the 100 μM ACh records is found. In records of 300 μM ACh the conduction is not influenced. Special care will be taken in analysis of records produced with high concentrations of Ebd or ACh to prevent the conclusion of false kinetic channel characteristics.

5.2. Open time distribution and dependences

Starting to investigate the kinetic properties of ligand-gated ion channels, the most intriguing observation is the channel opening in fast succession with short gaps, barely resolvable even with the high-resolution setup used here. I will start with the investigation of open period distributions, produced by plotting the number of events of defined duration ranges using a logarithmic binning method (Figure 11). It is well known that the conclusions that can be drawn from the inspection of apparent open period distributions are ambiguous if not all of the gaps in the record can be resolved properly (Colquhoun & Sakmann, 1985). This will be the case and that is why the term "apparent" is used in the context of observed openings. Nonetheless detailed exploration can give a coarse overview of the activation characteristics and clues for further investigation. The issue of unresolved gaps should be kept in mind in the further course.

For analysis using the program EKDIST (DC-programs) the smallest resolvable open and shut time duration was set to be 6 μs. Exceptions were made for 2 of the records using 100 μM ACh as agonist. Due to amplitude reduction values of 8 and 10 μs were considered to be save for these records, so that no events were missed at the imposed resolution. The open period histograms for all agonists show similar distribution characteristics, as a minimum of 2 components is always obvious to visual inspection.

Former electrophysiological investigations of nAChRs proposed a minimum of 2 or 3 open period components (Colquhoun D. and Sakmann B., 1985; Parzefall et al., 1998; Hallermann et al., 2005) to describe the distributions, see also Models 1 and 2 correspondingly. To test if fitting a mixture of 3 exponential probability density functions (pdfs) gives significantly better results compared to a mixture of 2 exponential pdfs, least squares fits for both constellations were performed and the logarithmic likelihood ratio (LLR) was calculated. With a LLR value exceeding 4.6 the probability of accepting 3 components by mistake although 2 components are sufficient is smaller than 1 % and can be considered to be save (Rao, 1973; Horn 1987). LLR values for experiments of the same concentration and agonist diverge highly in some cases (see supplementary table 1). The mean LLRs for the used ACh concentrations are heterogeneous and show no concentration dependent tendency. Less than half of the values exceed a LLR of 4.6, but the total mean for ACh is 5.00±1.55 . For CCh and Ebd more than half of the mean LLR values for the used concentrations surpass the critical value with total means of 10.69±3.71 and 13.26±4.20, correspondingly. For CCH and Ebd the LLRs show a roughly indirect logarithmic concentration dependency that may resemble the intermediate open time component frequency decrease, observable in 3-component probability density function fitting. Global application of the 3-component approach seems to be appropriate for the generation of acurately fitted distributions.
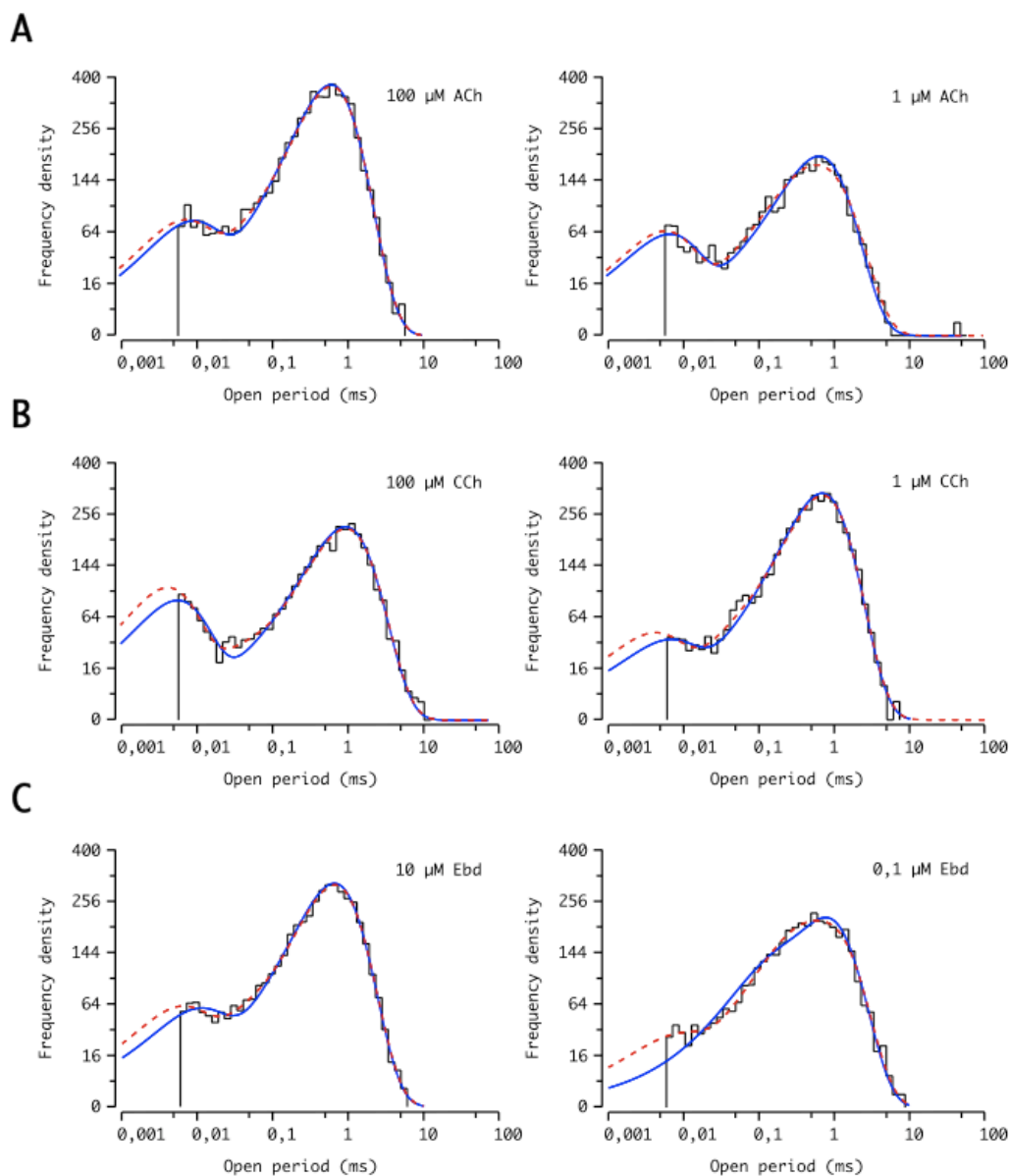
Figure 11: Open period histograms for distinct agonists. Each histogram shows 3-component (dashed red line) versus 2-component (continuous blue line) least square fits of probability density functions for openings. 3 component fits generate significantly better results than 2 components trials (see Table 1: LLR analysis) in most, but not all of the records.

Using 3 components, the comparison of lengths (Figure 12 A) does not reveal any significant concentration dependences for ACh and CCh. For Ebd the obvious decrease of the longest component duration for concentrations $\geq$ 30 µM can be attributed to an effective channel block. τ_3 for Ebd decreases from a total mean of 0.83±0.035 ms for concentrations < 30 µM to values of 0.33±0.007 ms in 30 µM

records. In the record, where 100 µM Ebd has been used, the component length of 0.13 ms is not anymore significantly different from the intermediate component τ_2 of 0.11 ms (see supplementary Table 2). In accordance with the findings derived from analysis of apparent shut time distributions the heavy blocking effect can be assumed to start at concentrations of 10 µM. Due to this finding epibatidine records ≥ 10 µM will be excluded from further analysis.

Since none of the lengths is significantly concentration dependent we compared total means for each agonist (Table 1, for detailed information supplementary table 2). A clear tendency between the agonists becomes visible, as the smallest values are always from Ebd, the intermediate ones from ACh and the largest values are always found for CCh. The longest component τ_3 of CCh and Ebd differs significantly at a P-level of < 0.001.

	ACh	CCh	Ebd
τ_1	6.19±0.711 µs	7.43±2.337 µs	5.35±0.759 µs
τ_2	0.177±0.0423 ms	0.279±0.0704 ms	0.129±0.0226 ms
τ_3	0.968±0.113 ms	1.186±0.077 ms	0.805±0.040 ms

Table 1: Mean open period component lengths for agonists. The mean component lengths ± s.e.m. are shown. A clear tendency for component length is apparent in the form that the smallest value is always from Ebd the intermediate from ACh and the longest value from CCh. The means differ significantly for τ_3 values of CCH and Ebd (P<0.001) only.
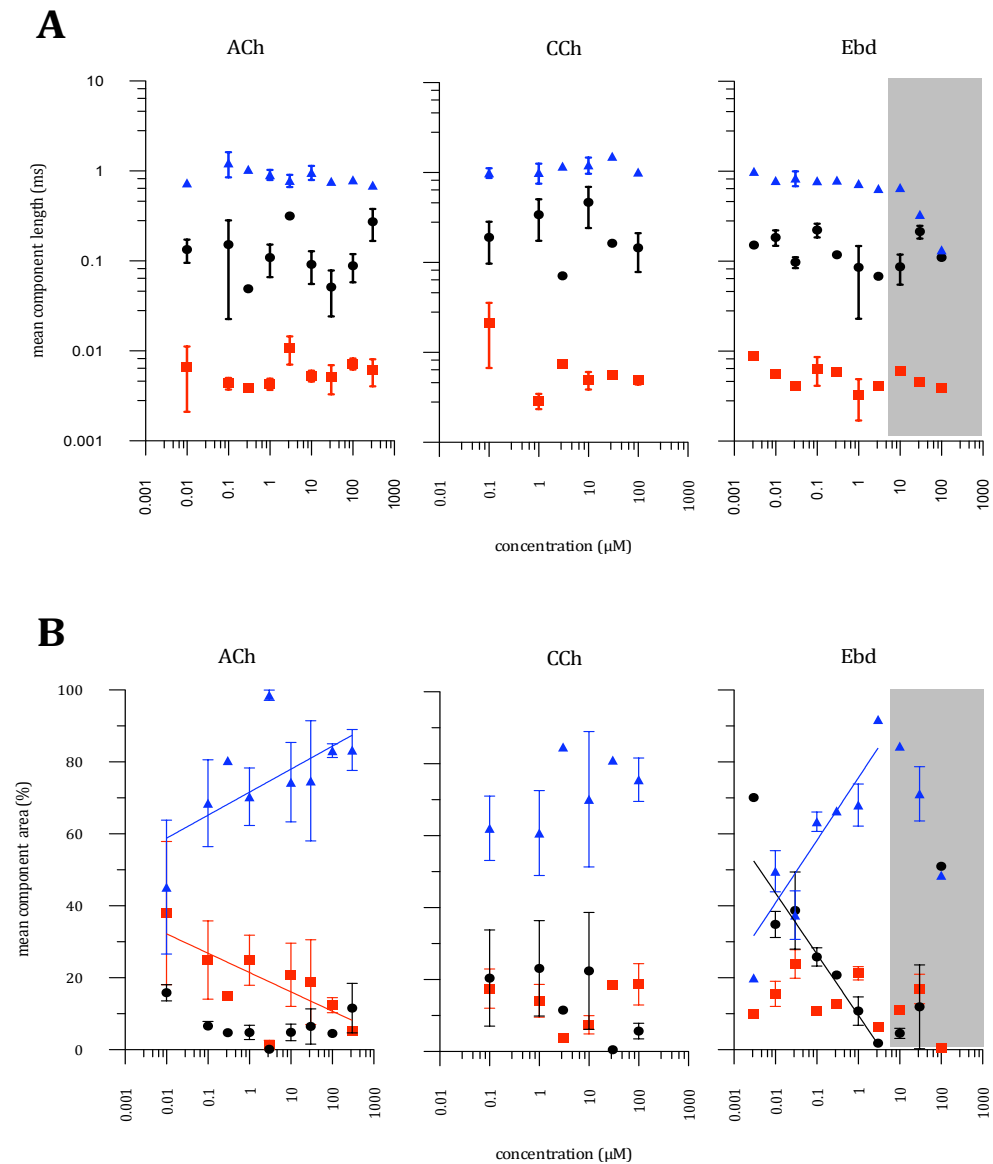
Figure 12: Open time component distributions: Histograms of open period distributions were fitted with a mixture of 3 component probability density functions. The obtained values are plotted as mean values with error bars (s.e.m.). Red rectangles: shortest component (τ_1), black dots: intermediate component (τ_2), blue triangles: longest component (τ_3). The grey area marks agonist concentrations where channel block is observed. (A) Comparison of time constants. No significant trends can be observed except for Ebd with τ_3 decreasing at concentrations higher than 10 µM caused by blocking (compare to shut time distributions in Figure 13). (B) Dependences of component areas. Trend lines are plotted for components that show a significant non-zero slope. Red rectangles: a significant concentration dependent decrease in shortest component areas (τ_1) for Ach appears but is not conserved for CCh and Ebd. Black dots: for CCh and especially striking in case of Ebd the intermediate component (τ_2) diminishes with increasing concentration, but can only be shown to have a significant slope for Ebd. The frequency of the longest component τ_3 (blue triangles) increases with concentration for all agonists (compare to supplementary table 2) and is significantly non-zero for ACh and Ebd.

The blocking effect for Ebd is comparably evident in the frequency of open period components as described by the fraction of total area (Figure 11B) covered by the probability density functions that were fitted. Beginning from 10 μM the area covered by the longest component τ_3 of Ebd continuously drops off from 84.4±0.86 % down to 71.2±7.5 % (30 μM) finally resulting in an area of 48.5 % for the 100 μM record. Accordingly the intermediate component area increases from 4.56±1.40 % to 51 % from 10 to 100 μM. Considering that the component lengths of τ_2 and τ_3 for 100 μM are not longer conspicuously distinguishable, the distribution would better be fitted by 2 components. In this case the longest component would have vanished and the intermediate component would describe 99.5 % of the opening events instead.

Disregarding concentrations where block is observed for Ebd, the area of the longest component (τ_3) shows a clear concentration dependent increase for all agonists. By fitting simple semilog-line functions to the data (see methods), a logarithmic concentration dependent slope is revealed to be weakest for CCh, slightly stronger for ACh and strongest for Ebd with mean slope values of 5.40±4.62 ms/μM, 6.39±2.78 ms/μM, 17.40±3.42 ms/μM, respectively. The frequency increase of τ_3-openings is consistent for all agonists, even though the slope of the fitted functions turns out to be significantly non-zero for ACH (P<0.05) and Ebd (P<0.001), but not for CCH. Since most of the open time is constituted by events of the longest component type (τ_3) these observations reflect the findings that CCh is known to be the least effective activator and Ebd the most effective one (Zhang et al., 1995; Prince & Sine, 1998a, 1998b).

Short and intermediate components show a differential behaviour that depends on the nature of the agonist. The frequency of the shortest openings (τ_1) decreases concentration dependently for Ach and Ebd with corresponding slopes of -5.37±2.28 and -0.39±2.13 ms/μM, but is only significantly non-zero for ACh (P<0.05). For CCh the slope of the fastest component (τ_1) is very small 0.004±2.17 ms/μM. In contrast a striking concentration dependent decrease in frequency of openings can be observed for open periods of the τ_2-type for Ebd with a

significant slope of -17.00±2.93 ms/µM (P<0.001). For CCh the slope is found to be non significant with -5.20±4.70 ms/µM and appears to lack concentration dependency for ACh with a slope of -0.90±0.85 ms/µM.

Even though a small decrease in current amplitude was detected when ACh was used in concentrations of 100 µM, we did not find any other evidence for channel block at ACh concentrations of 100 or 300 µM.

5.3. Shut time distribution and dependences

Similar to open period distributions, example graphs of the frequency density of shut times show the main features of gaps in Figure 13. The most eye-catching observation is the high abundance of very short gaps at the resolution-limit of 6 µs that is consistently present in all distributions. Even though the high-resolution recording setup has been used gaps of this group can not be completely resolved. Fitting a mixture of pdfs predicts a high proportion of gaps beyond the resolution limit of 6 µs. These unresolved shut periods would prune the apparent open periods described above to shorter conducting dwells if resolved. The predicted number of gaps assumes that about 81% (total mean) of the gaps were constantly missed. For comparison, a portion of short openings is similarly missed, but the numbers are substantially lower. About 16% of openings were missed by the detection method.

One the most pressing questions in this context is, how dwell times that stem from one component in a dwell time distribution, i.e. where events have been missed, correlate to adjacent events of the opposed type. The knowledge of these correlations allows correct interpretation of distributions, as missed events can be taken into consideration. Furthermore the information of correlation of different types of events gives direct clues how several states of channel activity may be linked with each other in possible kinetic mechanisms. Dependency plots like shown in Figure 25 thus can suggest the kinetic relationships between

dwell time events (Magleby & Song, 1992). While going on in the analysis of the data the correlation issue will be reconsidered.
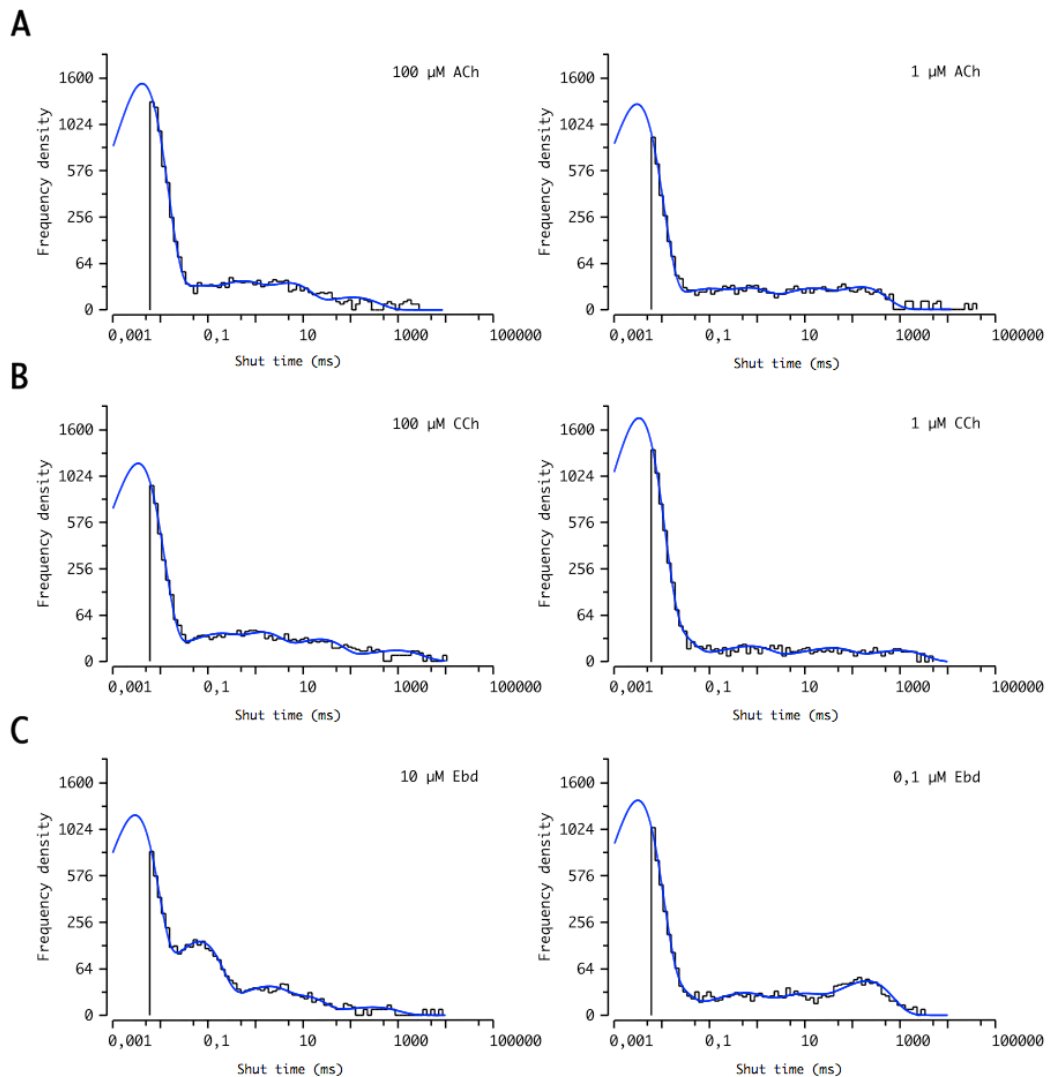
Figure 13: Shut time distributions and fitted pdfs for ACh CCh and Ebd. The same records as in Figure 10 were used. All distributions show a clear, very fast shut time component at the resolution limit and a mostly uniform distribution of higher shut time components, except for (C) in the case of 10μM Ebd, where a second component of about 0.1 ms clearly emerges. The rising component resembles the observed block in the elementary current traces of Figure 10, that was only shallow in the 10 μM trace but clearly visible in case of the 100 μM record.

An additional eye-catching attribute is the rise of a slightly longer shut time population in the example plot of 10 μM Ebd (Figure 13C). A population of short gaps of slightly less than 0.1 ms duration manifests clearly compared to gap distributions of other agonists, resembling the short gaps intervening long

periods of channel activation that have already been observed in the example trace of Figure 10 (see 10 and 100 µM traces of Ebd).

As for apparent open period distributions a mixture of probability density functions was fitted to the shut time distributions. For most records a mixture of 5 pdfs was sufficient, only 2 records needed to be fitted by a mixture of 6 pdfs to account for the broader distribution of shut times and ensure a stable fitting process.

Plotting the pdf component lengths and proportional areas clearly reveals details of the blocking effect. The second shortest component frequency (τ_2 in Figure 14B, top row) starts to rise drastically at a concentration of 10 µM Ebd. Changes affecting the shortest component τ_1 firstly become obvious at a concentration of 30 µM Ebd, when the relative area of τ_1 starts to drop off drastically (Figure 14B, top row). The decline of the area of τ_1 in the fitting process is mainly based on the growth of the second component and on the fact that the components overlap to a high degree. Regarding the component length we find a lengthening of all components at high Ebd concentrations. However the lengthening may be based on the enormous growth of the second component and its influence on the fitting process and therefore may be artificial. Additional experimental data is needed and additional analysis has to be performed to support a proper interpretation of the blocking effect observed here.

In accordance with the observations from open period distributions, data of Ebd concentrations of 10 µM and higher will be excluded from further analysis.

As one might expect for increasing agonist concentrations and the regularly resulting increase in overall channel activity, there should be obvious evidence for concentration dependently decreasing component characteristics. Indeed a decrease in lengths and areas for some of the components can be found for all agonists.

A

B
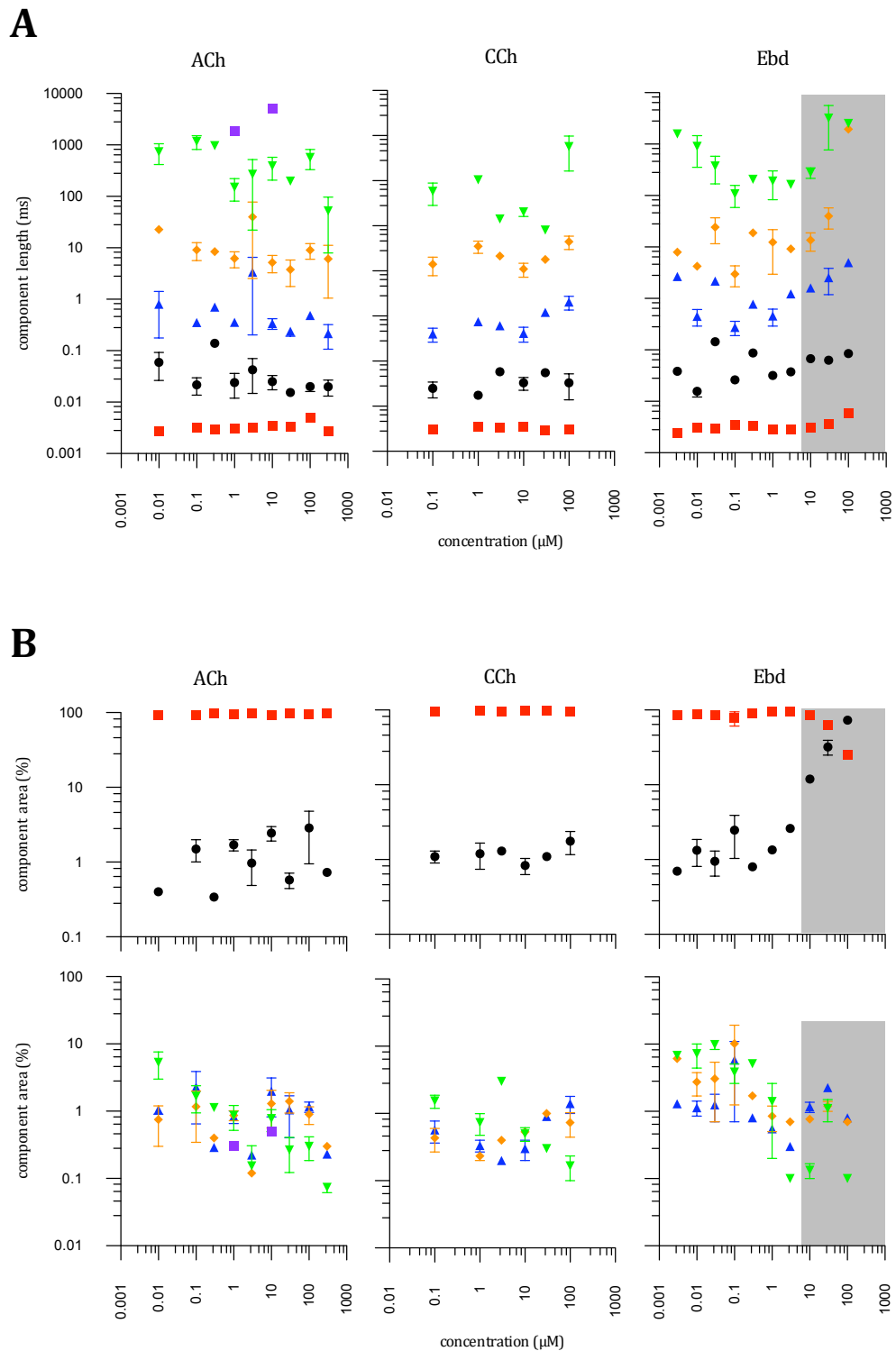
Figure 14: Distribution of shut time components: components derive from simultaneous fitting of 5 to 6 probability density functions to shut time distributions. Red rectangles (τ_1), black dots (τ_2), blue triangles (τ_3), orange rhombs (τ_4), green triangles (τ_5) and violet rectangles (τ_6). The grey area marks agonist concentrations where channel block is observed. (A) significant concentration dependency of the components can only be found for the longest shut time component τ_5, getting shorter with increased concentration (see supplementary table 3: shut time distributions). Grey bar: component lengths of Ebd progressively increase. The effect is induced by channel block. (B) top row: τ_1 and τ_2: the areas of

the two shortest components do not show concentration dependency. Grey bar: The changes at high concentrations of Ebd (> 3μM) originate from the blocking effect. Bottom row: τ_3, τ_4, τ_5 and τ_6: a consistent decrease of component areas while increasing agonist concentration can be observed for the τ_5-component for all agonists.

The shortest and second shortest gap components do not show concentration dependent changes, but remain stable in length and relative frequency for all records. The shortest gap component turns out to be the most stable one with total mean lengths of 3.3±0.23 μs, 3.2±0.11 μs and 3.0±0.14 μs and 95.7±0.8 %, 96.6±0.4 % and 88.42±2.53 % of the total area for Ach, CCh and Ebd respectively. Similar but with broader dispersion, the second fastest component τ_2 features component lengths of 40.8±13.1 μs, 36.9±6.7 μs, 54.4±17.2 μs and component areas of 1.3±0.30 %, 1.2±0.13 % and 1.5±0.30 % for Ach, CCh and Ebd correspondingly (for details see supplementary table 3).

Since a great number of detected gaps is of the shortest component and very similar length values of about 3 μs are found, the fitted pdfs can be deemed to give good estimates for the real component length and the predicted number of events. The predicted number is composed by the number of detected gaps plus the predicted number of gaps beyond the resolution limit in the fitting process of pdfs.

The lengths of τ_3-components do not change with increasing agonist concentration, just as the length of τ_4-components. The associated component areas for ACh and CCh do not change either but for Ebd both areas show a slight concentration dependent decrease.

The τ_5 component areas show significant non-zero slopes for Ach (P<0.0001), CCh and Ebd (P<0.05): -0.42±0.08 %/μM -0.19±0.10 %/μM and -0.20±0.10 %/μM. The fact, that it was necessary to fit 6 components to 2 of the distributions of ACh does not influence the significance of the data presented here. An analysis excluding these records did not alter the overall picture. The components length are found to decrease concentration dependently and significant for Ach (P<0.05) and Ebd (P<0.01) with slopes of -0.14±0.06 %/μM and -0.57±0.21 %/μM.

For CCh the 100µM records show consistently elevated τ_5 component lengths that may be based on desensitization of the channel. The lower concentrations show decreasing length values with a slope of -0.15±0.14 %/µM.

5.4. Burst analysis

Bursts are defined as periods of single channel activation, consisting of openings intervened by gaps shorter than a defined critical shut time (t_{crit}). By using the on cell patch clamp technique it cannot be assured that, even though no overlapping openings have been observed, all openings originate from the same receptor molecule. For further analysis of agonist-induced channel gating it is crucial to determine a reasonable dead time to segment the record into periods of channel activation, that were elicited by the activity of one single receptor molecule. There exists a broad spectrum of methods to introduce t_{crit} , all relying on the features observed in shut time distributions, strictly speaking on the observation of significant characteristics.

5.4.1. Separation of bursts

Basically two outstanding findings were made by the investigation of shut time distributions that can be used for the definition of t_{crit}: The observation that gaps of the τ_1 type constitute the most stable parameter to be observed and account for at least 80 % of gaps detected in the record. The second observation is that the τ_5-component area reveals an indirect concentration dependent significant decrease for all agonists and therefore may reflect the expected concentration dependent increase in channel activation. Direct evidence for differences that are based on the existence of differing numbers of active channels in the recorded patch could not be found.

To test whether the variation of the critical shut time and its inherent influence on the distribution of burst lengths reveals any clues, e.g. about the number of

channels in the patch, an analysis of the dependency of burst time distribution on the choice of the critical shut time t_{crit} was performed. For better understanding an example overview of burst length distributions, generated by stepwise increase of the critical shut time, was created, beginning from the resolution limit of 6µs (Figure 15).
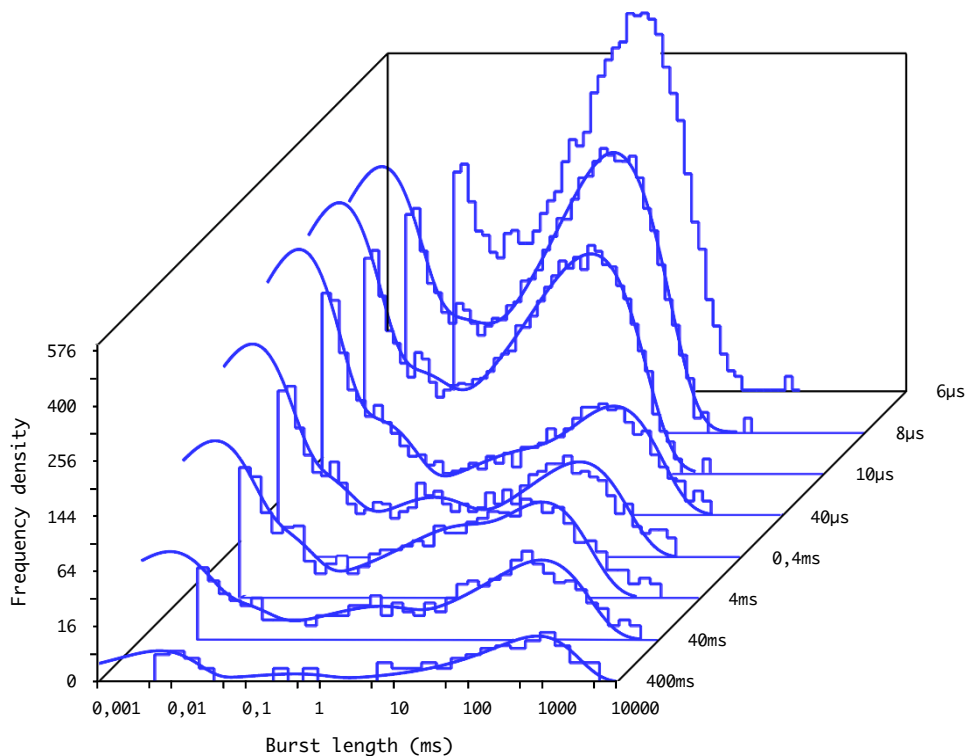
Figure 15: Development of the burst composition dependent on the choice of t_{crit}. The critical shut time was altered from resolution limit of 6µs, resembling the open time distribution for the dataset (back plane), to higher shut time values, which causes the bursts to fuse into longer stretches of the record. Note that burst components are very robust in moderate ranges of t_{crit} from about 40µs to 40ms. For details see supplementary Table 4 and Figure 18. The most dramatic changes take place between t_{crit} of 8 µs and 40µs. Note that it was never necessary to use more than 4 components to properly fit the burst distribution for any t_{crit}.

By increasing the critical shut time, starting from the resolution limit, more and more events fuse to prolonging stretches of alternating openings and gaps. At the resolution limit the distribution resembles the apparent open period distribution for the record. By sensitively increasing t_{crit} in a stepwise mode the way open period components fuse to bursts of differing lengths, including all gaps that are smaller than t_{crit}, can be traced. As t_{crit} is further enlarged more of the openings combine to bursts or fuse with already formed burst fragments to

proper burst events. Bursts melt with other bursts as well to form long stretches of channel activation, altogether reducing the overall number of events in the burst length distribution. In the example record shown in Figure 15 it is very obvious that increasing t_{crit} to 8, 10 and 40 µs mainly involves long openings in the fusion process, whereas short openings on the lower end of the distribution remain consistent with the distribution of apparent open periods as shown in the back plane. This observation is in accordance with the correlation of adjacent dwell times as shown in Figure 25, that is that long openings highly correlate with very short gaps.

The fusion of the longest openings to bursts, dramatically changes the distribution of bursts for burst lengths longer then 100 µs, while t_{crit} is increased from 6 to 40 µs. At 40 µs a mixture of 4 probability density functions is needed to properly fit the distribution of burst lengths. Increasing t_{crit} beyond 40 µs leads to progressive fusion of short openings into bursts, causing only moderate changes in burst lengths, but altogether broadening the distribution.

These findings can be further generalized by comparison of parameters, derived by fitting of the burst distributions while t_{crit} was increased. Figure 16 shows two example records from ACh. The method is found to give very similar results for all agonists and this in turn may be based on the very similar distribution of gaps in all the records.

The parameters derived from burst distributions upon prolongation of the critical shut time exhibits some unique features. The length of the longest burst distribution component τ_4 has a steep increase when t_{crit} is increased from resolution barrier to about 40 µs. A phase of moderate changes for t_{crit}-values of 40 µs to about 30 ms follows. Finally a period of steeper increase for values above 30 ms can be observed. The same observations can be made if other agonists and concentrations are investigated.

A comparable observation can be made from the development of areas for the shortest and longest burst components τ_1 and τ_4 over the change of t_{crit}: a period of high transformation in component area for low t_{crit} values is followed by a

relatively stable stage and is terminated by a interval of high change in component area.

The longest component accounts for the majority of the channel current, offering the physiological most meaningful fraction of channel activation and thereby determining the decay rate of synaptic currents (Wyllie et al., 1998; Hatton et al., 2003). If a direct comparison to the total numbers of events that are covered by the respective pdfs is drawn (compare Figure 15 and 16), it is revealed that the striking increase in relative component area of short bursts is caused by a heavy loss in burst numbers covered by the longest component pdf at low t_{crit} values. For high t_{crit} values the opposite effect takes place as the decrease in total numbers of the short burst component covered by the τ_1-pdf leads to a heavy non-proportional increase of τ_4 component area compared to the total numbers covered by this pdf.
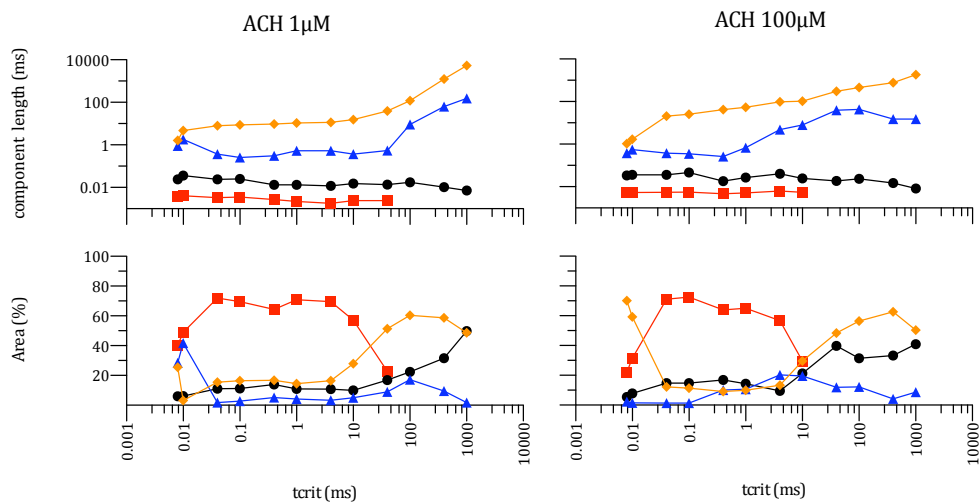
Figure 16: Change of burst components and associated areas on successive prolongation of t_{crit}. A mixture of 4 probability density functions (τ_1 to τ_4) was fitted to every burst distribution as t_{crit} was increased in a stepwise mode and the successive change of the pdfs component lengths and corresponding relative area were plotted. Red rectangles (τ_1), black dots (τ_2), blue triangles (τ_3), orange rhombs (τ_4). The steep change in component 4 (orange rhombs) at small t_{crit} from 6 to 40 µs in pdf component length and relative area resembles the fast fusion of open periods that are separated by very short gaps,. The plateau primarily prominent in component 4 depicts the robust phase of burst components, where only moderate changes in component length as well as component area take place in comparison to the drastic increase of t_{crit}. At high t_{crit} values single activation sequences melt to longer stretches ultimately fusing to a single series of open and shut times resembling the whole record.

Other than expected no direct clues for differing numbers of active channels could be determined. However, the exploration of burst time distributions in dependency of the critical shut time gives some interesting hints that help guiding further investigations. Between t_{crit} values of 6 to 40 µs gaps mainly fuse with events of the longest pdf component of open period distributions. When t_{crit} is further prolonged, the burst distribution is comparatively little affected until values of 30 ms are reached. Thus choosing a t_{crit} between about 40 µs and 30 ms would be uncritical, as the main results depend negligibly on the exact choice of the value. In other words the exact choice is not meaningful. Defining t_{crit} to about 40µs, when dense clustering of long openings and moderate change of distributions take turn, may deliver a more significant tool.

5.4.2. Burst time distributions

While doing single channel records and in the process of idealizing records I realized that channel openings seem to divide in two groups: Long periods of channel activation that are interrupted by very short gaps and short single openings outside of the long activation periods. The observations described above show that one of the unique features of shut time distributions for high-resolution recordings is the presence of an extraordinary significant group of gaps with a mean duration of about 3 µs. The investigation of burst time distributions dependent on the value of the critical shut time suggests that these very short gaps tend to fuse with the longest type of open periods to bursts of very high open probability. According to the significance of the choice of t_{crit} described above, the dead time for the burst definition will be constrained to include only the shortest gaps in bursts.

The critical shut time was defined by eye, since the standard methods using diverse misclassification criteria did not work for all of the records. The critical value was chosen to lie in the sharp bend of shut time distributions, right after the dropping phase of very short gaps. The resulting values of t_{crit} lie between 30 and 70 µs. The generated distributions of burst times have been fitted by a

mixture of 4 probability density functions, that will be further denoted as τ_1 to τ_4 according to their component length from shortest to longest (see Figure 17).
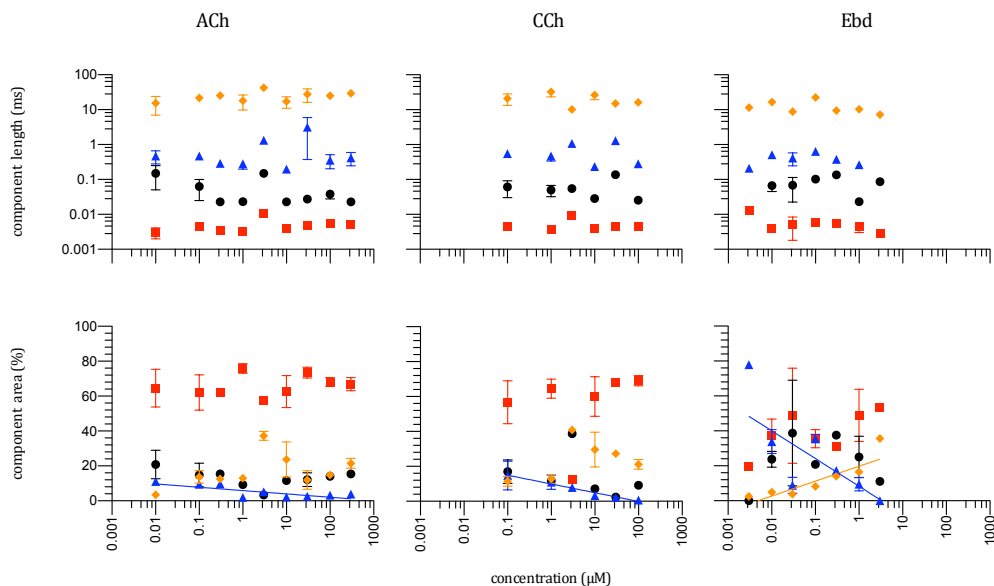
Figure 17: Analysis of burst time distributions. t_{crit} has been chosen by eye to lie in the sharp bend of shut time distribution, right after the dropping phase of shortest gaps. The distributions have been fitted by a mixture of 4 pdfs. Lengths and areas of the 4 pdfs are plotted as τ_1 to τ_4, according to the component length. Red rectangles (τ_1), black dots (τ_2), blue triangles (τ_3), orange rhombs (τ_4). Trend lines are plotted for components that show a significantly concentration dependent non-zero slope. The shortest component τ_1 (red squares) is the most frequent one and separates clearly for ACh and CCh but not for Ebd. The area of τ_3 decreases slightly in a log-concentration dependent manner for all agonists as depicted by the continuous blue lines. The longest burst time component τ_4 is the most important one in the physiological sense, since it accounts for the majority of total open time of the receptor. τ_4 does not show a clear concentration dependency for the component length, but its relative frequency increases slightly with increasing concentration and is only significant when epibatidine was used as agonist.

The component lengths do not bare concentration dependency for any of the agonists but the mean lengths are found to differ between the agonists (Table 2). The shortest (τ_1) and second shortest component length (τ_2) do not differ significantly between the agonists, with overall mean values of 5.3 ± 0.54 µs (τ_1) and 61.6 ± 9.78 µs (τ_2). On the other hand the second longest (τ_3) and longest component (τ_4) of the distributions differ significantly between Ebd and the other agonists (ACh and CCh). As shown in Table 2 the length difference is

about 2 fold between Ebd elicited τ_3 and τ_4 bursts and the ones found for ACh or CCh (see supplementary Table 4 for detailed information).

Agonist	mean τ_1 (µs) ± s.e.m.	mean τ_2 (µs) ± s.e.m.	mean τ_3 (µs) ± s.e.m.	mean τ_4 (ms) ± s.e.m.
Ach	4.9 ± 0.78	57.5 ± 17.8	773 ± 316.4	24.7 ± 2.75
CCh	5.1 ± 0.88	59.5 ± 16.6	653 ± 178.6	20.1 ± 3.29
Ebd	5.8 ± 1.23	68.7 ± 17.3	345 ± 79.3	12.3 ± 2.02

Table 2: Burst length distribution component lengths. A comparison of component lengths reveals a significant decrease in the longest (τ_4) and second longest (τ_3) component lengths for Ebd compared to ACh and CCh. The component length is reduced to about half of the duration for the same component type of ACH or CCh. For the 2 short components no length difference can be found between the agonists.

The mean relative area of the shortest component (τ_1) of Ebd 39.22±4.49 % is significantly lower than for the other agonists: ACH and CCh: 65.9±1.96 % and 55.2±8.75 %, respectively. Bursts of the second longest component type (τ_3) show a significant slight decrease in component area of -1.91±0.47 %/µM, -5.01±1.65 %/µM and -15.9±5.10 %/µM, for ACh, CCh and Ebd correspondingly. The relative frequency of the longest component shows a slight increase for all agonists and turns out to be strongest and significantly log-concentration dependent for Ebd (0.28±0.06 %/µM) only.

Thus burst length distributions for Ebd elicited channel currents reveal substantially differing kinetic characteristics that may derive from opposed site selectivity of Ebd for the receptor binding sites compared to ACh or CCh. Relationships concerning differences between agonists and the resulting differences in binding site affinity will be further interpreted in the discussion part.

While trying to calculate open probabilities describing the increase in channel activity, I realized that based on the method of on-cell patch clamping it is impossible to calculate a reliable value for the whole record, even though an overall very inconsistent concentration dependent increase in open probability for the records can be observed. In fact, in most investigations, open probability calculation is based on the fragmentation of records into bursts, as stretches with

openings that derive from one channel only. The burst definition used here is substantially different and open probabilities would intrinsically be independent of agonist concentrations.

However, when the relative frequencies are compared to the real frequencies of events in the record, an overall increase in burst events is obvious (compare to Figure 19 A). Even though the uncertain number of channels in the record biases the observed frequency of burst events, the frequency of all burst components can be deemed to increase, if only single channels would have been observed. This notion is supported by the relationship, that the records open probability increases with increasing concentration for all agonists and that accordingly the possible number of channels that might be present in a recorded membrane patch decreases inversely. In other words the observed frequency of events will be closer to true single channel event frequency in higher concentrations, but further away in lower concentrations. The increase in true single channel event frequency can therefore be assumed even steeper than the measurable increase in frequency, even though the total numbers might be lower.

5.5. Dissection into single openings and dense bursts

Breaking up the record into small stretches of activation with only the shortest gaps included leads to a distribution of bursts that I already considered to be made up of detached short openings and longer openings that are clustered in long bursts. To test this hypothesis I further analysed the distribution of bursts by differentiating between single openings and bursts consisting of 2 and more open periods intermitted by shortest gaps, therefore further referred to as dense bursts.
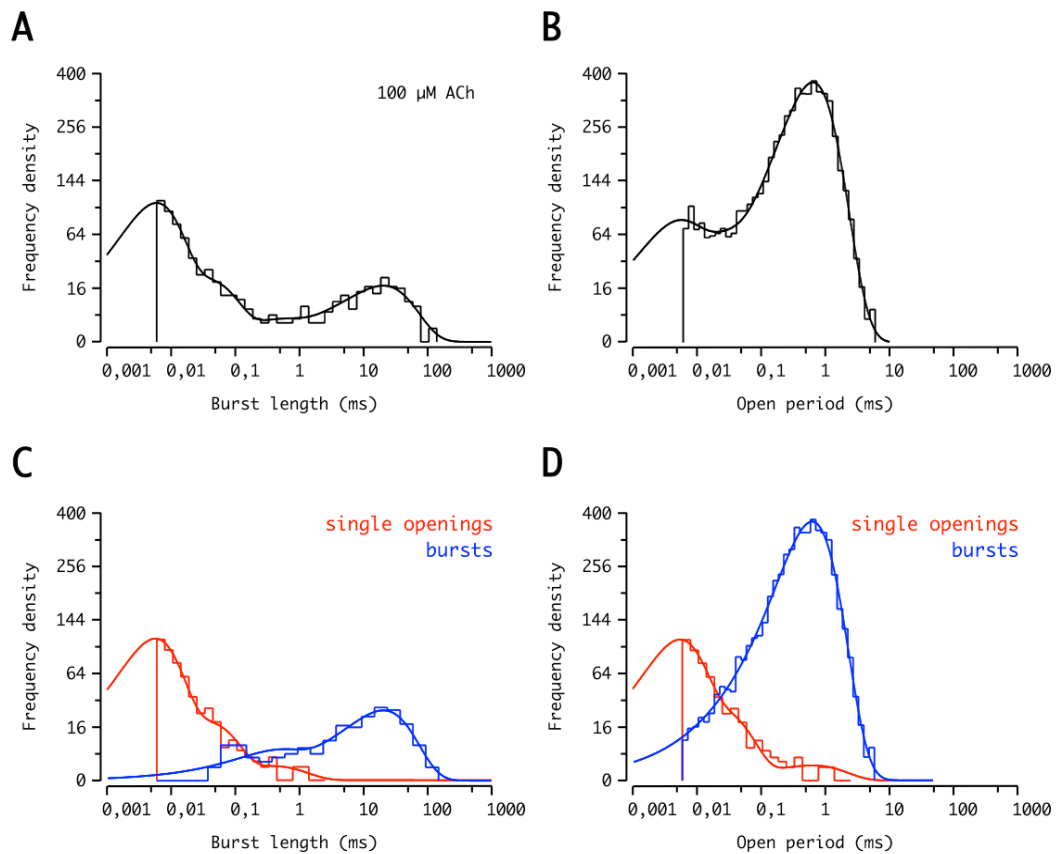
Figure 18: Single openings vs. clustered openings in dense bursts. The critical shut time was set to 40μs for this record (10μM ACh). (A) The burst time distribution was fitted by a mixture of 4 probability density functions. (C) By differentiating between single openings (red) and bursts of multiple openings (blue) it becomes quite obvious that shortest bursts are almost exclusively constituted by single openings, whereas bursts of the 2 longer burst component types τ_3 and τ_4 are mostly dependent on bursts of multiple openings. (B) The open period distribution of the record with fitted mixture of 3 pdfs. (D) 3 pdfs of the same component lengths were fitted to distributions of single openings and openings that constitute bursts of multiple openings. Choosing a t_{crit} this short leads to single openings that are mostly of the shortest and intermediate open period component types (compare to τ_1 and τ_2 of Figure 11). Contrarily, bursts with more than one opening, which are most of the bursts of the 2 longest burst time components (compare to C), are nearly unexceptionally composed of long openings of the τ_3-open period component type.

The classification of burst times (Figure 18 A) into single openings and dense bursts of multiple openings (Figure 18 C) shows a good separation of single openings mainly constituting the shortest and second shortest bursts on one hand and dense bursts that are mainly covered by the pdfs of the τ_3 and τ_4 type-pdfs on the other hand. In case of the example record shown in Figure 18 (10 μM ACh) a dissection of open period distribution in detached short openings and open periods grouped in dense bursts reveals that fitting of only one probability

density function is sufficient to cover the distribution of grouped openings. In comparison, single openings need to be fitted by a mixture of 2 to 3 probability density functions. Further details of the composition of bursts and single openings will be analysed in the following sections.
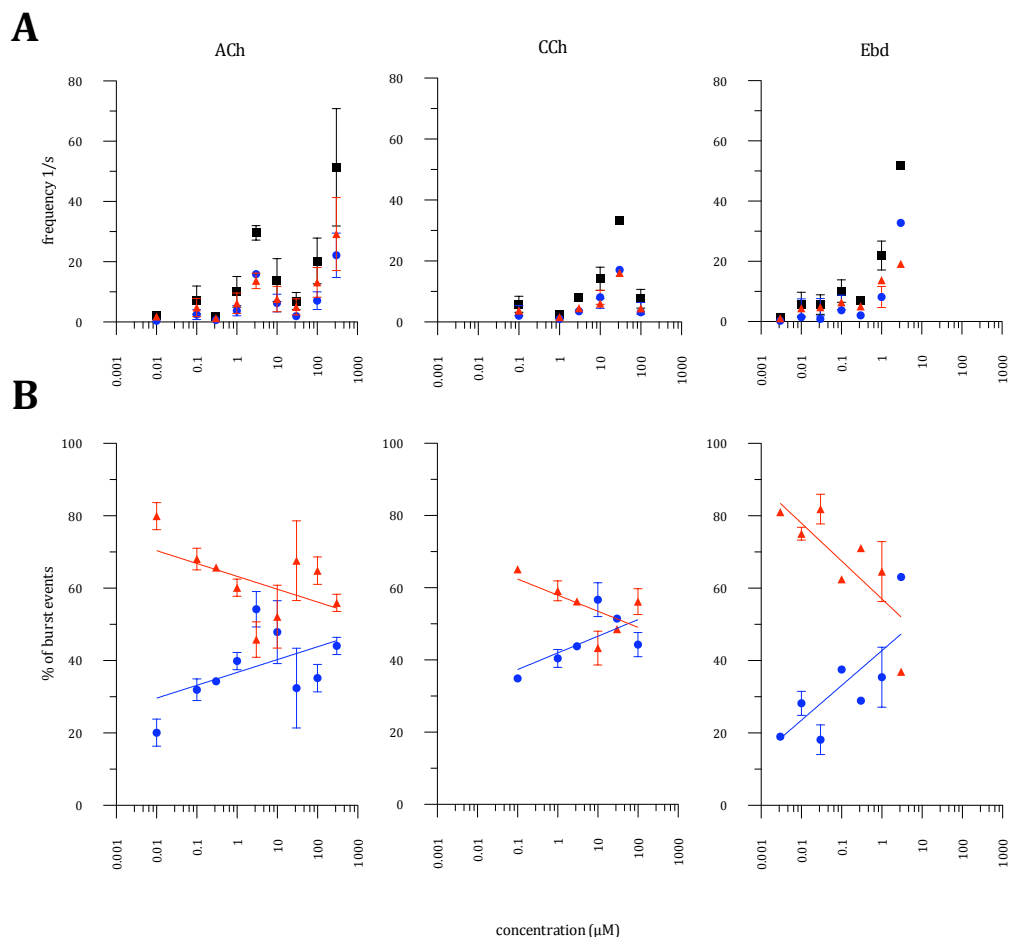
Figure 19: Frequencies of single openings and dense bursts. (A) The mean frequencies of burst events (black squares) are shown in comparison to mean frequencies of single openings (red triangles) and bursts of more than 1 opening (blue dots). An overall increase in frequency can be observed for all groups. As the potential number of channels in the recorded patch decreases with increasing open probability, the frequency of openings that originate from one channel only is expected to increase similarly. (B) By calculating the percentage of single openings and dense bursts the biasing problem of the number of channels in the patch can be disposed revealing the relative changes in the 2 groups of activation.

Imposing the findings of observed frequency increase to single openings and dense bursts, an increase in frequency of both types of activations that is biased by the uncertainty of channel number in the patch can be observed (Figure 18A). The frequency of burst events increases log-concentration dependent with a slope of 2.95±1.05 1/s*μM, 1.76±1.16 1/s*μM and 6.81±2.06 1/s*μM for ACh, CCh and Ebd, in that order. By normalizing the frequency of observed dense bursts and single openings to the frequency of all observed burst events, the biasing problem by unknown channel number can be disposed and the shift in channel activation for dense bursts versus single openings is revealed. The relative frequency of dense bursts increases in a log-concentration dependent way as the relative number of single events decreases accordingly for all three agonists: 3.55±1.89 %/μM, 4.62±1.93 %/μM and 9.62±3.00 %/μM, ACh, CCh and Ebd respectively.

5.5.1. Agonist dependency of single openings

With the goal to further characterize the properties of single openings in detail, distributions were fitted by a mixture of three probability density functions, like it was done for dwell time distributions for open periods of the whole record. Since open periods of intermediate length were barely dissolvable in normal open period distributions and the length constant of the according intermediate pdf may be poorly estimated two approaches to test this speculation have been used. Distributions of single openings were fitted with a mixture of pdfs that were not constrained and for comparison with pdfs where time constants were fixed to the values obtained before by fitting of normal apparent open period distributions.
Figure 20 shows an overview of results obtained by the two procedures. Concerning the length constants of the probability density functions no clear tendency of improvement in estimates is observable even though resulting component lengths always show slight variances. The length of the longest pdf component (τ_3) for Ebd is the only exception to show a clear difference, as the length is significantly reduced (paired t-test, P<0.01) from 0.77±0.02 ms to 0.34±0.02 ms in the free fitting approach. As most of the long openings are found to cluster in dense bursts, long single openings may resemble misclassified

events. Additionally the events of the longest open period component are found to highly correlate with shortest gaps, and as these are poorly resolved the length of long openings cannot be deemed reliable for interpretation.

Believing that the fitting process with unconstrained pdfs gives results that are more accurate for openings of the intermediate pdf component as obtained by fitting of whole record open period distributions, further interpretation will be restricted to the results of the "free fit" approach unless otherwise stated.

Observation of corresponding component areas reveals a diverse picture. The kinetics of short and intermediate single openings are very similar for ACh and CCh, but clearly differing from the picture that is drawn when Ebd is used for channel activation. The relative amount of shortest component type openings elicited by epibatidine is much smaller than for the native agonist or CCh and is particularly deviating at low agonist concentrations. Accordingly the areas for the intermediate and long component are elevated but differ to a considerable degree for the "fixed fit" and the "free fit" approaches used to characterize the distributions. The differences for τ_3 lead back to the discrepancy in fitted component lengths in the 'free fit' approach compared to the 'fixed fit' method. The reduced component length in the free fit approach leads to changed classification of events of intermediate length that are covered by the intermediate component, when using the 'fixed fit' method.

τ_1-component areas increase log-concentration dependently for all agonists with slopes of 4.75±1.51 %/μM, 8.23±2.70 %/μM and 11.69.0±4.74 %/μM for ACh, CCh and Ebd, respectively. Similarly the areas covered by the intermediate pdf component type exhibit a log-concentration dependent decrease for all agonists: -3.25±1.30 %/μM, -2.70±1.66 %/μM and -7.44.0±5.54 %/μM, in the same order as above (for details see supplementary Table 5).
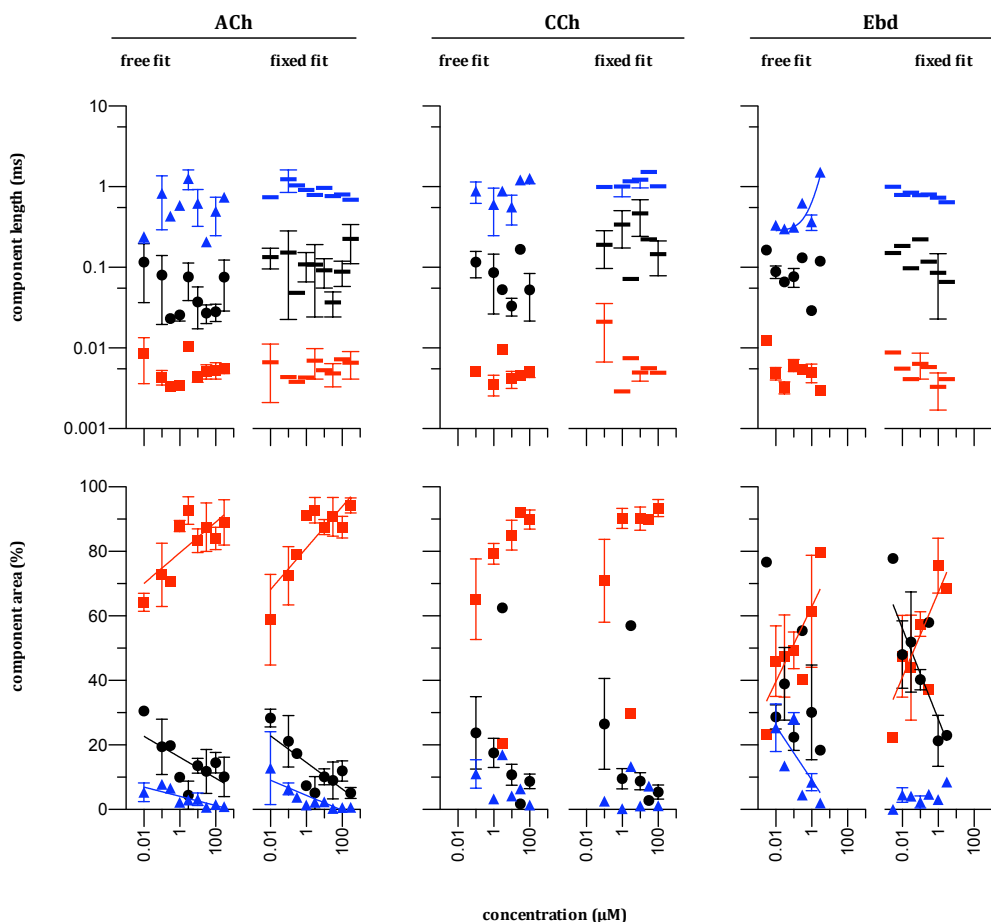
Figure 20: Analysis of bursts consisting of only one opening. Distributions of single openings were fitted with a mixture of 3 probability density functions. Two alternative approaches were tested: pdfs were directly fitted to the distributions without any constraints (free fit) and pdfs with constrained time constants, derived from the fitting of open period distributions (fixed fit), were fitted. The 2 different methods turn out to give very similar results. Trend lines are shown if concentration dependent, significant non-zero slopes are detected. The component lengths of the second and third components (black and blue) in the free fit approach are slightly shortened. The corresponding areas reveal a diverse picture: The frequency of very short single openings of the τ_1 type (red squares) increases in a concentration dependent way while intermediate single openings (black dots) become more rare. For ACh this observation exhibits significance in both fitting approaches (see trend lines). For CCh the overall picture is very similar to ACh even though the significance was lost. Using Ebd as an agonist activates the receptor in a more different way, as the shortest openings are much less frequent at low concentrations compared but show a much steeper increase with increasing concentration. Similarly the intermediate single openings are much more frequent in low concentrations of Ebd than for other agonists and drop off in a steep concentration dependent manner. The 2 fitting approaches reveal a severe difference in the fitting of longest openings for Ebd in determination of component length as well as frequency.

The similarity in the activation of single openings for the agonist acetylcholine and carbamoylcholine may reflect their ability of binding. As they are known to feature similar site selectivity, but differ to a certain level in the overall binding affinity, the preferential triggering of τ_1-openings for both agonists can be assumed to be elicited by the preferred binding site. The more infrequently observed intermediate openings can accordingly be allocated to the binding of agonist molecules to the secondary binding site. The overall reduced binding affinity for CCh, deduced from binding experiments may be reflected by the concentration shift in component areas observable between the two agonists.

The decreased frequency of τ_1 and the elevated frequency of τ_2 openings when Ebd is used would be in accordance with the findings from binding experiments, that Ebd has opposing site selectivity. On the other hand, similar as for the native agonist and CCh the frequency of the shortest opening type dominates when high Ebd concentrations are used.

Obviously the nature of the agonist is capable of actuating the channels opening characteristics. Single openings are commonly thought to be elicited by singly occupied receptors, with only one agonist molecule bound to either one of the two available binding sites. According to this hypothesis, the difference in activation kinetics concerning single openings of the short and intermediate component may be based on the ability of the two differing binding sites to briefly activate the receptor. This assumption would be in agreement with previous findings by Hallermann and colleagues in 2005, where openings of the short and intermediate component were interpreted as openings derived from the singly occupied receptor states (compare to Figure 4, model 2).

The longest single opening component frequency (τ_3) decreases significantly for ACh in both approaches. For Ebd the significant decrease in frequency for the free fit approach is ambiguous as it may be based on the change in estimated component length. For CCh the longest component is not found to decrease significantly nor consistently. Suggesting that τ_3 single openings are most

probably openings of dense bursts that have been misclassified, the findings for this group may not improve interpretation.

The derivation of openings of the longest component is a delicate question, as it is the most important one in the physiological sense by accounting for the majority of charge carried by receptor openings. Longest openings are found to cluster almost exclusively in bursts of multiple openings that will be investigated in the following section.

5.5.2. Agonist dependency of dense bursts – short and long activations

In dense bursts the channel is in the conducting state for 98.9±0.04 % of the time (mean±s.e.m. for all records) and accounts for a minimum of 88.8 % of the total channel current. Mean values for ACh, CCh and Ebd are 98.6±0.60 %, 98.5±0.39 % and 91.6±2.99 % respectively. Based on these impressive values the characterization of dense bursts is of uppermost importance in the physiological sense.

The total frequency of dense bursts increases log-concentration dependently with a slope of 2.95±1.05 1/s*μM, 1.76±1.16 1/s*μM and 6.81±2.06 1/s*μM for acetylcholine, carbamoylcholine and epibatidine, correspondingly (compare also to Figure 9). Fitting a mixture of 4 probability density functions with fixed time constants to the distributions of burst with multiple openings reveals that dense bursts are indeed practically unexceptionally of the two longest burst time component types (τ_3 and τ_4, Figure 21). The lengths were fixed to the values of time constants obtained by fitting of the normal burst length distribution. The component areas of the second longest and longest component vary in a concentration dependent manner. The relative frequency of the longest burst component increases just inversely as the relative frequency of the second longest component decreases and reaches a maximum of nearly 100 % dense burst component area for ACh and CCh at concentrations of 1 μM and 3 μM respectively. Slopes for the log-concentration dependent change in τ_4 component area before the maximum is reached are 17.89±8.56 %/μM and 13.43±17.53 %/μM, ACH and CCh respectively. The component areas of τ_3 bursts

behave basically counteracting. For Ebd the slope for the increase in τ_4-area is 27.01±5.17 %/µM and the component seems to reach the maximum at about 3 µM agonist concentration.
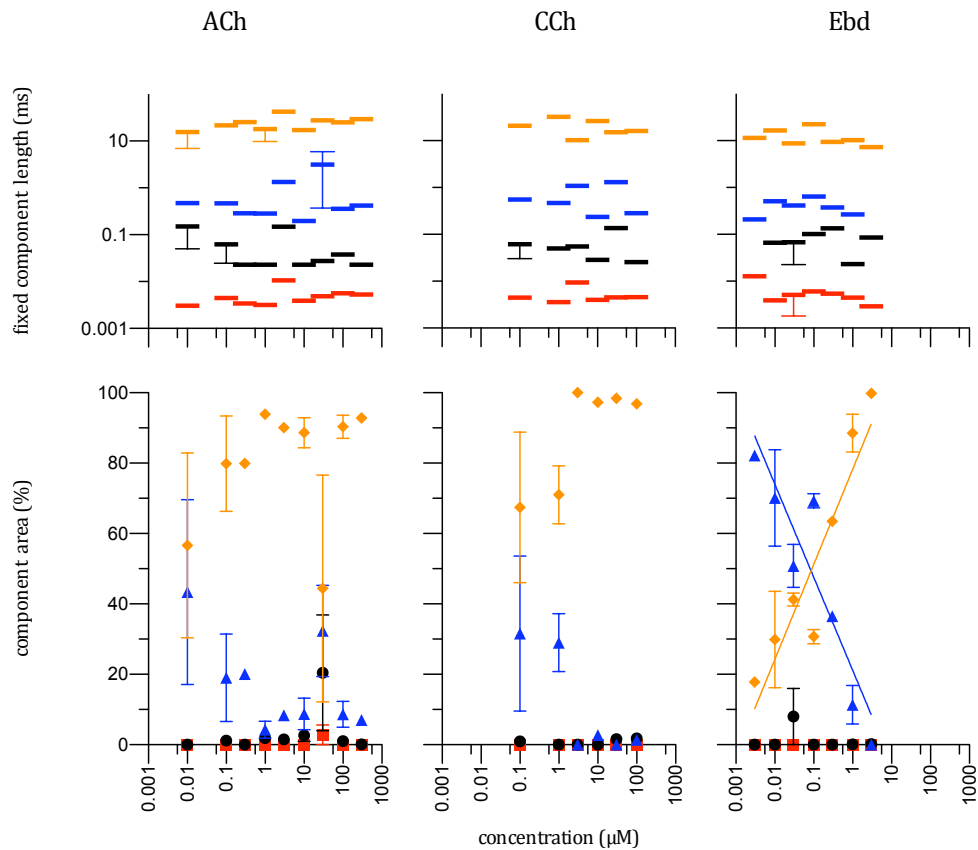
Figure 21: Analysis of burst time distributions for bursts with multiple openings. The distributions of dense bursts were fitted with a mixture of 4 pdfs with component lengths constrained to the values obtained by the fitting process of the normal burst length distributions. Only trend lines of significantly non-zero slope are shown. Dense bursts are practically exclusively of the longest and second longest burst length components (τ_4 orange rhombs and τ_3 blue triangles). For ACh and CCh most of the bursts are of the longest component type τ_4 (orange rhombs) and show a strong concentration dependent increase. Bursts of the second longest component τ_3 (blue triangles) show a counteracting concentration dependent decrease in frequency. Using Ebd as agonist elicits primarily bursts of the second longest type τ_3 at low concentrations, that is surpassed in frequency at concentrations > 0.1 µM. The 2 components reveal a significant concentration dependent frequency (P < 0.001) for Ebd only.

The analysis of dense bursts with more than 2 openings clearly shows that dense bursts are of 2 groups with differing concentration dependent frequency characteristics. As described above the dense burst lengths of Ebd show a clear

aberration from the ones found for ACh and CCh, being about half as long in mean duration (Table 2). Long bursts are predominant when ACh or CCh are used as agonists. For Ebd the overall picture is different with short bursts being the predominant type at low agonist concentration that are excelled at concentrations > 0.1 µM by long dense bursts. Based on the observation that the two dense burst types differ substantially in activation kinetics, a minimum of 2 different kinetic states that hold the possibility to reopen repeatedly in very short succession.

Interestingly the distributions of component areas for dense bursts look very much the same like the distributions for single openings investigated above. The diagrams for Ebd reveal distinct kinetic behaviour in response to the agonist in both distribution types analysed here. To point out the analogy between the two different distributions: the long component of dense bursts tends to perform similar to the short single openings, whereas the shorter type of dense bursts behaves more accordingly to the longer type of single openings.

Another question is why these distinct properties cannot be observed in detail in the overall burst distribution (Figure 17). Dividing bursts into single openings and dense bursts increases the contrast between the different components, as the tendencies described for the single opening and dense burst distributions can be observed to some degree in the overall burst distribution as well.

5.5.3. Openings in dense bursts

When differentiating the open period distribution in Figure 18 into single openings and openings clustered in dense bursts, the stunning observation of burst openings being only of the longest open period component type was made. Further analysis of open periods clustered in dense bursts will be performed to test this discovery for all records.

5.5.3.1. Apparent opening length

Distributions of open periods in dense bursts were fitted with either a mixture of 2 pdfs or a simple one component pdf to test whether more than 1 component is

needed to sufficiently describe the observed open periods in dense bursts. The opening distributions were fitted perfectly using a mixture of 2 probability density functions, but only 5 out of 54 records have slightly better fitting results compared to simple 1 component pdf fits. These 5 records were found in ACh driven single channel records only and no dependency on agonist concentration was observable. A possible cause could be improved signal to noise ratio as a higher number of short openings may be detected in this case and better fits with 2 pdfs could result. No indication for improved signal to noise ratios was found for these records.

It is self-evident that the observed deviation in the fitting process using 2 or 1 component pdfs may be based on the nature of the dense burst distribution that has to be fitted by a mixture of 2 pdfs. More precisely the existence of two burst types, may result in openings of distinct mean dwell times. At least the problem may simply be based on misclassified events that truly belong to single openings and therefore should not have been clustered. These assumptions will be investigated in the next section.

The very meaning why the number of components is so important is based on the possibility to calculate the true mean open time for dense bursts, if openings and gaps included in this kind of bursts essentially derive from simple exponential distributions (Colquhoun & Sakmann, 1985; Colquhoun & Sigworth, 1995). The predicted length and number of bursts and of gaps in bursts, needed for the calculation, is expected to be well estimated as described above. To ensure that the calculation is justifiable, the dwell time lengths will be investigated on dependency in the sequence of openings in dense bursts in the next section.

5.5.3.2. Position dependent dwell time length

To test whether the sparsely remaining short open period events that are found in dense bursts of 5 records are evenly distributed in the sequence of dwell times, open periods were analysed dependent on their position in the sequence of events. This analysis was performed for all records and accordingly conducted for gap lengths in dense bursts.

Dwell time lengths were not found to change dependent on their position in the sequence of events in the bursts, but it turned out that both, first openings and first gaps in bursts show a slight aberration of the mean length (Figure 22). First gaps bear a significantly (paired t-test, P<0.05) prolonged dwell time of +14.39±2.05 % to 10.94±0.51μs for acetylcholine, +7.03±0.88 % to 10.49±0.19 μs for Carbamoylcholine and +5.50±0.56 % to 10.14±0.20 μs for epibatidine.
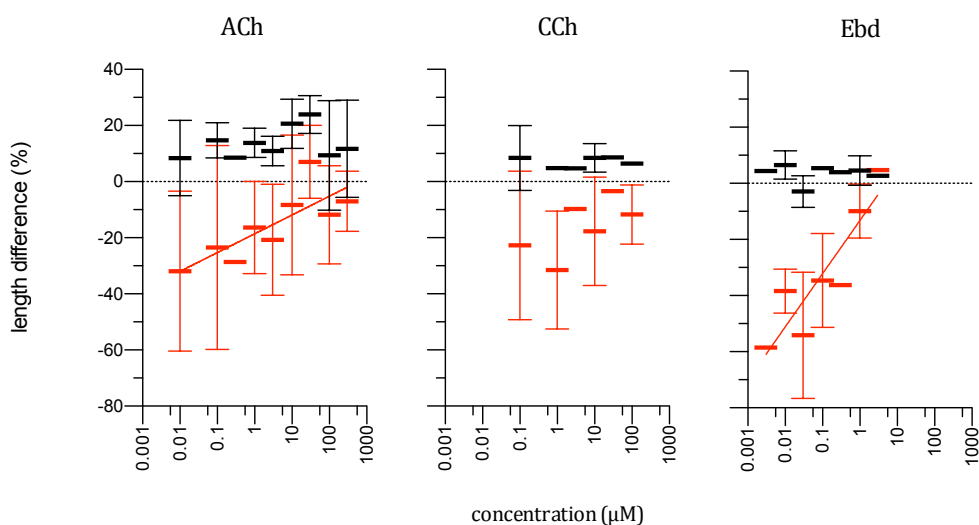
Figure 22: Dependency of dwell time length on position in the burst. For bursts with 2 and more openings open periods (red) and gaps (black) have been analysed for dependency on their position in the sequence of alternating open and shut events. Except for the first open and the first shut event in a burst no dependencies on sequence position were found. The length difference in % plotted here is based on the observed length of the first event of its kind compared to the mean length of all other events in dense bursts. The first opening event is revealed to be consistently shorter than average opening events in a burst (red). The first opening event is 19.7%, 20.4% and 27.5 % shorter than average for ACH, CCh and Ebd correspondingly. All agonists seem to show a concentration dependent approach of this length to the average length of other openings when the agonist concentration is increased. The dependency is significant for ACh and Ebd only. The first gap (black) in a burst turns out to be significantly longer than the average gap in a burst with a mean increase of 14.4%, 7.0% and 5.5% in event length for ACh, CCh and Ebd respectively, but does not expose any concentration dependency.

Openings elicited by ACh and Ebd show a significantly log-concentration dependent increase with a slope of 7.79±0.17 %/μM and 18.97±4.08 %/μM correspondingly. For Carbamoylcholine the reduction in first open time length is not found to be significantly concentration dependent with a slope of 6.15±3.50

%/µM but the mean length is significantly reduced by 20.91±4.19 % to 0.75±0.074 ms. Most likely the concentration dependency is comparable to ACh but may be less pronounced and therefore harder to be described by significance tests. By further investigation, pooling first openings from records of the same concentration it became clear, that the effect is based on 2 differing clases of openings. However fitting a mixture of 2 pdfs to the distributions was ambiguous as the numbers were still to low to give good estimates for the components. Comparison with component lengths for single openings and the mean length of openings in dense bursts suggest that the reduction is caused by missclassified single openings, being attached to dense bursts.

Exclusion of first openings of bursts did not improve the fitting of simple pdfs to the 5 records where improved fitting was detected with a mixture of 2 pdfs.

To further test whether openings of the shorter dense burst component show deviant mean lengths the distribution of bursts was investigated in detail. Since the mean duration of short dense bursts is much lower than the mean length observed for long dense bursts (about 100 fold) the minimum number of openings included in bursts was increased in a stepwise fashion (n>2, 3, 4, 5, 6) and the according burst distribution was fitted with a mixture of 2 pdfs. The component lengths was constrained to the values obtained by the fitting of dense burst distributions shown above to determine the critical number (n_{crit}) of openings that has to be exceeded to gain burst distributions with only long bursts included. Using this definition of n_{crit}, one has to be aware of the misclassification problem that may arise by this procedure but the primary goal to generally test for reduced opening length should not be critically influenced by this problem. By further fitting 1 component pdfs to the apparent open time distributions of bursts with n openings (n<n_{crit}) no significantly differing component lengths were found. Additionally no influence on distributions of open periods of long bursts was detected if bursts of n openings with n>n_{crit} were investigated.

The events that cause the slightly increased number of short openings in dense bursts in the 5 ACh records are most probably evenly distributed among long

openings and are suggested to have no significance for the calculation of true mean opening length in dense bursts.

5.5.3.3. Opening length - recalculated

By using the approach described by D. Colquhoun and B. Sakmann in 1985 the true mean opening length for bursts can be generated using the following relationship:

$$\mu_{open} = \frac{\mu_{burst} - \mu_{gap} * n_{gaps/burst}}{n_{gaps/burst} + 1}$$

The true mean length (μ_{open}) can be calculated as the mean open time per burst divided by the mean number of openings per bursts. The mean number of openings per burst is the mean number of gaps per burst ($n_{gaps/burst}$) plus 1. $n_{gaps/burst}$ can easily be calculated by dividing the predicted total number of gaps in bursts by the predicted total number of dense bursts in the record. The mean open time per burst is ill estimated, because of the high number of predicted gaps and therefore has to be replaced by the mean burst length (μ_{burst}) minus the predicted mean duration the channel is closed in bursts ($\mu_{gap}*n_{gaps/burst}$). μ_{gap} being the estimated mean gap length.

The mean open time length calculated by this procedure proofs to be very stable when compared to the values obtained for the intermediate open period component of apparent opening distributions (Figure 23 B). The mean values are 171±19.0 μs, 206±23.4 μs and 146±10.6 μs for ACH, CCh and Ebd, respectively (see also supplementary Table 7). Thus, similar to the observed reduction of dense bursts lengths for Ebd, the mean calculated opening length for Ebd is substantially shortened to roughly half of the calculated open period length for ACh or CCh.
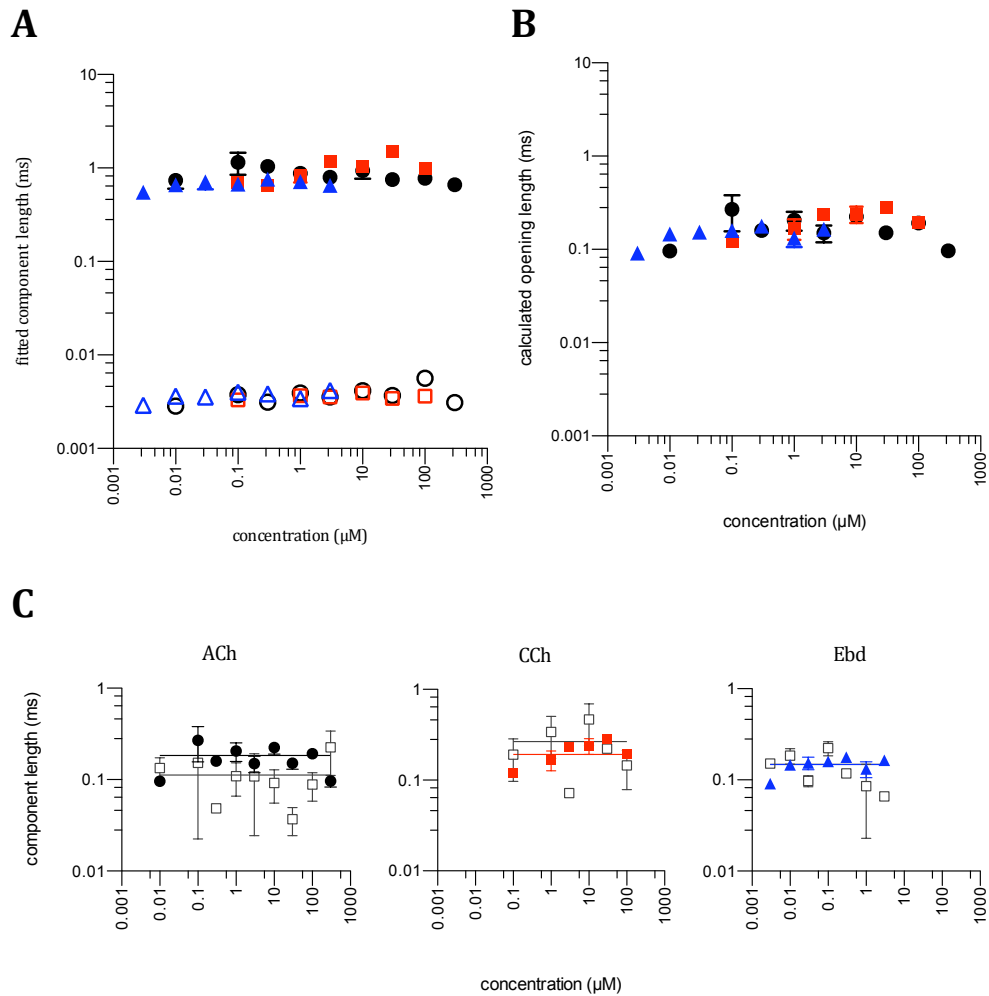
Figure 23: Recalculation of open length in dense bursts. (A) Apparent open periods clustered in dense bursts can be fitted by a simple 1-component pdf. The component length is shown by filled symbols: black dots depict ACh; red squares, CCh; blue triangles, Ebd. The corresponding contours depict the predicted mean lengths of gaps in dense bursts and are also of the simple exponential distribution type. (B) For this very special case it is possible to estimate the true mean length for openings as introduced by Colquhoun & Sakmann in 1985. The calculated true opening length is found to be very similar for ACH and CCH but slightly reduced for Ebd. (C) As the calculated true mean opening length is considerably reduced compared to the ones observed in apparent open period distributions (compare to A) the obtained values are compared to the fitted intermediate component of apparent open period distributions that are found to be not significantly different. It is quite notable that the calculated values show less variance from the overall mean value then the values of the intermediate opening component obtained by the fitting of dwell time distributions.

5.5.4. Reassembling the open period distribution

The calculation of the true mean open time in dense bursts gives values that are strongly shortened if compared to the values obtained by the fitting process of apparent openings in dense bursts, because the large predicted number of unresolved gaps. Besides the decrease in dwell time length this recalculation has the additional effect that the number of openings contained in bursts is much higher than the observed number. To demonstrate this enormous difference, a hypothetical open period distribution is shown in Figure 24, depicting the observed apparent open period distribution and the calculated pdfs from observed openings in dense bursts and single openings and a pdf illustrating the calculated true mean open time. To give a glimpse of what an open distribution might look like, if dense burst openings could be observed at infinite resolution, a mixture of pdfs obtained from single openings and the one predicted by calculation of the true mean open time in dense bursts is plotted.

At this point the reader should be aware that the hypothetical open period distribution shown here can not expected to have the true shape of an open time distribution as it could be observed if resolution of the setup would be infinite for several reasons. Even though the calculated true mean open period length for dense bursts may be very accurate, detailed assumptions about the open periods that are observed as single openings cannot be absolutely reliable. It may well be that short gaps have been missed that would fragment additional single openings into shorter units. Additionally the number of short events would increase accordingly. According to our dissection into single openings and bursts with more than 1 opening these disintegrated openings would be removed from single opening distribution and be added to dense burst distribution. Generally we assume this to be the most likely case for the longest single openings (τ_3) that were already considered to be misclassified.
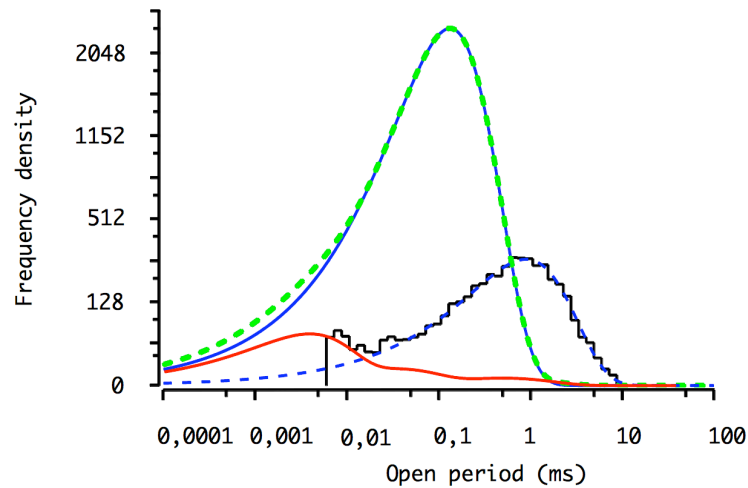
Figure 24: Reconstituted open period distribution. The original apparent open period distribution for an example record (ACh, 1 µM, t_{crit}=50µs) is shown. The calculated curves were obtained by fitting the distributions of single openings (continuous red line) and dense bursts (broken blue line). The calculated true mean length and number of openings in dense bursts was used to depict the according pdf that would cover such a distribution (continuous blue line). An hypothetical open period distribution was reconstituted by combining the findings from single opening distributions and recalculated true mean opening length in dense bursts (broken green line).

5.5.5. Correlation of activations

For the investigation of single channel recordings in terms of mechanism it is of special interest to characterize the relationships between different kinds of dwell times. Associations between dwell times can be suggested from investigations of correlation calculations and be visualized by dependency plots (Magleby & Song, 1992). Dependency plots can help to find correlations in the observed data and can be used to suggest the kinetic structure of the channel. Thus they can reveal correlations of kinetic states of distinct lifetimes that can be interpreted in the framework of structural findings and kinetic models.
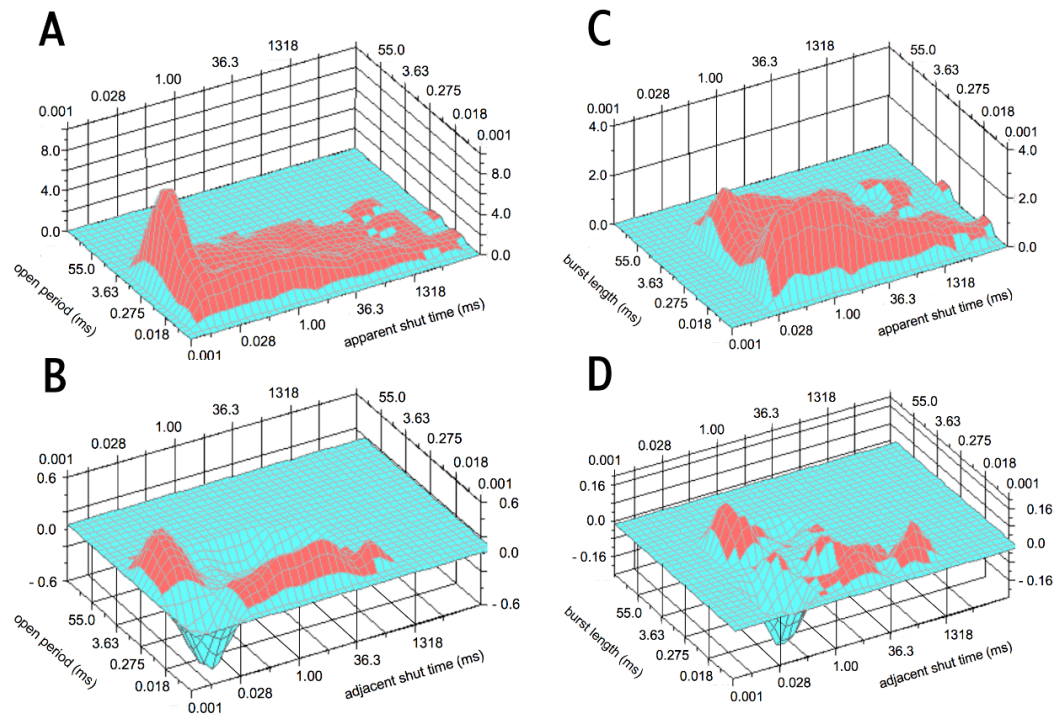
Figure 25: Bivariate distributions and dependency plots of dwell times and bursts. The plots show data of an example record using ACh (10μM) (A) The bivariate distribution shows apparent open periods and shut times without imposing correlation. (B) The correlation dependency plot for apparent dwell times suggest a strong correlation of long openings with shortest gaps and further correlation of short openings with gaps longer than the t_{crit} of 40μs used for this record. (C) Bivariate distribution for the observed bursts with apparent shut times as if events were evenly distributed. (D) To further investigate correlations of bursts with adjacent gaps (preceding and following) dependency plots were assembled. Shut times start at 40μs as shorter gaps are included in the burst events used for the correlation calculation. The dependency plot suggests less well-defined areas of correlation that can be highly variable between records. However, dense bursts can be constantly found to correlate preferentially with gaps shorter than ≈1ms and single openings to rather correlate with longer gaps.

Figure 25A shows a simple bivariate distribution of apparent open periods and gaps when no correlation is imposed. By calculating correlation coefficients for the binned data a dependency plot can be generated. The dependency plot for observed dwell times (Figure 25B) shows strong correlation of long openings with short gaps as they were clustered in our analysis for dense bursts. Short openings correlate well with shut times longer than gaps of the shortest type. This observation is consistent for all of the records and very similar results have already been published for high-resolution data (Hallermann et al., 2005; Parzefall et al., 1998).

As we investigated burst distributions we found single openings to be clearly separated from long openings clustered in dense bursts. The remaining shut times are mostly evenly distributed over the whole range between t_{crit} and the upper end of the distribution. To investigate the connectivity between dense bursts, single openings and adjacent gaps, we investigated dependency plots of bursts, defined by the critical shut time, and adjacent dwell times (Figure 25D). Dense bursts are found to preferentially correlate with short gaps between t_{crit} and about 1ms. This observation is also consistent with dependency plots of other records. Short bursts, i.e. single openings, on the other hand associate preferentially with longer gaps. However, dependency plots of channel activations in the sense of bursts and especially of single openings show considerable variability in dependency plots between records allowing only assumptions about a general scheme for correlation of channel activations.

6. Discussion

In the following section the results will be discussed and the described characteristics will be interpreted in the framework of previously proposed kinetic models for the nicotinic acetylcholine receptor channel. Finally a modified kinetic model will be presented that fulfils the demands of the kinetic features in channel activation and an outlook of future plans will be given.

6.1. Reliability of dwell time distributions

Since the very beginning of single channel research missed dwell times have been a problem for the reliable interpretation of apparent event distributions. Application of the high-resolution recording method allowed for the determination of correlations for apparent dwells and the well predicted missed events can be used for a reliable interpretation of the results.

6.1.1. Single openings

Even though the field clearly emerged and advanced techniques like the high-resolution patch clamp are available dwells cannot be resolved completely yet. The problem can be bypassed by sensible interpretation of events in the background of correlation, if the dependencies of dwells are homogeneous and distinct, as could be shown for the high-resolution data used in this study.

Short and intermediate single openings highly correlate with long gaps as was shown in previous publications (Parzefall et al., 1998; Hallermann et al., 2005). Single openings therefore cannot be influenced by the existence of short undetected gaps.

Furthermore the distribution of the number of openings per burst were found to have a component close to unity (data not shown). Following Colquhoun and Hawkes (1982) and Colquhoun & Sakmann (1985) a component with unit mean implies that there is at least one burst component that has only one opening per burst and thus cannot have gaps in the burst that may have been missed due to insufficient resolution.

On the other hand sparsely observed long single openings have the same length as long apparent openings that were shown to highly correlate with shortest gaps and are found to cluster in dense bursts. Hence, openings of this type are suggested to resemble missclassified events that should belong to dense bursts instead.

6.1.2. Burst distributions and openings in dense bursts

The definition of bursts includes events of the shortest gap component only. Implying that all gaps longer than the critical shut time do not have any influence on the distribution of bursts. Since short openings are found to be highly correlated with gaps longer than the dead time, unresolved openings are automatically excluded from having any influence on burst distributions. Even though the burst definition used in this study is substantially different from the conventional burst distrbutions, burst distributions can be deemed reliable as undetected dwells do not substantially change these distributions (Colquhoun & Sakmann, 1985; Colquhoun & Sigworth, 1995)

Since both, openings and partially undetected gaps in dense bursts, could be shown to belong to a single class (component) of events it was possible to recalculate the true mean opening length in dense bursts. The procedure delivered very consistent values over the concentration ranges that were used for the different agonists. By doing so the biasing problem of undetected short gaps could be elliminated.

6.2. Agonist dependent channel activations

Dense bursts are almost exclusively constituted by openings of the longest apparent open period component and, per definition, of shortest shut time distribution component gaps. Investigation of correlation plots of bursts versus adjacent gaps, suggest that dense bursts occur in clusters as they correlate

preferentially with gaps < 10 ms, whereas single openings are found to be mostly adjacent to longer shuttings. Like suggested in previous studies (Colquhoun & Sakmann, 1985; Hallermann et al., 2005) short openings appear to be well separated from other activations.

6.2.1. Single openings are site specific

Ebd is the only agonist in this study that is able to elicit second longest single openings in higher frequency than shortest openings at low agonist concentrations, when the receptor can be expected to be mostly in one of its singly occupied states. In accordance with Ebds unique site selectivity for the α-γ site, it can be concluded that the agonist preferentially binds to this site and thus is able to particularly elicit openings of the second shortest single opening component.

It is most likely that shortest openings arise from singly as well as doubly occupied channel states as relative frequencies in burst distributions are found to stay constant, or when only single openings are investigated even increase. Thus, ACh and CCh that posses a higher affinity for the α-δ binding site elicit short openings by preferential binding to this site. By lacking the concentration dependent decrease in frequency short openings have to be elicited by doubly bound receptor molecules as well.

This interpretation further implies that a possible mechanistic receptor model cannot be a sequential model without support for differing binding sites, but has to offer the possibility to generate short single openings from a doubly liganded state. This possibility is given by the 'primed-states' model published by Mukhtasimova and colleagues in 2009.

6.2.2. Dense burst length depend on the nature of the agonist

Dense bursts are consituted of openings that are mostly similar in length and can be considered independent of the nature of the agonist. This is in line with the findings of Lape and colleagues that found the final opening and closing rate of

the receptor to be mostly independent of the nature of the agonist. They also describe that on the other hand partial and full agonists posses different ability to actuate the receptor into its highly efficient burst state. The ability of an agonist to take effect on the effectiveness of channel gating thus is not based on the ability to change the final close to open reaction or vice versa, but relies on locking and holding the receptor in a preactivated state.

Dense bursts constitute the longest and second longest components of the normal burst length distribution. The length of burst components does not differ significantly between ACh and CCh, but the burst lengths for Ebd driven currents show a significant reduction by a factor of about 0.5 .

Long dense bursts for Ach and CCh have a mean component length of about 24.7 ms and 20.14 ms accordingly. The component length for Ebd is significantly different with a mean length of about 12 ms. Hence, the proportion of the long burst lengths for the three agonists ACh : CCh : Ebd is: 1.0 : 0.8 : 0.5 .

The second longest burst component has very similar length proportions, as mean lengths of about 0.77 ms, 0.65 ms and 0.35 ms are found for ACh, CCh and Ebd respectively. Thus the length proportion is exactly the same 1.0 : 0.8 : 0.5 .

6.2.3. Dense burst frequencies reveal the origin of burst states

Mostly important short dense bursts and long dense bursts exhibit another unique feature: the concentration dependency of burst types differs substantially. Long dense bursts rise in frequency with increased agonist concentration as one would expect as this is in line with the hypothesis that dense bursts emerge from doubly liganded receptor states (Colquhoun & Sakmann, 1985; Lape et al., 2008; Mukhtasimova et al., 2009).

Short dense bursts do not seem to derive from doubly liganded channels since their relative frequency declines when the concentration is increased. Short dense bursts can therefore be suggested to derive from singly liganded receptor states, as a concentration dependent drop out of the burst state is only possible by binding of an additional agonist molecule. Furthermore the pathway leading out of the dense burst state cannot arise directly from a basal shut state, as this

would shorten the lifetime of the short dense-burst state in a concentration dependent manner. This implies that in a possible kinetic mechanism the basic singly occupied receptor state, able to bind a second molecule of agonist, and the invariant shut state from which openings are elicited in short dense bursts have to be two distinct states. Hence, a mechanism including at least one additional state as described in the flipped state model (model 3) or the primed state model (model 4) is required.

Furthermore the short dense bursts, similar to long single openings, are the preferentially elicited channel activations when Ebd is used in low concentrations. The proportion difference in relative frequencies appears to be in good accordance with differences in binding site selectivity in that way that ACh and CCh primarily select for the α-δ binding site but Ebd possesses a strong antithetic selectivity for the α-γ site. Thus Ebd preferentially binds to the α-γ site thereby causing the receptor to elicit openings different from the short single openings preferentially produced by ACh and CCh.

6.3. Discussion of previously published kinetic models

6.3.1. The 'flip-state' mechanism

Lape and colleagues proposed an enhanced version of model 1 in 2008 that distinguishes not only between binding and gating but additionally separating early stages in the conformational wave (Purohit et al., 2007) from the ultimate close-open reactions. The introduced states most likely resemble the closing in of the C-loop around the bound ligand. Performing a very elegant essay using agonists (ACh) and partial agonists (TMA), they were able to show that the reduction in partial agonists ability to activate the receptor is not due to the diminished ability to open the receptors gate, but leads back to an earlier stage as the conformational wave spreads through the receptor molecule.

The group found the channels final opening and closing rate not to vary greatly upon full or partial agonist binding. The difference was shown to derive from the

reduced ability of partial agonists to push the receptor to its flip states. The results described here are clearly contraindicative, at least when it comes to the channels shutting rates that define the length of the openings.

Similar to model 1 the mechanism is not compatible with the results desribed here.

6.3.2. The 'primed states' model

As a logical progression to the flip-state model Mukhtasimova and colleagues published a model including two intermediate levels of shut states that are proposed to represent the sequential movement of the C-loops. When it comes to our data the model proposed by Lape et al. essentially lacks one conformational state, that probably was not necessary to describe their data: openings that arise from the singly occupied flip-state and from the doubly occupied flip-state show greatly differing kinetics, implying that the flipped receptor states have to resemble different conformational states. Accordingly the binding rate directly connecting the flip-states in the mechanism is a compound of the rate for binding and the rate for the subsequent conformational change. The resulting intermediate state, where 2 agonist molecules are bound but the conformational change has not yet happened, is missing.

The primed states model adapts 2 levels of conformational change, singly primed states and doubly primed states, and thus discerns between the second binding step and the induced conformational change. Comprising this hybrid doubly bound singly primed state this model is able to allow single openings from doubly bound receptors, even though the group didn't have the necessity of using this feature of the mechanism to fit their data.

Discerning between singly and doubly primed states brings the further advantage that single short openings as well as dense bursts can be elicited from singly occupied receptors. The frequency of the singly bound doubly primed state, from which bursts are possible, decreases with increasing agonist concentration.

The complexity of the high-resolution data demands a model differentiating the two binding sites provided by the embryonic nAChR architecture. Thus an additional short-lived open state is missing in this study and its frequency has to be dependent on the nature of the agonist, correlating with differences in site selectivity.

6.4. A primed state model with binding site discrimination

To incorporate all the characteristics found by the investigations described in this study I propose a kinetic mechanism based on the primed states model as introduced by Mukhtasimova et al. in 2009, but with resolved binding site diversity (Figure 26). The possibility of reaching primed states from unliganded receptors is excluded for simplification, even though the existence of such states may be quite reasonable. Nevertheless the model gets quite complex when the two binding sites are distinguished and a number of combinations of singly primed and doubly primed states become visible.

According to the site selectivity of the agonists short single openings can be elicited by binding of agonist to the α-δ site, being less frequent for Ebd compared to ACh or CCh.

The frequency of short openings does not decrease with increasing receptor concentration implying that an additional open state for doubly liganded receptors ($A_\gamma A_\delta'$), other than the highly effective long dense burst state exists allowing short openings at high agonist concentrations.

Long single openings, showing a slight decease with increasing agonist concentration can be restricted to single occupied receptors or be less effectively accomplished by an additional doubly liganded receptor state. As a strong difference in relative frequency is observable between Ebd and ACh or CCh and the site selectivity of the agonists differ correspondingly, second longest single openings can be suggested to derive from the singly primed, α-γ occupied receptor states ($A_\gamma'R_\delta$ and $A_\gamma'A_\delta$).

Model 5: primed states model with resolved binding site diversity
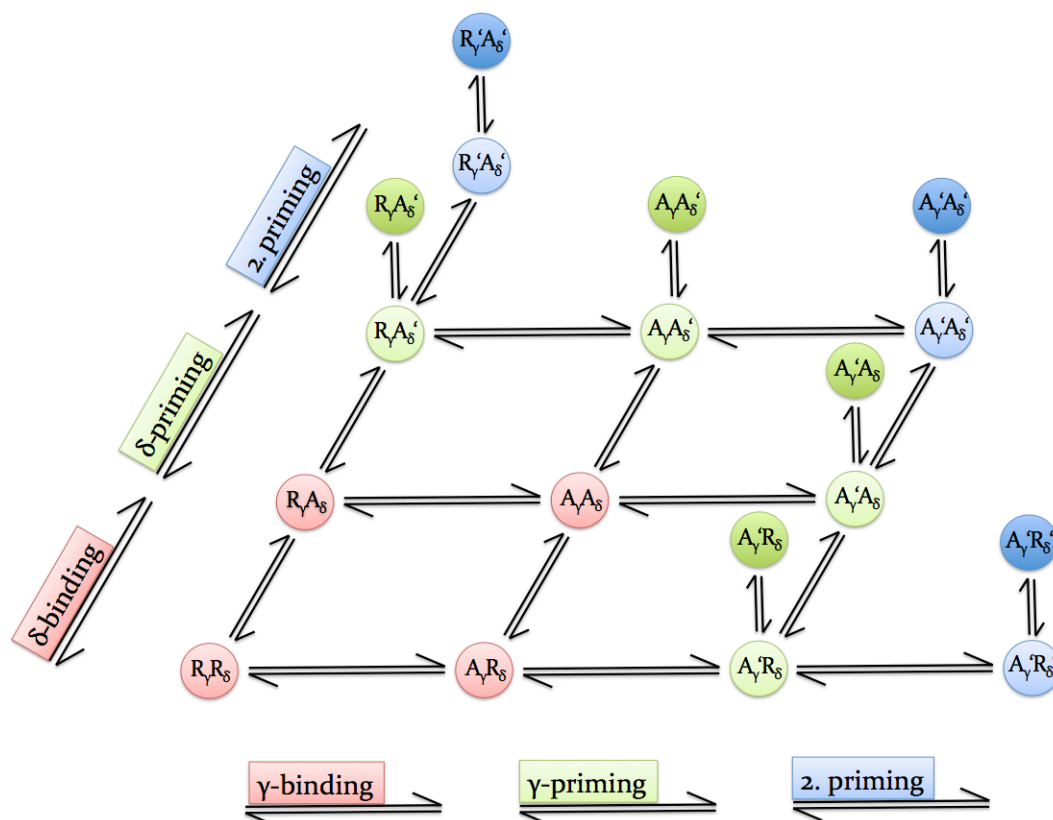
Figure 26: Primed states model with resolved binding site diversity. The proposed model is based on the primed states model published in 2009 by Mukhtasimova and colleagues. The published model (model 4) did not distinguish the two structurally differing binding sites and was modified to allow binding site diversity. The possibility to prime and open the channel from its unliganded state as found in the original model is not needed and discarded for simplification. The first priming levels are suggested to allow single openings, whereas the second priming levels permit the generation of dense bursts. R is for the receptor binding sites without bound agonists, whereas A denotes that one molecule of the agonist was bound at the respective binding site, denoted in subscript δ or γ, for α-δ and α-γ binding site respectively. The priming states are described by apostrophes assigned to the according binding site and for enhancing the overview by coloured spheres in green for singly primed or blue for doubly primed receptors. Open-close reactions are depicted by vertical arrows and the according open state darker in colour than the according shut state from which it arises.

Short dense bursts show a consistent concentration dependent decrease in relative frequency for all agonists and an overall elevated relative frequency for Ebd compared to Ach and CCh. I suggest the existence of a highly effective dense

burst state for the singly liganded α-γ binding site ($A_\gamma'R_\delta'$). Additionally a doubly primed state may exist for the α-δ site, but being less effectively reached, meaning that self priming of the α-γ site is less probable for the receptor used in this study.

Long dense bursts are most likely to be elicited by doubly liganded doubly primed receptors only and their relative frequency increases indifferently for all agonists used here. The increase is steepest for Ebd and may reflect the overall elevated affinity of the molecule to the binding sites.

Long dense bursts and short dense bursts have the same calculated true mean opening length and possess gaps of the same length. This is found for all three agonists. Gaps do not even differ between the agonist types used in this study and therefore may reflect an intrinsic channel characteristic. The calculated mean true opening lengths in dense bursts is found to differ considerably between the agonists used for channel activation by a factor of roughly 2 between Ebd and ACh or CCh. This finding suggests that there is a crosstalk between the agonist binding sites and the channels gate, which is in accordance with the suggestions made by Mukhtasimova and colleagues in 2009.

6.5. Channel block with Ebd

While performing the initial analysis of apparent dwell distributions a heavy blocking effect at high Ebd concentrations of $\geq 10\mu M$ was described. The blocking effect manifests as additional gaps, considerably longer than gaps of the fastest shut time component, are introduced in enduring periods of activation. The gaps elicited by the blocking effect are found to have a sharp roll off, so this may be a hint towards an allosteric blocking mechanism. At high Ebd concentrations the longest apparent open period distribution component vanishes and only the shortest and intermediate open component remain. Without additional experimental evidence to determine the type of block mechanism trustworthy, e.g. open channel block versus allosteric blocking, it is not possible to characterize the findings properly.

6.6. Outlook

It would be interesting whether a direct comparison with nAChRs of other species or of the adult type reveals other kinetic characteristics, when similar experiments are performed, helping to explain how far structural differences between subunits alter the picture of elicited receptor currents.

Further investigations using blockers that specifically disable one binding site might additionally improve insights in binding site diversity of the nAChR and may help to explain how different states of kinetic mechanisms are accomplished. The channel block observed for Ebd has to be further investigated. Performing additional experiments might shed light on the nature of block for this molecule and could help to predict the actions of this very potent agonist at high concentrations.

7. Table of figures

8. References

Akk G, Sine S, Auerbach A (1996) Binding sites contribute unequally to the gating of mouse nicotinic alpha D200N acetylcholine receptors. J Physiol 496: 185-196.

Bocquet N, Prado de Carvalho L, Cartaud J, Neyton J, Le Poupon C, Taly A, Grutter T, Changeux JP, Corringer PJ (2007) A prokaryotic proton-gated ion channel from the nicotinic acetylcholine receptor family. Nature 445: 116-119.

Brejc K, van Dijk WJ, Klaassen RV, Schuurmans M, van Der Oost J, Smit AB, Sixma TK (2001) Crystal structure of an ACh-binding protein reveals the ligand-binding domain of nicotinic receptors. Nature 411: 269-276.

Brenner HR & Sakmann B (1983) Neurotrophic control of channel properties at neuromuscular synapses of rat muscle. J Physiol 337: 159-171.

Chakrapani S, Auerbach A (2005) A speed limit for conformational change of an allosteric membrane protein. Proc Natl Acad Sci USA 102: 87-92.

Chakrapani S, Bailey TD, Auerbach A (2004) Gating dynamics of the acetylcholine receptor extracellular domain. J Gen Physiol 123: 341-356.

Colquhoun D & Sigworth FJ (1995) Fitting & statistical analysis of single channel records. In Single-Channel Recording, 2nd edn, ed Sakman B & Neher E, Plenum Press, New York pp. 483-585

Colquhoun D, Hatton CJ, Hawkes AG (2003) The quality of maximum likelihood estimates of ion channel rate constants. J Physiol 547: 699-728.

Colquhoun D, Hawkes AG (1982) On the stochastic properties of bursts of single ion channel openings and of clusters of bursts. Philos Trans R Soc Lond B Biol Sci 300: 1-59.

Colquhoun D, Sakmann B (1981) Fluctuations in the microsecond time range of the current through single acetylcholine receptor ion channels. Nature 294: 464-466.

Colquhoun D, Sakmann B (1985) Fast events in single-channel currents activated by acetylcholine and its analogues at the frog muscle end-plate. J Physiol 369: 501-557.

Colquhoun D, Sivilotti LG (2004) Function and structure in glycine receptors and some of their relatives. Trends Neurosci 27: 337-344.

Colquhoun D, Unwin N, Shelly C, Hatton CJ, Sivilotti L (2003) Nicotinic acetylcholine receptors. In Burger's Medicinal Chemistry & Drug Discovery Volume II, Drug Discovery and Drug Development, 6th edn, ed Abraham DJ, Wiley, New York, pp. 357-405.

Corringer PJ, Baaden M, Bocquet N, Delarue M, Dufresne V, Nury H, Prevost M, Van Renterghem C (2010) Atomic structure and dynamics of pentameric ligand-gated ion channels: new insight from bacterial homologues. J Physiol 588: 565-572.

Corringer PJ, Le Novère N, Changeux JP (2000) Nicotinic receptors at the amino acid level. Annu Rev Pharmacol Toxicol 40: 431-458.

del Castillo J, Katz B (1955) Local activity at a depolarized nerve-muscle junction. J Physiol 128: 396-411.

del Castillo J, Katz B (1955) On the localization of acetylcholine receptors. J Physiol 128: 157-181.

del Castillo J, Katz B (1957) Interaction at end-plate receptors between different choline derivatives. Proc R Soc Lond B Biol Sci 146: 369-381.

del Castillo J, Katz B (1957) A study of curare action with an electrical micromethod. Proc R Soc Lond B Biol Sci 146: 339-356.

Dudel J, Hallermann S, Heckmann M (2000) Quartz glass pipette puller operating with a regulated oxy-hydrogen burner. Pflügers Arch 441: 175-180.

Fatt P, Katz B (1950) Membrane potentials at the motor end-plate. J Physiol 111: 46p-47p.

Fatt P, Katz B (1950) Some observations on biological noise. Nature 166: 597-598.

Fatt P, Katz B (1952) Spontaneous subthreshold activity at motor nerve endings. J Physiol 117: 109-128.

Feldberg W, Fessard A, Nachmansohn D (1940) The cholinergic nature of the nervous supply to the electric organ of the Torpedo (*Torpedo marmorata*). J Physiol 97: 3-4.

Franke C, Költgen D, Hatt H, Dudel J (1992) Activation and desensitization of embryonic-like receptor channels in mouse muscle by acetylcholine concentration steps. J Physiol 451: 145-158.

Gao F, Bren N, Burghardt TP, Hansen S, Henchman RH, Taylor P, McCammon JA, Sine SM (2005) Agonist-mediated conformational changes in acetylcholine-binding protein revealed by simulation and intrinsic tryptophan fluorescence. J Biol Chem 280: 8443-8451.

Göpfert H & Schäfer H (1938) Über den direkt und indirekt erregten Aktionsstrom und die Funktion der motorischen Endplatte. Pflügers Arch 239: 597-619.

Grosman C, Zhou M, Auerbach A (2000) Mapping the conformational wave of acetylcholine receptor channel gating. Nature 403: 773-776.

Hallermann S, Heckmann S, Dudel J, Heckmann M (2005) Short openings in high resolution single channel recordings of mouse nicotinic receptors. J Physiol 563: 645-662.

Hamill OP, Marty A, Neher E, Sakmann B, Sigworth FJ (1981) Improved patch-clamp techniques for high-resolution current recording from cells and cell-free membrane patches. Pflügers Arch 391: 85-100.

Hansen SB, Wang HL, Taylor P, Sine SM (2008) An ion selectivity filter in the extracellular domain of Cys-loop receptors reveals determinants for ion conductance. J Biol Chem 283: 36066-36070.

Hatton CJ, Shelley C, Brydson M, Beeson D, Colquhoun D (2003) Properties of the human muscle nicotinic receptor, and of the slow-channel myasthenic syndrome mutant epsilonL221F, inferred from maximum likelihood fits. J Physiol 547: 729-760.

Horn R (1987) Statistical methods for model discrimination. Applications to gating kinetics and permeation of the acetylcholine receptor channel. Biophys J 51: 255-263.

Jackson MB (1999) Ligand-gated channel: postsynaptic receptors and drug targets. Adv Neurol 79: 511-524.

Kalamida D, Poulas K, Avramopoulou V, Fostieri E, Lagoumintzis G, Lazaridis K, Sideri A, Zouridakis M, Tzartos SJ (2007) Muscle and neuronal nicotinic acetylcholine receptors. Structure, function and pathogenicity. FEBS J 274: 3799-3845.

Karlin A (1967) On the application of "a plausible model" of allosteric proteins to the receptor for acetylcholine. J Theor Biol 16: 306-320.

Karlin A (1993) Structure of nicotinic acetylcholine receptors. Curr Opin Neurobiol 3: 299-309.

Karlin A. (2002) Emerging structure of the nicotinic acetylcholine receptors. Nat Rev Neurosci 3: 102-114.

Katz B, Miledi R (1973) The effect of atropine on acetylcholine action at the neuromuscular junction. Proc R Soc Lond B Biol Sci 184: 221-226.

Kelley SP, Dunlop JI, Kirkness EF, Lambert JJ, Peters JA (2003) A cytoplasmic region determines single-channel conductance in 5-HT3 receptors. Nature 424: 321-324.

Kistler J, Stroud RM (1981) Crystalline arrays of membrane-bound acetylcholine receptor. Proc Natl Acad Sci USA 78: 3678-3682.

Költgen D, Brinkmeier H, Jockusch H (1991) Myotonia and neuromuscular transmission in the mouse. Muscle Nerve 14: 775-780.

Kuffler SW, Yoshikami D (1975) The distribution of acetylcholine sensitivity at the post-synaptic membrane of vertebrate skeletal twitch muscles: iontophoretic mapping in the micron range. J Physiol 244: 703-730.

Labarca P, Zapata O, Beltran C, Darszon A (1995) Ion channels from the mouse sperm plasma membrane in planar lipid bilayers. Zygote 3: 199-206.

Langley JN (1906) Croonian Lecture, 1906. On nerve endings and on special excitable substances in cells. Proc Roy Soc Ser B 78: 170-194.

Lape R, Colquhoun D, Sivilotti LG (2008) On the nature of partial agonism in the nicotinic receptor superfamily. Nature 454: 722-727.

Lester HA, Dibas MI, Dahan DS, Leite JF, Dougherty DA (2004) Cys-loop receptors: new twists and turns. Trends Neurosci 27: 329-336.

McManus OB, Blatz AL, Magleby KL (1987) Sampling, log binning, fitting, and plotting durations of open and shut intervals from single channels and the effects of noise. Pflügers Arch 410: 530-553.

Miyazawa A, Fujiyoshi Y, Stowell M, Unwin N (1999) Nicotinic acetylcholine receptor at 4.6 A resolution: transverse tunnels in the channel wall. J Mol Biol 288: 765-786.

Miyazawa A, Fujiyoshi Y, Unwin, N (2003) Structure and gating mechanism of the acetylcholine receptor pore. Nature 410: 949-955.

Mukhtasimova N, Lee WY, Wang HL, Sine SM (2009) Detection and trapping of intermediate states priming nicotinic receptor channel opening. Nature 459: 451-455.

Nastuk W (1953) The electrical activity of the muscle cell membrane at the neuromuscular junction. J Cell Physiol 42: 249-272.

Neher E & Sakmann B (1976) Single-channel currents recorded from membrane of denervated frog muscle fibres. Nature 260: 799-802.

Ohno K, Wang HL, Milone M, Bren N, Brengman JM, Nakano S, Quiram P, Pruitt JN, Sine SM, Engel AG (1996) Congenital myasthenic syndrome caused by decreased agonist binding affinity due to a mutation in the acetylcholine receptor epsilon subunit. Neuron 17: 157-170.

Parzefall F, Wilhelm R, Heckmann M, Dudel J (1998) Single channel currents at six microsecond resolution elicited by acetylcholine in mouse myoballs. J Physiol 512: 181-188.

Prince RJ & Sine SM (1998) Epibatidine activates muscle acetylcholine receptors with unique site selectivity. Biophys J 75: 1817-1827.

Prince RJ & Sine SM (1998) Epibatidine binds with unique site and state selectivity to muscle nicotinic acetylcholine receptors. J Biol Chem 273: 7843-7849.

Purohit P, Mitra A, Auerbach A (2007) A stepwise mechanism for acetylcholine receptor channel gating. Nature 446: 930-933.

Rao CR (1973) Linear statistical interference and its application. 2nd edn, John Wiley & Sons Inc, New York

Raymond V & Sattelle DB (2002) Novel animal-health drug targets from ligand-gated chloride channels. Nat Rev Drug Discov 1: 427-436.

Ripoll DR, Faerman CH, Axelsen PH, Silman I, Sussman JL (1993) An electrostatic mechanism for substrate guidance down the aromatic gorge of acetylcholinesterase. Proc Natl Acad Sci USA 90: 5128-5132.

Sigworth FJ & Neher E (1980) Single Na+ channel currents observed in cultured rat muscle cells. Nature 287: 447-449.

Sigworth FJ & Sine SM (1987) Data transformations for improved display and fitting of single-channel dwell time histograms. Biophys J 52: 1047-1054.

Sine SM & Engel AG (2006) Recent advances in Cys-loop receptor structure and function. Nature 440: 448-455.

Sine SM, Kreienkamp HJ, Bren N, Maeda R, Taylor P (1995) Molecular dissection of subunit interfaces in the acetylcholine receptor: identification of determinants of alpha-conotoxin M1 selectivity. Neuron 15: 205-211.

Sine SM & Taylor P (1981) Relationship between reversible antagonist occupancy and the functional capacity of the acetylcholine receptor. J Biol Chem 256: 6692-6699.

Smit AB, Syed NI, Schaap D, van Minnen J, Klumperman J, Kits KS, Lodder H, van der Schors RC, van Elk R, Sorgedrager B, Brejc K, Sixma TK, Geraerts WP (2001) A glia-derived acetylcholine-binding protein that modulates synaptic transmission. Nature 411: 261-268.

Taly A, Delarue M, Grutter T, Nilges M, Le Novère N, Corringer PJ, Changeux JP (2005) Normal mode analysis suggests a quaternary twist model for the nicotinic receptor gating mechanism. Biophys J 88: 3954-3965.

Taly A, Corringer PJ, Guedin D, Lestage P, Changeux JP (2009) Nicotinic receptors: allosteric transitions and therapeutic targets in the nervous system. Nat Rev Drug Discov 8: 733-750.

Unwin N (2005) Refined structure of the nicotinic acetylcholine receptor at 4A resolution. J Mol Biol 346: 967-989.

Unwin N, Miyazawa A, Li J, Fujiyoshi Y (2002) Activation of the nicotinic acetylcholine receptor involves a switch in conformation of the alpha subunits. J Mol Biol 319: 1165-1176.

Vogel Z, Sytkowski AJ, Nirenberg MW (1972) Acetylcholine receptors of muscle grown in vitro. Proc Natl Acad Sci USA 69: 3180-3184.

Wang HL, Auerbach A, Bren N, Ohno K, Engel AG, Sine SM (1997) Mutation in the M1 domain of the acetylcholine receptor alpha subunit decreases the rate of agonist dissociation. J Gen Physiol 109: 757-766.

Xie Y, Cohen JB (2001) Contributions of Torpedo nicotinic acetylcholine receptor gamma Trp-55 and delta Trp-57 to agonist and competitive antagonist function. J Biol Chem 276: 2417-2426.

Zhang Y, Chen J, Auerbach A (1995) Activation of recombinant mouse acetylcholine receptors by acetylcholine, carbamylcholine and tetramethylammonium. J Physiol 486: 189-206.

Zhou Y, Pearson JE, Auerbach A (2005) Phi-value analysis of a linear, sequential reaction mechanism: theory and application to ion channel gating. Biophys J 89: 3680-3685.

9. Supplementary tables

Table 1: LLRs of opentime distributions - 2 vs 3 components

[ACh]	exp. No.	LLR	[ACh]	exp. No.	LLR
300	26	0,92	3	31	0,00
	27	1,17		32	-0,08
	Mean	1,05		Mean	-0,04
100	1	0,65	1	11	8,41
	2	0,68		12	0,55
	3	-0,08		13	14,22
	Mean	0,42		Mean	7,73
30	29	10,30	0,3	33	4,04
	30	0,03			
	Mean	5,16	0,1	16	4,99
				17	3,09
10	6	9,90		18	2,92
	7	10,63		Mean	3,67
	8	0,19			
	9	9,59	0,01	21	8,57
	Mean	7,58		22	3,17
				Mean	5,87

[CCh]	exp. No.	LLR	[CCh]	exp. No.	LLR
100	1	10,11	3	21	1,83
	2	7,21			
	3	5,88	1	11	3,53
	Mean	7,73		12	13,73
				13	63,00
30	20	0,10		Mean	26,75
10	6	9,17	0,1	16	20,07
	7	24,10		17	25,17
	8	0,00		18	17,21
	Mean	11,09		Mean	20,82

[Ebd]	exp. No.	LLR	[Ebd]	exp. No.	LLR
100	20	0,67	0,3	24	24,92
30	21	-0,19	0,1	11	31,92
	22	0,00		12	31,62
	Mean	-0,09		13	35,47
				Mean	33,00
10	1	3,36			
	2	1,25	0,03	25	13,08
	3	8,63		26	42,88
	Mean	4,41		Mean	27,98
3	23	0,18	0,01	16	48,54
				17	19,47
1	7	9,03		18	12,36
	8	6,80		Mean	26,79
	Mean	8,96			
			0,003	27	5,78

Table 2:components & areas of open period distributions

		Component length (ms)			Area (%)		
[Ach]	exp. No.	Tau1	Tau2	Tau3	Tau1	Tau2	Tau3
300	26	0,0090	0,339	0,72	3,92	18,47	77,62
	27	0,0041	0,111	0,66	6,32	4,68	89,01
	Mean	0,0066	0,225	0,69	5,12	11,57	83,31
100	1	0,0055	0,028	0,64	14,20	3,70	82,20
	2	0,0090	0,110	0,85	14,70	4,90	80,40
	3	0,0072	0,127	0,91	8,20	5,00	86,80
	Mean	0,0072	0,088	0,80	12,37	4,53	83,13
30	29	0,0033	0,024	0,69	14,15	74,19	11,66
	30	0,0064	0,049	0,84	30,59	11,37	58,04
	Mean	0,0049	0,037	0,77	22,37	42,78	34,85
10	6	0,0043	0,044	0,95	18,60	4,10	77,30
	7	0,0065	0,173	1,35	15,10	4,10	80,80
	8	0,0066	0,132	1,04	4,10	0,00	95,90
	9	0,0038	0,018	0,52	45,50	11,10	43,50
	Mean	0,0053	0,092	0,97	20,83	4,83	74,38
3	31	0,0098	0,024	0,66	0,02	0,00	99,98
	32	0,0041	0,192	0,92	2,59	0,31	97,10
	Mean	0,0070	0,108	0,79	1,31	0,15	98,54
1	11	0,0053	0,168	0,71	23,70	8,30	68,00
	12	0,0044	0,134	0,90	13,50	1,40	85,20
	13	0,0032	0,025	1,12	37,50	4,70	57,80
	Mean	0,0043	0,109	0,91	24,90	4,80	70,33
0,3	33	0,0038	0,048	1,04	14,90	4,72	80,38
0,1	16	0,0048	0,028	0,92	8,60	5,30	86,20
	17	0,0031	0,017	0,78	20,60	5,40	74,00
	18	0,0052	0,412	2,00	45,60	9,10	45,40
	Mean	0,0044	0,152	1,23	24,93	6,60	68,53
0,01	21	0,0021	0,095	0,81	57,90	13,60	26,60
	22	0,0112	0,173	0,66	18,10	18,10	63,80
	Mean	0,0067	0,134	0,74	38,00	15,85	45,20

Table 2:components & areas of open period distributions

[Cch]	exp. No.	Component length (ms)			Area (%)		
		Tau1	Tau2	Tau3	Tau1	Tau2	Tau3
100	1	0,0039	0,0234	0,985	29,80	4,20	65,90
	2	0,0057	0,159	1,13	10,50	2,90	86,60
	3	0,0052	0,254	0,926	15,80	10,00	74,20
	Mean	0,0049	0,145	1,01	18,70	5,70	75,57
30	20	0,0056	0,164	1,52	18,50	0,50	81,00
10	6	0,0058	0,217	1,21	5,20	6,10	88,70
	7	0,0028	0,915	1,66	12,50	54,90	32,50
	8	0,0063	0,268	0,79	4,60	6,20	89,20
	Mean	0,0050	0,467	1,22	7,43	22,40	70,13
3	21	0,0074	0,071	1,18	3,80	11,50	84,70
1	11	0,0033	0,0585	0,694	12,90	3,20	83,80
	12	0,0018	0,329	0,813	22,50	18,00	53,50
	13	0,0036	0,631	1,5	6,90	48,20	44,90
	Mean	0,0029	0,340	1,00	14,10	23,13	60,73
0,1	16	0,0066	0,367	0,987	8,10	47,10	44,80
	17	0,0068	0,158	1,21	27,00	6,30	66,70
	18	0,05	0,0473	0,784	17,40	7,90	74,70
	Mean	0,0211	0,191	0,99	17,50	20,43	62,07

Table 2:components & areas of open period distributions

[Ebd]	exp. No.	Component length (ms)			Area (%)		
		Tau1	Tau2	Tau3	Tau1	Tau2	Tau3
100	20	0,0039	0,110	0,13	0,50	51,00	48,50
30	21	0,0041	0,248	0,33	12,80	23,60	63,60
	22	0,0051	0,179	0,34	21,00	0,30	78,70
	Mean	0,0046	0,214	0,33	16,90	11,95	71,15
10	1	0,0057	0,032	0,66	12,40	4,30	83,30
	2	0,0059	0,085	0,64	11,60	2,30	86,10
	3	0,0065	0,143	0,67	9,10	7,10	83,80
	Mean	0,0060	0,087	0,66	11,03	4,57	84,40
3	23	0,0041	0,066	0,64	6,40	1,80	91,80
1	7	0,0017	0,023	0,78	23,10	14,70	62,20
	8	0,0049	0,148	0,68	19,40	6,80	73,90
	Mean	0,0033	0,085	0,73	21,25	10,75	68,05
0,3	24	0,0058	0,118	0,80	12,80	20,80	66,40
0,1	11	0,0035	0,152	0,82	10,40	20,80	68,80
	12	0,0108	0,286	0,90	11,20	27,70	61,20
	13	0,0048	0,230	0,63	10,90	28,90	60,20
	Mean	0,0064	0,223	0,79	10,83	25,80	63,40
0,03	25	0,0038	0,084	1,00	19,90	49,40	30,70
	26	0,0044	0,111	0,68	27,80	28,00	44,20
	Mean	0,0041	0,098	0,84	23,85	38,70	37,45
0,01	16	0,0059	0,241	0,86	12,40	27,70	59,90
	17	0,0044	0,194	0,85	22,50	37,30	40,20
	18	0,0063	0,118	0,66	11,70	39,50	48,80
	Mean	0,0055	0,184	0,79	15,53	34,83	49,63
0,003	27	0,0088	0,151	1,00	9,90	70,10	20,00

Table 3:components & areas of shut time distributions

[Ach]	exp. No.	Component length (ms)						Area (%)					
		Tau1	Tau2	Tau3	Tau4	Tau5	Tau6	Tau1	Tau2	Tau3	Tau4	Tau5	Tau6
300	26	0,0029	0,027	0,32	11,2	96,5		98,66	0,77	0,23	0,28	0,06	
	27	0,0026	0,013	0,11	1,1	7,9		98,68	0,69	0,23	0,32	0,09	
	Mean	0,0027	0,020	0,21	6,1	52,2		98,67	0,73	0,23	0,30	0,07	
100	1	0,0041	0,026	0,48	7,8	698,2		96,10	0,90	1,50	1,30	0,10	
	2	0,0063	0,012	0,63	14,8	915,7		90,60	6,70	1,20	1,00	0,50	
	3	0,0047	0,022	0,34	4,5	104,7		97,50	1,00	0,80	0,40	0,30	
	Mean	0,0050	0,020	0,48	9,0	572,9		94,73	2,87	1,17	0,90	0,30	
30	29	0,0031	0,013	0,29	5,8	207,8		95,31	0,71	1,70	1,87	0,41	
	30	0,0036	0,018	0,19	1,8	190,3		98,10	0,44	0,40	0,93	0,12	
	Mean	0,0033	0,015	0,24	3,8	199,0		96,70	0,58	1,05	1,40	0,26	
10	6	0,0029	0,011	0,49	4,8	641,1		94,30	4,00	1,20	0,40	0,10	
	7	0,0035	0,018	0,46	2,6	76,9		95,10	2,30	0,90	0,80	1,00	
	8	0,0034	0,047	0,21	10,7	769,7		96,70	1,70	0,40	0,50	0,60	
	9	0,0038	0,025	0,20	2,7	76,3	5035	87,30	1,80	5,40	3,50	1,40	0,50
	Mean	0,0034	0,025	0,34	5,2	391,0		93,35	2,45	1,98	1,30	0,78	
3	31	0,0032	0,070	6,53	77,4	518,1		99,18	0,49	0,21	0,12	0,00	
	32	0,0031	0,015	0,20	2,5	22,2		97,89	1,45	0,23	0,12	0,31	
	Mean	0,0031	0,043	3,37	40,0	270,1		98,53	0,97	0,22	0,12	0,15	
1	11	0,0027	0,014	0,41	10,5	290,6		96,20	1,20	0,90	0,90	0,80	
	12	0,0031	0,010	0,27	3,9	81,0		96,50	2,20	0,50	0,60	0,30	
	13	0,0035	0,048	0,40	4,3	81,2	1880	94,30	1,70	1,10	1,10	1,50	0,30
	Mean	0,0031	0,024	0,36	6,2	150,9		95,67	1,70	0,83	0,87	0,87	
0,3	33	0,0029	0,139	0,70	8,5	971,9		97,83	0,34	0,29	0,40	1,13	
0,1	16	0,0031	0,014	0,24	8,1	688,7		96,60	1,40	0,80	0,50	0,80	
	17	0,0030	0,038	0,40	3,7	961,9		97,40	0,70	0,50	0,20	1,10	
	18	0,0036	0,013	0,42	15,5	1847,0		86,10	2,40	5,50	2,80	3,10	
	Mean	0,0032	0,022	0,35	9,1	1165,9		93,37	1,50	2,27	1,17	1,67	
0,01	21	0,0025	0,026	0,18	25,1	416,1		90,00	0,00	1,20	1,20	7,60	
	22	0,0029	0,092	1,42	20,4	1058,0		95,40	0,40	0,90	0,30	3,00	
	Mean	0,0027	0,059	0,80	22,8	737,1		92,70	0,20	1,05	0,75	5,30	

Table 3:components & areas of shut time distributions

[Cch]	exp. No.	Component length (ms)						Area (%)					
		Tau1	Tau2	Tau3	Tau4	Tau5	Tau6	Tau1	Tau2	Tau3	Tau4	Tau5	Tau6
100	1	0,0031	0,018	0,68	18,3	719,1		94,60	1,80	2,20	1,20	0,30	
	2	0,0032	0,071	2,86	68,2	13818,0		98,10	0,70	1,00	0,20	0,10	
	3	0,0028	0,010	2,59	46,6	2627,0		95,30	2,80	1,00	0,80	0,10	
	Mean	0,0030	0,033	2,04	44,4	5721,4		96,00	1,77	1,40	0,73	0,17	
30	20	0,0029	0,055	1,21	17,9	80,9		96,80	1,10	0,90	1,00	0,30	
10	6	0,0037	0,054	0,72	6,8	263,5		97,10	1,20	0,50	0,50	0,70	
	7	0,0037	0,021	0,25	18,6	222,4		97,80	0,80	0,20	0,60	0,50	
	8	0,0033	0,024	0,28	7,7	123,6		98,40	0,50	0,20	0,50	0,30	
	Mean	0,0036	0,033	0,41	11,1	203,2		97,77	0,83	0,30	0,53	0,50	
3	21	0,0033	0,058	0,61	21,3	141,7		95,10	1,30	0,20	0,40	3,00	
1	11	0,0034	0,023	1,02	20,8	772,7		98,20	0,90	0,40	0,30	0,30	
	12	0,0032	0,019	0,63	56,3	987,1		98,30	0,60	0,20	0,20	0,70	
	13	0,0037	0,011	0,60	28,5	1387,0		96,10	2,10	0,40	0,20	1,20	
	Mean	0,0034	0,018	0,75	35,2	1048,9		97,53	1,20	0,33	0,23	0,73	
0,1	16	0,0026	0,014	0,39	13,7	1178,0		96,80	0,70	0,20	0,10	2,20	
	17	0,0033	0,016	0,17	3,5	207,4		95,90	1,30	0,90	0,60	1,30	
	18	0,0031	0,044	0,64	24,9	365,9		96,40	1,30	0,60	0,60	1,10	
	Mean	0,0030	0,025	0,40	14,0	583,8		96,37	1,10	0,57	0,43	1,53	

Table 3:components & areas of shut time distributions

		Component length (ms)						Area (%)					
[Ebd]	exp. No.	Tau1	Tau2	Tau3	Tau4	Tau5	Tau6	Tau1	Tau2	Tau3	Tau4	Tau5	Tau6
100	20	0,0058	0,085	4,95	1959,0	2520,0		25,20	73,30	0,80	0,70	0,10	
30	21	0,0038	0,068	3,86	57,6	5626,0		56,70	39,40	2,20	1,00	0,70	
	22	0,0033	0,057	1,19	22,3	768,4		69,90	24,90	2,30	1,40	1,50	
	Mean	0,0036	0,063	2,53	40,0	3197,2		63,30	32,15	2,25	1,20	1,10	
10	1	0,0029	0,066	1,63	9,6	296,9		86,00	11,60	1,50	0,80	0,10	
	2	0,0032	0,064	1,27	7,1	160,4		86,40	11,70	0,80	0,90	0,20	
	3	0,0029	0,071	1,87	24,0	382,2		85,60	12,50	1,20	0,60	0,10	
	Mean	0,0030	0,067	1,59	13,6	279,8		86,00	11,93	1,17	0,77	0,13	
3	23	0,0028	0,038	1,23	9,2	164,3		96,30	2,60	0,30	0,70	0,10	
1	7	0,0028	0,030	0,29	3,0	82,7		95,10	1,20	0,60	0,50	2,60	
	8	0,0028	0,034	0,62	21,8	301,0		96,70	1,50	0,50	1,20	0,20	
	Mean	0,0028	0,032	0,45	12,4	191,9		95,90	1,35	0,55	0,85	1,40	
0,3	24	0,0033	0,087	0,78	18,8	206,1		91,60	0,80	0,80	1,70	5,10	
0,1	11	0,0032	0,034	0,28	3,2	193,9		95,20	0,70	0,50	0,90	2,60	
	12	0,0033	0,026	0,42	5,2	107,6		93,50	1,40	0,90	1,60	2,60	
	13	0,0041	0,019	0,13	0,6	22,5		44,40	5,30	16,00	28,00	6,30	
	Mean	0,0035	0,026	0,27	3,0	108,0		77,70	2,47	5,80	10,17	3,83	
0,03	25	0,0027	0,136	2,12	11,6	169,0		81,90	0,60	0,70	5,40	11,40	
	26	0,0033	0,152	2,21	36,9	582,9		87,90	1,30	1,80	0,70	8,30	
	Mean	0,0030	0,144	2,17	24,3	376,0		84,90	0,95	1,25	3,05	9,85	
0,01	16	0,0031	0,014	0,38	3,5	624,3		94,40	2,00	0,90	0,90	1,80	
	17	0,0032	0,011	0,22	4,2	1975,0		83,40	1,70	0,80	2,80	11,30	
	18	0,0031	0,022	0,76	5,1	122,7		84,90	0,30	1,70	4,50	8,60	
	Mean	0,0031	0,016	0,45	4,2	907,3		87,57	1,33	1,13	2,73	7,23	
0,003	27	0,0024	0,039	2,66	8,0	1573		85,00	0,70	1,30	6,10	6,80	

Table 4:components & areas of burst distributions

[Ach]	exp. No.	Component length (ms)				Area (%)			
		Tau1	Tau2	Tau3	Tau4	Tau1	Tau2	Tau3	Tau4
300	26	0,0064	-	0,25	29,7	70,60	0,00	5,10	24,30
	27	0,0042	0,023	0,59	29,2	63,10	15,40	2,70	18,70
	Mean	0,0053	0,023	0,42	29,5	66,85	7,70	3,90	21,50
100	1	0,0053	0,038	0,39	21,8	71,40	15,10	1,50	11,90
	2	0,0056	0,020	0,07	20,6	63,10	16,10	6,50	14,40
	3	0,0060	0,056	0,60	32,4	69,80	10,80	1,60	17,90
	Mean	0,0056	0,038	0,36	24,9	68,10	14,00	3,20	14,73
30	29	0,0043	0,028	0,37	16,1	76,50	16,00	0,90	6,60
	30	0,0054	0,027	5,91	39,4	70,40	8,20	4,20	17,20
	Mean	0,0049	0,027	3,14	27,8	73,45	12,10	2,55	11,90
10	6	0,0029	0,025	0,29	19,6	73,00	12,10	1,20	13,70
	7	0,0040	0,030	0,27	33,1	69,80	11,20	2,90	16,20
	8	0,0049	0,011	0,14	11,4	35,20	7,50	3,70	53,70
	9	0,0039	0,025	0,10	4,3	72,50	15,60	0,80	11,00
	Mean	0,0039	0,023	0,20	17,1	62,63	11,60	2,15	23,65
3	31	0,0095	0,118	1,19	40,3	59,10	2,00	5,00	39,80
	32	0,0118	0,179	1,47	44,6	55,40	4,60	5,30	34,70
	Mean	0,0107	0,149	1,33	42,5	57,25	3,30	5,15	37,25
1	11	0,0034	0,025	0,35	8,2	70,70	11,60	1,70	16,00
	12	0,0035	0,026	0,38	34,2	76,80	9,10	2,40	11,80
	13	0,0026	0,018	0,11	11,6	80,00	7,20	1,70	11,20
	Mean	0,0032	0,023	0,28	18,0	75,83	9,30	1,93	13,00
0,3	33	0,0034	0,023	0,29	25,4	62,30	15,40	9,70	12,50
0,1	16	0,0051	0,024	0,26	24,3	43,30	26,40	10,60	19,70
	17	0,0029	0,025	0,51	28,8	64,90	14,90	12,80	7,30
	18	0,0054	0,138	0,64	11,5	78,00	3,00	5,00	14,10
	Mean	0,0045	0,063	0,47	21,5	62,07	14,77	9,47	13,70
0,01	21	0,0020	0,249	0,28	6,9	75,40	12,70	8,80	3,00
	22	0,0041	0,050	0,66	24,0	53,80	29,00	13,30	3,90
	Mean	0,0031	0,150	0,47	15,5	64,60	20,85	11,05	3,45

Table 4:components & areas of burst distributions

[Cch]	exp. No.	Component length (ms)				Area (%)			
		Tau1	Tau2	Tau3	Tau4	Tau1	Tau2	Tau3	Tau4
100	1	0,0039	0,026	0,23	10,3	73,70	9,00	0,10	17,30
	2	0,0047	0,028	0,26	22,9	63,70	9,20	0,70	26,40
	3	0,0051	0,022	0,36	15,4	69,80	9,20	1,20	19,70
	Mean	0,0046	0,025	0,28	16,2	69,07	9,13	0,67	21,13
30	20	0,0045	0,137	1,30	15,1	68,10	2,40	2,20	27,30
10	6	0,0045	0,031	0,29	17,3	42,40	10,00	3,40	44,20
	7	0,0022	0,018	0,17	39,8	81,10	5,70	2,60	10,60
	8	0,0053	0,037	0,25	21,7	56,50	5,80	3,80	34,00
	Mean	0,0040	0,029	0,24	26,3	60,00	7,17	3,27	29,60
3	21	0,0094	0,055	1,08	10,2	12,50	38,70	7,90	40,80
1	11	0,0032	0,020	0,23	40,2	72,20	14,00	3,00	10,80
	12	0,0028	0,049	0,51	14,3	67,40	9,70	13,30	9,60
	13	0,0048	0,081	0,67	42,3	54,00	11,60	16,50	17,90
	Mean	0,0036	0,050	0,47	32,3	64,53	11,77	10,93	12,77
0,1	16	0,0043	0,123	0,72	35,7	32,50	30,00	31,10	5,90
	17	0,0046	0,027	0,36	12,1	72,20	7,50	6,60	13,70
	18	0,0045	0,034	0,58	14,7	65,50	13,50	6,50	14,50
	Mean	0,0045	0,061	0,55	20,8	56,73	17,00	14,73	11,37

Table 4:components & areas of burst distributions

[Ebd]	exp. No.	Component length (ms)				Area (%)			
		Tau1	Tau2	Tau3	Tau4	Tau1	Tau2	Tau3	Tau4
3	23	0,0029	0,086	-	7,3	53,30	11,10	0,00	35,60
1	7	0,0059	0,024	0,24	12,1	34,00	36,90	13,30	15,70
	8	0,0030	0,022	0,29	8,5	63,80	13,30	5,70	17,20
	Mean	0,0045	0,023	0,27	10,3	48,90	25,10	9,50	16,45
0,3	24	0,0054	0,135	0,38	9,4	31,10	37,60	17,30	14,00
0,1	11	0,0076	0,135	0,63	25,2	27,10	23,90	39,80	9,20
	12	0,0059	0,073	0,68	19,7	34,60	21,20	35,40	8,90
	13	0,0047	0,098	0,61	22,3	44,90	17,30	31,20	6,60
	Mean	0,0061	0,102	0,64	22,4	35,53	20,80	35,47	8,23
0,03	25	0,0084	0,114	0,58	8,2	21,40	69,00	4,30	5,40
	26	0,0018	0,023	0,25	9,3	75,90	8,50	13,40	2,20
	Mean	0,0051	0,068	0,41	8,8	48,65	38,75	8,85	3,80
0,01	16	0,0035	0,031	0,50	17,5	53,40	16,00	21,00	9,60
	17	0,0038	0,104	0,65	17,5	37,70	23,70	36,30	2,30
	18	0,0044	0,065	0,38	14,7	21,30	31,50	44,30	2,90
	Mean	0,0039	0,067	0,51	16,6	37,47	23,73	33,87	4,93
0,003	27	0,0128	-	0,21	11,5	19,60	0,00	77,90	2,50

Table 5: components & areas of single opening distributions

fixed fit approach'		Component length (ms)			Area (%)		
[Ach]	exp. No.	Tau1	Tau2	Tau3	Tau1	Tau2	Tau3
300	26	0,0090	0,339	0,72	96,60	3,40	0,00
	27	0,0041	0,111	0,66	91,90	6,80	1,30
	Mean	0,0066	0,225	0,69	94,25	5,10	0,65
100	1	0,0055	0,028	0,64	80,80	18,20	1,00
	2	0,0090	0,110	0,85	90,90	8,40	0,70
	3	0,0072	0,127	0,91	90,80	9,20	0,00
	Mean	0,0072	0,088	0,80	87,50	11,93	0,57
30	29	0,0033	0,024	0,69	84,70	14,70	0,60
	30	0,0064	0,049	0,84	96,70	3,30	0,00
	Mean	0,0049	0,037	0,77	90,70	9,00	0,30
10	6	0,0043	0,044	0,95	86,70	11,70	1,60
	7	0,0065	0,173	1,35	93,50	6,20	0,30
	8	0,0066	0,132	1,04	87,70	6,10	6,20
	9	0,0038	0,018	0,52	82,30	16,40	1,30
	Mean	0,0053	0,092	0,97	87,55	10,10	2,35
3	31	0,0098	0,024	0,66	96,70	0,00	3,30
	32	0,0041	0,192	0,92	88,80	10,20	1,20
	Mean	0,0070	0,108	0,79	92,75	5,10	2,25
1	11	0,0053	0,168	0,71	90,90	7,60	1,50
	12	0,0044	0,134	0,90	92,90	6,50	0,60
	13	0,0032	0,025	1,12	90,00	8,00	2,00
	Mean	0,0043	0,109	0,91	91,27	7,37	1,37
0,3	33	0,0038	0,048	1,04	78,90	17,30	3,80
0,1	16	0,0048	0,028	0,92	59,20	34,60	6,20
	17	0,0031	0,017	0,78	68,40	21,90	9,70
	18	0,0052	0,412	2,00	89,70	7,00	3,30
	Mean	0,0044	0,152	1,23	72,43	21,17	6,40
0,01	21	0,0021	0,095	0,81	44,80	31,10	24,10
	22	0,0112	0,173	0,66	72,90	25,60	1,50
	Mean	0,0067	0,134	0,74	58,85	28,35	12,80

Table 5: components & areas of single opening distributions

fixed fit approach'		Component length (ms)			Area (%)		
[Cch]	exp. No.	Tau1	Tau2	Tau3	Tau1	Tau2	Tau3
100	1	0,0039	0,0234	0,985	88,20	9,80	2,00
	2	0,0057	0,159	1,13	95,10	3,40	1,50
	3	0,0052	0,254	0,926	97,00	3,00	0,00
	Mean	0,0049	0,145	1,01	93,43	5,40	1,17
30	20	0,0056	0,164	1,52	89,90	2,80	7,20
10	6	0,0058	0,217	1,21	83,30	13,70	3,00
	7	0,0028	0,915	1,66	95,40	4,60	0,00
	8	0,0063	0,268	0,79	91,80	8,00	0,20
	Mean	0,0050	0,467	1,22	90,17	8,77	1,07
3	21	0,0074	0,071	1,18	29,70	57,00	13,30
1	11	0,0033	0,0585	0,694	91,70	7,60	0,70
	12	0,0018	0,329	0,813	94,70	5,30	0,00
	13	0,0036	0,631	1,5	84,30	15,70	0,00
	Mean	0,0029	0,340	1,00	90,23	9,53	0,23
0,1	16	0,0066	0,367	0,987	45,30	54,60	0,10
	17	0,0068	0,158	1,21	85,10	10,50	4,40
	18	0,05	0,0473	0,784	82,30	14,50	3,20
	Mean	0,0211	0,191	0,99	70,90	26,53	2,57

Table 5: components & areas of single opening distributions

fixed fit approach'		Component length (ms)			Area (%)		
[Ebd]	exp. No.	Tau1	Tau2	Tau3	Tau1	Tau2	Tau3
3	23	0,0041	0,066	0,64	68,50	23,00	8,50
1	7	0,0017	0,023	0,78	67,10	29,20	3,70
	8	0,0049	0,148	0,68	84,10	13,40	2,50
	Mean	0,0033	0,085	0,73	75,60	21,30	3,10
0,3	24	0,0058	0,118	0,80	37,30	58,00	4,70
0,1	11	0,0035	0,152	0,82	53,90	40,10	6,00
	12	0,0108	0,286	0,90	53,40	45,70	0,90
	13	0,0048	0,230	0,63	65,10	34,90	0,00
	Mean	0,0064	0,223	0,79	57,47	40,23	2,30
0,03	25	0,0038	0,084	1,00	27,70	67,40	4,90
	26	0,0044	0,111	0,68	60,20	36,40	3,40
	Mean	0,0041	0,098	0,84	43,95	51,90	4,15
0,01	16	0,0059	0,241	0,86	70,20	29,00	0,80
	17	0,0044	0,194	0,85	46,00	50,00	4,00
	18	0,0063	0,118	0,66	26,30	65,10	8,60
	Mean	0,0055	0,184	0,79	47,50	48,03	4,47
0,003	27	0,0088	0,151	1,00	22,20	77,80	0,00

Table 5: components & areas of single opening distributions

free fit approach'		Component length (ms)			Area (%)		
[Ach]	exp. No.	Tau1	Tau2	Tau3	Tau1	Tau2	Tau3
300	26	0,0064	0,123	-	96,00	4,00	0,00
	27	0,0048	0,029	0,74	82,00	16,20	1,80
	Mean	0,0056	0,076	0,74	89,00	10,10	0,90
100	1	0,0050	0,026	0,31	79,80	18,90	1,30
	2	0,0076	0,041	0,99	90,90	8,40	0,70
	3	0,0034	0,018	0,19	81,30	16,20	2,50
	Mean	0,0053	0,028	0,49	84,00	14,50	1,50
30	29	0,0041	0,020	0,21	80,00	18,60	1,40
	30	0,0062	0,034	-	95,00	5,00	0,00
	Mean	0,0052	0,027	0,21	87,50	11,80	0,70
10	6	0,0029	0,020	0,23	85,20	13,20	1,60
	7	0,0061	0,097	1,51	92,20	7,30	0,50
	8	0,0049	0,015	0,47	74,80	16,20	9,00
	9	0,0039	0,017	0,28	81,00	17,50	1,60
	Mean	0,0045	0,037	0,62	83,30	13,55	3,18
3	31	0,0096	0,039	1,61	96,90	0,00	3,10
	32	0,0114	0,113	0,92	88,40	8,80	2,80
	Mean	0,0105	0,076	1,26	92,65	4,40	2,95
1	11	0,0037	0,026	0,51	84,50	12,60	2,90
	12	0,0038	0,033	0,50	88,90	9,30	1,90
	13	0,0027	0,019	0,76	90,20	8,10	1,80
	Mean	0,0034	0,026	0,59	87,87	10,00	2,20
0,3	33	0,0033	0,023	0,43	70,60	19,80	6,60
0,1	16	0,0051	0,024	0,30	55,10	35,60	9,30
	17	0,0026	0,016	0,28	74,20	16,30	9,50
	18	0,0054	0,201	1,90	88,90	6,40	4,70
	Mean	0,0044	0,080	0,83	72,73	19,43	7,83
0,01	21	0,0134	0,196	0,20	67,00	30,60	2,40
	22	0,0036	0,037	0,28	61,40	30,40	8,20
	Mean	0,0085	0,116	0,24	64,20	30,50	5,30

Table 5:components & areas of single opening distributions

free fit approach'		Component length (ms)			Area (%)		
[Cch]	exp. No.	Tau1	Tau2	Tau3	Tau1	Tau2	Tau3
100	1	0,0039	0,021	1,11	87,20	10,80	2,00
	2	0,0048	0,022	1,07	86,60	11,20	2,20
	3	0,0067	0,115	1,64	95,80	4,20	0,00
	Mean	0,0051	0,053	1,27	89,87	8,73	1,40
30	20	0,0045	0,167	1,21	91,90	1,70	6,40
10	6	0,0048	0,039	0,97	76,00	17,10	6,90
	7	0,0022	0,017	0,19	91,10	6,50	2,40
	8	0,0054	0,044	0,52	88,10	8,60	3,20
	Mean	0,0041	0,033	0,56	85,07	10,73	4,17
3	21	0,0095	0,053	0,88	20,50	62,50	17,00
1	11	0,0027	0,012	0,18	79,20	18,30	2,60
	12	0,0024	0,042	0,32	84,80	9,40	5,80
	13	0,0056	0,205	1,31	73,70	24,90	1,40
	Mean	0,0036	0,086	0,60	79,23	17,53	3,27
0,1	16	0,0047	0,145	0,56	43,00	46,00	11,00
	17	0,0061	0,169	1,40	86,30	10,20	3,40
	18	0,0046	0,034	0,69	66,20	15,10	18,70
	Mean	0,0051	0,116	0,88	65,17	23,77	11,03

Table 5: components & areas of single opening distributions

free fit approach'		Component length (ms)			Area (%)		
[Ebd]	exp. No.	Tau1	Tau2	Tau3	Tau1	Tau2	Tau3
3	23	0,0030	0,119	1,51	79,60	18,40	2,00
1	7	0,0063	0,026	0,29	44,10	44,80	11,10
	8	0,0037	0,032	0,45	78,80	15,40	5,80
	Mean	0,0050	0,029	0,37	61,45	30,10	8,45
0,3	24	0,0054	0,131	0,63	40,20	55,40	4,50
0,1	11	0,0079	0,116	0,33	40,20	28,10	31,70
	12	0,0062	0,066	0,37	48,00	24,70	27,30
	13	0,0043	0,048	0,24	59,80	14,50	25,70
	Mean	0,0061	0,077	0,31	49,33	22,43	28,23
0,03	25	0,0027	0,065	0,30	34,80	50,20	15,00
	26	0,0038	0,067	0,30	60,30	27,70	12,00
	Mean	0,0033	0,066	0,30	47,55	38,95	13,50
0,01	16	0,0066	0,104	0,41	64,60	23,40	11,90
	17	0,0039	0,104	0,34	46,60	26,80	26,70
	18	0,0041	0,057	0,25	26,70	35,90	37,40
	Mean	0,0049	0,088	0,33	45,97	28,70	25,33
0,003	27	0,0125	0,164		23,30	76,70	

Table 6: components & areas of dense burst distributions

[Ach]	exp. No.	Component length (ms)				Area (%)			
		Tau1	Tau2	Tau3	Tau4	Tau1	Tau2	Tau3	Tau4
300	26	0,0064	-	0,25	29,7	0,00	0,00	6,80	93,20
	27	0,0042	0,023	0,59	29,2	0,10	0,20	7,20	92,50
	Mean	0,0053	0,023	0,42	29,5	0,05	0,10	7,00	92,85
100	1	0,0053	0,038	0,39	21,8	0,00	0,10	16,00	83,90
	2	0,0056	0,020	0,07	20,6	0,00	0,00	5,60	94,40
	3	0,0060	0,056	0,60	32,4	0,00	2,90	4,40	92,70
	Mean	0,0056	0,038	0,36	24,9	0,00	1,00	8,67	90,33
30	29	0,0043	0,028	0,37	16,1	5,60	36,90	45,30	12,20
	30	0,0054	0,027	5,91	39,4	0,00	4,00	19,40	76,60
	Mean	0,0049	0,027	3,14	27,8	2,80	20,45	32,35	44,40
10	6	0,0029	0,025	0,29	19,6	0,00	7,00	3,20	89,80
	7	0,0040	0,030	0,27	33,1	0,00	3,50	11,80	84,70
	8	0,0049	0,011	0,14	11,4	0,00	0,00	0,00	100,00
	9	0,0039	0,025	0,10	4,3	0,00	0,00	19,90	80,10
	Mean	0,0039	0,023	0,20	17,1	0,00	2,63	8,73	88,65
3	31	0,0095	0,118	1,19	40,3	0,00	3,10	7,80	89,00
	32	0,0118	0,179	1,47	44,6	0,00	0,00	8,90	91,10
	Mean	0,0107	0,149	1,33	42,5	0,00	1,55	8,35	90,05
1	11	0,0034	0,025	0,35	8,2	0,00	3,70	0,00	96,30
	12	0,0035	0,026	0,38	34,2	0,00	1,90	4,60	93,50
	13	0,0026	0,018	0,11	11,6	0,00	0,00	8,20	91,80
	Mean	0,0032	0,023	0,28	18,0	0,00	1,87	4,27	93,87
0,3	33	0,0034	0,023	0,29	25,4	0,00	0,00	20,10	79,90
0,1	16	0,0051	0,024	0,26	24,3	0,00	0,00	14,60	85,40
	17	0,0029	0,025	0,51	28,8	0,00	3,50	42,40	54,10
	18	0,0054	0,138	0,64	11,5	0,00	0,00	0,00	100,00
	Mean	0,0045	0,063	0,47	21,5	0,00	1,17	19,00	79,83
0,01	21	0,0020	0,249	0,28	6,9	0,00	0,00	17,10	82,90
	22	0,0041	0,050	0,66	24,0	0,00	0,00	69,60	30,40
	Mean	0,0031	0,150	0,47	15,5	0,00	0,00	43,35	56,65

Table 6: components & areas of dense burst distributions

[Cch]	exp. No.	Component length (ms)				Area (%)			
		Tau1	Tau2	Tau3	Tau4	Tau1	Tau2	Tau3	Tau4
100	1	0,0039	0,026	0,23	10,3	0,00	2,10	0,70	97,20
	2	0,0047	0,028	0,26	22,9	0,00	3,20	1,80	95,00
	3	0,0051	0,022	0,36	15,4	0,00	0,00	1,70	98,30
	Mean	0,0046	0,025	0,28	16,2	0,00	1,77	1,40	96,83
30	20	0,0045	0,137	1,30	15,1	0,00	1,60	0,00	98,40
10	6	0,0045	0,031	0,29	17,3	0,00	0,00	0,10	99,90
	7	0,0022	0,018	0,17	39,8	0,00	0,00	3,10	96,90
	8	0,0053	0,037	0,25	21,7	0,00	0,00	5,00	95,00
	Mean	0,0040	0,029	0,24	26,3	0,00	0,00	2,73	97,27
3	21	0,0094	0,055	1,08	10,2	0,00	0,00	0,00	100,00
1	11	0,0032	0,020	0,23	40,2	0,00	0,00	14,70	85,30
	12	0,0028	0,049	0,51	14,3	0,00	0,00	43,10	56,90
	13	0,0048	0,081	0,67	42,3	0,00	0,00	29,20	70,80
	Mean	0,0036	0,050	0,47	32,3	0,00	0,00	29,00	71,00
0,1	16	0,0043	0,123	0,72	35,7	0,00	0,00	74,70	25,30
	17	0,0046	0,027	0,36	12,1	0,00	2,90	2,20	94,90
	18	0,0045	0,034	0,58	14,7	0,00	0,00	17,90	82,10
	Mean	0,0045	0,061	0,55	20,8	0,00	0,97	31,60	67,43

Table 6: components & areas of dense burst distributions

[Ebd]	exp. No.	Component length (ms)				Area (%)			
		Tau1	Tau2	Tau3	Tau4	Tau1	Tau2	Tau3	Tau4
3	23	0,0029	0,086	-	7,3	0,00	0,20	0,00	99,80
1	7	0,0059	0,024	0,24	12,1	0,00	0,00	16,80	83,20
	8	0,0030	0,022	0,29	8,5	0,00	0,20	5,90	93,90
	Mean	0,0045	0,023	0,27	10,3	0,00	0,10	11,35	88,55
0,3	24	0,0054	0,135	0,38	9,4	0,00	0,00	36,50	63,50
0,1	11	0,0076	0,135	0,63	25,2	0,00	0,00	70,00	30,00
	12	0,0059	0,073	0,68	19,7	0,00	0,00	65,50	34,50
	13	0,0047	0,098	0,61	22,3	0,00	0,00	72,40	27,60
	Mean	0,0061	0,102	0,64	22,4	0,00	0,00	69,30	30,70
0,03	25	0,0084	0,114	0,58	8,2	0,00	16,00	44,70	39,40
	26	0,0018	0,023	0,25	9,3	0,00	0,00	56,90	43,10
	Mean	0,0051	0,068	0,41	8,8	0,00	8,00	50,80	41,25
0,01	16	0,0035	0,031	0,50	17,5	0,00	0,00	42,80	57,20
	17	0,0038	0,104	0,65	17,5	0,00	0,00	85,70	14,30
	18	0,0044	0,065	0,38	14,7	0,00	0,00	81,80	18,20
	Mean	0,0039	0,067	0,51	16,6	0,00	0,00	70,10	29,90
0,003	27	0,0128	-	0,21	11,5	0,00	0,00	82,20	17,80

Table 7: calculation of true mean opening length

[ACh]	exp. No.	dense bursts (2 components)		gaps in dense bursts			calculated values for openings in dense bursts	
		predicted Length	predicted number	predicted Length	total predicted number	predicted number per burst	calculated number	calculated length
(µM)		μ_{burst} (ms)	n_{burst}	μ_{gap} (ms)	n_{gaps}	$n_{gaps/burst}$	$n_{gaps/burst}+1$	μ_{open} (ms)
300,00	26	27,29	26,04	0,0033	6269,25	240,8	241,8	0,110
300,00	27	27,26	40,05	0,0029	12739,30	318,1	319,1	0,083
100,00	1	18,62	184,13	0,0045	19416,00	105,5	106,5	0,170
100,00	2	19,85	190,94	0,0072	17147,50	89,8	90,8	0,212
100,00	3	30,02	124,45	0,0052	18728,90	150,5	151,5	0,193
30,00	29	12,61	59,94	0,0036	5586,51	93,2	94,2	0,130
30,00	30	31,43	46,22	0,0038	8231,51	178,1	179,1	0,172
10,00	8	11,72	252,13	0,0038	15456,60	86,0	87,0	0,200
10,00	9	3,60	147,08	0,0042	21301,90	88,2	89,2	0,315
10,00	6	17,75	179,75	0,0037	12513,30	49,6	50,6	0,228
10,00	7	28,49	241,55	0,0049	3193,80	21,7	22,7	0,154
3,00	31	36,18	26,04	0,0034	7697,23	295,6	296,6	0,119
3,00	32	40,51	35,02	0,0037	7689,08	219,6	220,6	0,180
1,00	11	8,11	229,24	0,0035	13407,40	58,5	59,5	0,133
1,00	12	32,16	118,14	0,0038	19580,00	165,7	166,7	0,189
1,00	13	11,38	418,14	0,0044	15534,20	37,2	38,2	0,294
0,30	33	20,68	48,15	0,0031	6114,51	127,0	128,0	0,159
0,10	16	21,06	145,63	0,0037	15508,60	106,5	107,5	0,192
0,10	17	15,47	124,56	0,0032	15011,40	120,5	121,5	0,124
0,10	18	12,76	37,02	0,0043	923,23	24,9	25,9	0,488
0,01	21	5,23	25,06	0,0026	1215,53	48,5	49,5	0,103
0,01	22	7,65	36,20	0,0030	2960,89	81,8	82,8	0,089

Table 7: calculation of true mean opening length

[CCh]	exp. No.	dense bursts (2 components)		gaps in dense bursts			calculated values for openings in dense bursts	
		predicted Length	predicted number	predicted Length	total predicted number	predicted number per burst	calculated number	calculated length
(μM)		μ_{burst} (ms)	n_{burst}	μ_{gap} (ms)	n_{gaps}	$n_{gaps/burst}$	$n_{gaps/burst}+1$	μ_{open} (ms)
100,00	1	10,70	289,01	0,0038	14169,2	49,0	50,0	0,210
100,00	2	22,55	451,97	0,0035	47430,3	104,9	105,9	0,209
100,00	3	15,07	110,17	0,0036	9540,16	86,6	87,6	0,169
30,00	20	15,98	122,32	0,0034	6753,65	55,2	56,2	0,281
10,00	6	17,80	283,31	0,0041	17147,2	60,5	61,5	0,285
10,00	7	38,69	184,23	0,0041	24185,3	131,3	132,3	0,288
10,00	8	20,97	158,25	0,0035	22415,1	141,6	142,6	0,144
3,00	21	10,59	120,07	0,0036	5236,51	43,6	44,6	0,234
1,00	11	34,25	88,76	0,0037	21989,4	247,7	248,7	0,134
1,00	12	21,40	110,41	0,0033	19128,6	173,2	174,2	0,120
1,00	13	29,58	252,48	0,0040	29057	115,1	116,1	0,251
0,10	16	9,40	111,55	0,0030	10259,5	92,0	93,0	0,098
0,10	17	10,75	200,11	0,0035	16541,7	82,7	83,7	0,125
0,10	18	11,02	201,31	0,0034	15620,3	77,6	78,6	0,137

Table 7: calculation of true mean opening length

[Ebd]	exp. No.	dense bursts (2 components)		gaps in dense bursts			calculated values for openings in dense bursts	
		predicted Length	predicted number	predicted Length	total predicted number	predicted number per burst	calculated number	calculated length
(μM)		μ_{burst} (ms)	n_{burst}	μ_{gap} (ms)	n_{gaps}	$n_{gaps/burst}$	$n_{gaps/burst}+1$	μ_{open} (ms)
3,000	23	7,70	82,1	0,0042	3670,7	44,7	45,7	0,164
1,000	7	10,04	231,7	0,0036	14216,1	61,3	62,3	0,158
1,000	8	7,95	257,1	0,0032	18542,1	72,1	73,1	0,106
0,300	24	6,03	176,8	0,0038	5735,9	32,4	33,4	0,177
0,100	11	7,81	313,6	0,0036	16072,3	51,2	52,2	0,146
0,100	12	6,91	313,3	0,0039	11527,2	36,8	37,8	0,179
0,100	13	6,43	339,7	0,0046	13505,1	39,8	40,8	0,153
0,030	25	3,96	97,2	0,0035	2044,1	21,0	22,0	0,177
0,030	26	3,96	132,1	0,0036	3804,3	28,8	29,8	0,129
0,010	16	9,71	220,8	0,0039	12591,9	57,0	58,0	0,163
0,010	17	2,98	80,4	0,0036	1353,7	16,8	17,8	0,164
0,010	18	2,86	164,3	0,0033	3943,4	24,0	25,0	0,111
0,003	27	1,99	82,0	0,0029	1667,6	20,3	21,3	0,091

11. PUBLICATIONS

Neuser K, Husse J, Stock P and Gerber B (2005) Appetitive olfactory learning in *Drosophila* larvae: effects of repetition, reward strength, age, gender, assay type and memory span. Anim Behav 69: 891-898.

Riemensperger T, Voeller T, Stock P, Buchner E and Fiala A (2005) Punishment prediction by dopaminergic neurons in *Drosophila*. Curr Biol 15: 1953-1960.

Erklärung

gemäß § 4 Absatz 3 der Promotionsordnung der Fakultät für Biologie der Bayerischen Julius-Maximilians Universität zu Würzburg vom 15. März 1999:

Hiermit erkläre ich, die vorgelegte Dissertation selbstständig angefertigt zu haben und keine anderen als die von mir angegebenen Quellen und Hilfsmittel benutzt zu haben. Alle aus der Literatur entnommen Stellen sind als solche kenntlich gemacht. Des Weiteren erkläre ich, dass die vorliegende Arbeit weder in gleicher noch ähnlicher Form bereits in einem anderen Prüfungsverfahren vorgelegen hat. Zuvor habe ich keine akademischen Grade erworben oder zu erwerben versucht.

Hanau, 25.07.2011   *Patrick M. Stock*

_____